

**SYNTHESIS AND CHARACTERIZATION OF HOLLOW AND POROUS
SILICA FINE PARTICLES VIA ORGANIC TEMPLATE ASSISTED WET-
CHEMICAL PROCESS**

(有機テンプレートを用いた液相法による中空、ポーラスシリカ微粒子
の合成と特性評価)

By
LUSI ERNAWATI

HIROSHIMA UNIVERSITY
SEPTEMBER 2017

**SYNTHESIS AND CHARACTERIZATION OF HOLLOW AND POROUS
SILICA FINE PARTICLES VIA ORGANIC TEMPLATE ASSISTED WET-
CHEMICAL PROCESS**

(有機テンプレートを用いた液相法による中空、ポーラスシリカ微粒子
の合成と特性評価)

A Thesis submitted to
The Department of Chemical Engineering
Graduate School of Engineering
Hiroshima University

By
LUSI ERNAWATI

In Partial Fulfillment of the Requirements
For the Degree of
Doctor of Engineering

Hiroshima University
September 2017

Approved by

Associate Professor Takashi Ogi
Advisor

Contents

Abstract	i
Contents	iv
List of Figures	vii
List of Tables	xii
1. Introduction	1
1.1 Silica nanoparticle and its growing demand in a wide range of markets.....	1
1.2 Hollow silica, properties and its applications.....	2
1.2.1 Template synthesis of hollow silica.....	4
1.2.2 Hard template synthesis	6
1.2.3 Soft template synthesis.....	7
1.2.4 Utilization of hollow silica spheres for thermal insulation purposes.....	8
1.2.5 Thermal conductivity of insulation material.....	8
1.2.6 Polymer based thermally conductive composite film.....	10
1.2.7 Nanotechnology and thermal insulation.....	11
1.3 Porous silica, properties and its applications.....	12
1.3.1 Synthesis of porous silica via emulsion process.....	13
1.3.2 Emulsion and classification of its phase behavior.....	15
1.3.3 Dynamic polystyrene template in oil/water emulsion system.....	16
1.4 Cationic polystyrene nanoparticle and its application.....	17
1.5 Objectives and outline of the dissertation.....	20
1.6 References.....	21
2. Hollow silica as an optically and thermally insulating polymer additive	26
2.1 Introduction.....	26
2.2 Experimental.....	27
2.2.1 Raw materials.....	27

2.2.2	Synthesis of PS particles.....	28
2.2.3	Synthesis of hollow silica particle.....	28
2.2.4	Preparation of PES/hollow silica composite film.....	29
2.2.5	Characterization.....	29
2.3	Results and discussions.....	30
2.3.1	Theoretical calculation of different required energy between TEOS and TMOS as silica source for hollow silica production.....	30
2.3.1.1	Calculation of required energy using TMOS in MeOH-water system.....	31
2.3.1.2	Calculation of required energy using TEOS in EtOH-water system.....	33
2.3.2	Polystyrene particle with controllable sizes.....	35
2.3.3	Effect of MeOH concentration on the formation of hollow silica.....	36
2.3.4	Effect of PS particle size on the outer diameter of hollow silica.....	40
2.3.5	Effect of TMOS concentration on the shell-thickness of hollow silica.....	42
2.3.6	Surface area and pore properties of hollow silica.....	47
2.3.7	Optical properties of the prepared hollow silica particle.....	48
2.3.8	Thermal conductivity of PES/hollow silica composite film.....	49
2.4	Conclusions.....	51
2.5	References.....	51
3.	Tunable synthesis of mesoporous silica particle with unique radially oriented pore structures from tetramethyl orthosilicate via oil-water emulsion process.....	56
3.1	Introduction.....	56
3.2	Experimental.....	58
3.2.1	Raw materials.....	57
3.2.2	Synthesis of mesoporous silica particle.....	58
3.2.3	Characterizations.....	59
3.3	Results and discussion.....	59

3.3.1	Effect of water-CTAB-oil weight ratios on the morphology mesoporous silica	59
3.3.2	Proposed formation mechanism of hierarchical mesoporous silica particle.....	64
3.3.3	Effect of initial styrene concentrations on the surface and pore properties of mesoporous silica particle.....	68
3.4	Conclusions.....	71
3.5	References.....	71
4.	Role of acetone in the formation of highly dispersed cationic polystyrene nanoparticle as a template for preparing hollow silica nanospheres.....	76
4.1	Introduction.....	76
4.2	Experimental.....	77
4.2.1	Raw materials.....	77
4.2.2	Preparation of cationic PS nanoparticle.....	77
4.2.3	Characterizations.....	78
4.3	Results and discussions.....	78
4.3.1	Influence of acetone/water mass ratio on PS particle sizes.....	78
4.3.2	Plausible formation mechanism of PS particle influenced by acetone addition.....	81
4.3.3	Influence of VA-004 initiator concentration on PS particle sizes and surface charge.....	85
4.3.4	Influence of reaction time on the yield and PS particle sizes.....	89
4.3.5	Synthesis of hollow silica using different sizes of PS particle.....	90
4.4	Conclusions.....	91
4.5	References.....	92
5.	Summary.....	96
5.1	Conclusions.....	96

Abstract

Silica nanoparticles are promising applications in many current and emerging areas of technology because of their nature advantages. The synthesis, properties and applications of silica particle have become a quickly expanding field of research. Nowadays, special attention has been paid to synthesis, control morphology and characterization of hollow and porous silica nanostructures in micron and/or submicron sized. Hollow silica is a special type of novel inorganic material with one or more cavities inside. In addition to the excellent properties, hollow silica exhibits unique characteristics, such as low density, high specific surface and good adsorption performance. While, porous silica has many useful characteristics, including high surface area, controllable morphology, feasible surface modifications, and biocompatibility, which are promising for various applications, such as catalyst, adsorption, separation, storage, optics, biomedical, etc. For practical application, the internal structure and the external morphology both of hollow and mesoporous silica particles have a significant influence on their practical applications. Therefore, it is important to develop facile methods to regulate both their pore structure and surface morphology.

This dissertation is focused on the development of synthesis of hollow and porous silica particles using tetramethyl-orthosilicate (TMOS) instead of tetraethyl-orthosilicate (TEOS) as silica source through organic-template assisted wet-chemical process. The use of TMOS rather than more typical TEOS has several potential advantages for practical applications, including fast reaction which enables the use of smaller-scale equipment and reduced energy cost. The role of polystyrene as a template particle along with hydrolysis/condensation of TMOS in deciding the final silica structure is described. Several synthesis parameters have also been carried out to investigate the effect of particles morphology. The brief descriptions of each chapter in this dissertation are shown below.

The background and motivation of the current research are described in **Chapter 1**. Basic explanation and review of previous researches on the synthesis and application of hollow and porous silica fine particles were also provided.

An improved synthesis route of hollow silica particles using TMOS and their applications as an optically and thermally insulating polymer additive are explained in **Chapter 2**. The results showed that as synthesized particles were successfully implemented into polymer films and permitted maintaining optical transparency while significantly improving the heat barrier properties of composite film. The shell-thickness of particle was controlled from 6.2 to 17.4 nm by increasing TMOS concentration and the diameter of particle from 95 to 430 nm through use of the different sizes of polystyrene particles. Hollow silica particle with the shell-thickness about 6.2 nm displayed a high light transmittance intensity up to 95%. Polyethersulfone (PES)/hollow silica composite films ($35 \pm 5 \mu\text{m}$ thick) exhibited a much lower thermal conductivity ($0.03 \pm 0.005 \text{ W m}\cdot\text{K}^{-1}$) than pure polymer films. The prepared particle has promising for cost and energy effective optical devices requiring thermal insulation.

Chapter 3 describes the synthesis of submicron sized spherical mesoporous silica particles using TMOS via an oil-water (O/W) emulsion process. The results showed that controlling water-surfactant-oil ratios in emulsion system leads to the formation of radially oriented structured of mesoporous silica with high specific surface area (up to $800 \text{ m}^2 \text{ g}^{-1}$) and large pore (20 nm) that will be most attractive for applications in catalysis and biomaterials. The characterization of the particles and how their morphology depends on the emulsions formed were detail studied. Additionally, the discussion of proposed mechanisms was also presented.

Chapter 4 a modified emulsion polymerisation synthesis route for preparing highly dispersed cationic polystyrene nanoparticles is described. The combined use of 2,2'-azobis[2-(2-imidazolin-2-yl) propane] di-hydrochloride (VA-044) as the initiator and acetone-water as the solvent medium afforded successful synthesis of cationic PS particles as small as 31 nm in diameter. This study provides important insights and a new methodology for further research and application, especially for synthesis and design of nanostructure materials.

Chapter 5 contains the summary of all chapters and direction for further research.

List of Figures

Figure 1.1.	Major application of silica nanoparticle in wide range of markets.	1
Figure 1.2	Hollow silica in wide applications.	3
Figure 1.3.	General formation of hollow silica by templating method.	5
Figure 1.4	Thermal conductivity depends on the temperature gradient, cross section, path length, and the properties of materials.	9
Figure 1.5	Polymer based thermally conductive composite film.	11
Figure 1.6	Nanotechnology and its application on high performance thermal insulation materials.	12
Figure 1.7	Synthesis pathway of the porous silica formation.	13
Figure 1.8	Mesoporous silica in wide range applications.	13
Figure 1.9	Classification of emulsion equilibrium based on WINSOR system.	15
Figure 1.10	Schematic of formation mechanism of mesoporous silica via dynamic polystyrene template through O/W emulsion process proposed by Nandyanto et.al.	16
Figure 1.11	Schematic of formation mechanism of mesoporous silica trough O/W emulsion process proposed by Gustafsson et.al.	17
Figure 1.12	General methods of preparation of polymeric nanoparticles and their principle involved in the mechanisms.	18
Figure 1.13	Organization and structure of chapters in the present dissertation.	20
Figure 2.1	Vapor-liquid equilibrium phase-diagram: (a) T-xy plot for MeOH-water, and (b) xy plot diagram for MeOH-water (<i>Copyright: 2006 John Wiley & Sons, Inc.</i>)	32
Figure 2.2	Vapor-liquid equilibrium phase-diagram: (a) T-xy plot for EtOH-water, and (b) xy plot diagram for EtOH-water (<i>Copyright: 2006 John Wiley & Sons, Inc.</i>)	34

-
- Figure 2.3 SEM images of polystyrene (PS) particles produced at different temperature and styrene/AIBA concentration: (a-c) at 90°C, using (a) 0.16/0.004, (b) 0.2/0.004 and (c) 0.4/0.004 (wt%); (d-f) at 80°C, using (d) 1.0/0.004, (e) 2.0/0.002, and (f) 4.0/0.004 (wt%), respectively 35
- Figure 2.4 SEM images of prepared hollow silica particle with different MeOH concentrations: (a) 0, (b) 30, (c) 50, (d) 75, and (e) 90 wt%. All the samples were prepared using PS particles of 116 nm in size. Hydrolysis of TMOS under various MeOH concentrations: At low concentration of MeOH, irregular gels and networks of particles are formed, (a-c). At higher concentration of MeOH, polystyrene template particles could be reliably coated with silica, (d, e). 36
- Figure 2.5 Hydrolysis and condensation of TMOS in MeOH-water system. The addition of MeOH or presence of partially hydrolyzed methoxy-silane species (bottom) slow down the overall condensation to silica (right) as $\text{CH}_3\text{-O-Si}$ is less reactive than Si-O-H . The amount of MeOH can be used to control the condensation rate of TMOS for controlled deposition of silica onto a template. 37
- Figure 2.6 Hollow silica is only formed at higher MeOH concentration (bottom) when the reaction rate is sufficiently low to suppress excessive nucleation (formation of free floating, new particles, (top)) and favoring deposition of silica onto surfaces or previously deposited silica nuclei on PS template surfaces. Here, surface growth fills the gaps between the porous shells and eventually leads to solid layers of silica (bottom). 38
- Figure 2.7 Fourier transform-infrared (FT-IR) spectra illustrate how the methoxy species (2870 cm^{-1}) and benzene rings of PS (8760 , 1500 , 1607 cm^{-1}) vanish during the reaction, and lead to the formation of silica (Si-O-Si bonds at 1080 and 1093 cm^{-1}): (a) pure PS template 39

- particles, (b) silica-coated PS particle before template removal, and (c) hollow silica particle.
- Figure 2.8 SEM and TEM images of hollow silica particles prepared with different PS diameter of: (a, b) 72, (c,d) 116, (e, f) 185, and (g, h) 380 nm. The molar ratio of $\text{NH}_4\text{OH}/\text{MeOH}$ and TMOS concentration were kept at 0.065 and 0.08 molL^{-1} , respectively. The coating process works well up to 180 nm. At 380 nm in size, homogeneous nucleation (i.e. independent of the template) leads to a second population of small particles (bottom) of 20 to 40 nm in size. 41
- Figure 2.9 The coating formation process becomes visible when using TEM (right side) instead of SEM for increasing shell-thickness. Hollow silica particles were prepared under various TMOS concentrations: (a, b) 0.025, (c, d) 0.04, (e, f) 0.06, (g, h) 0.08, and (I, j) 0.1 mol L^{-1} . Thin shells (top) appear grainy because of the growth of silica, where first a layer of small silica particles is deposited, and subsequently grows together through surface growth (i.e., direct deposition of silica onto previously formed silica surfaces (bottom)). 43
- Figure 2.10 Schematic illustration of the geometry of hollow silica sphere 44
- Figure 2.11 Shell-thickness of hollow silica particles can be controlled by changing TMOS concentrations. The layer thickness measured from TEM images well matches with the theoretical value when assuming even distribution of the silica on the surface of PS particle, and (b) Nitrogen (N_2) adsorption-desorption isotherms and BJH pore size distribution plots of hollow silica with 6.2 nm in shell-thickness. Adsorption and desorption volumes shown a significant hysteresis, typical for the presence of large cavities in a material. 47
- Figure 2.12 (a) Hollow silica is nearly fully transparent and stable over weeks in dispersion. photograph of the samples containing PS, silica-coated PS, hollow and dense silica particles with similar sizes were 48

provided, (b) Optical transmittance light spectra of the samples, (c) Transparent stability of hollow silica particles ($D_p=181$ nm and $L=6.2$ nm) as a function of measuring time, and (d) Optical transmittance light spectra of the prepared hollow silica particles with different shell-thickness. Inset of Figure 7(d) shows the correlation between shell-thickness and optical transparency of hollow silica at shorter ($\lambda=380$ nm) and longer ($\lambda=680$ nm) wavelength, respectively.

- Figure 2.13 (a) Hollow silica particle can be implemented into polymer films. 50
 Photograph of the succeed transparent composite film of PES/hollow silica, the film is indicated with the dotted line, the results of SEM images are shown in: (b) view from the top surface, (c) view from the bottom surface, and (d) cross sectional surface and the inset shows high magnification image.
- Figure 3.1 SEM images of MPS particles prepared using various 60
 water/CTAB/oil weight ratios: (a) MPS-a, 7.0:1.0:0.0; (b) MPS-b, 7.0:1.0:2.5; (c) MPS-c, 7.0:1.0:6.0; (d) MPS-d, 7.0:1.0:7.5; (e) MPS-e, 6.0:1.0:10.5; (f) MPS-f, 5.5:1.0:10.5; (g) MPS-g, 4.0:1.0:10.5; (h) MPS-h, 4.0:1.0:13.0; and (i) MPS-i, 4.0:1.0:14.0. Other synthesis conditions are summarized in Table 3.1.
- Figure 3.2 Photograph of MPS samples freshly prepared after cooling overnight 62
 and before centrifugation. The mixed precursor was left without mixing for 1 d prior to observing the presence of a transparent and translucent mixed solution (change of solution phase).
- Figure 3.3 TEM images of MPS particles prepared using various 63
 water/CTAB/oil weight ratios: (a) MPS-a, 7.0:1.0:0.0; (b) MPS-b, 7.0:1.0:2.5; (c) MPS-c, 7.0:1.0:6.0; (d) MPS-d, 7.0:1.0:7.5; (e) MPS-e, 6.0:1.0:10.5; (f) MPS-f, 5.5:1.0:10.5; (g) MPS-g, 4.0:1.0:10.5; (h) MPS-h, 4.0:1.0:13.0; and (i) MPS-i, 4.0:1.0:14.0.

Figure 3.4	A plausible formation mechanism of mesoporous silica through dynamic polystyrene template particle via O/W emulsion process.	64
Figure 3.5	(a) N ₂ adsorption-desorption isotherms and pore-size distribution plots for MPS-c particles; (b) low- and high-magnification TEM images of MPS-c particles; (c) N ₂ adsorption-desorption isotherms and pore-size distribution plots of MPS-f particles; and (d) low- and high-magnification TEM images of MPS-f particles	68
Figure 3.6	FT-IR spectra of (a) pure CTAB; (b, c) MPS-f particles before and after calcination; and (d, e) MPS-c particles before and after calcination.	70
Figure 3.7	XRD patterns of the calcined mesoporous silica particle and after reheat treatment	71
Figure 4.1	SEM and TEM images, and size distribution profiles of the PS particles prepared at different acetone/water mass ratios of (a, b, c) 0, (d, e, f) 0.28, (g, h, i) 0.67, (j, k, l) 1.04, and (m, n, o) 1.50. Other parameters were kept constant: VA-044 initiator/styrene mass ratio is 0.055; and reaction temperature at 60°C.	80
Figure 4.2	Schematic formation of the cationic PS nanoparticles influenced by differences in the diffusion rate of acetone in the emulsion system.	81
Figure 4.3	SEM images of the PS particles prepared at different acetone/water mass ratios of (a) 1.86, and (b) 2.33. Other parameters were kept constant: styrene and VA-044 initiator concentrations, 9.24 and 0.15 mol L ⁻¹ , respectively; reaction temperature, 60 °C, and reaction time, 8h.	82
Figure 4.4	Influence of the acetone/water composition on the average diameter of the PS particles and surface tension of the emulsion system.	83
Figure 4.5	Correlation between the acetone/water composition to the surface tension and the solubility parameter of styrene in the mixture solvent	84

-
- system calculated using Beerbower model (1971) and fitted using Koenhen-Smolders equation model (1975).
- Figure 4.6 SEM and TEM images, and zeta potential distribution (ζ) of the PS particles prepared at various VA-044 concentrations of (a, b, c) 0.0048, (d, e, f) 0.0091, (g, h, i) 0.0129, and (j, k, l) 0.0193 mol L⁻¹. Other parameters were kept constant: acetone/water mass ratio, 1.50; styrene, 9.24 mol L⁻¹; reaction temperature, 60°C. 85
- Figure 4.7 (a) Hydrodynamic diameter (R_h) distributions of the colloidal PS particles measured by DLS. (b) Force at distance, of the colloidal PS particles as a function of lag time, (τ). The inset shows an enlarged view at the shorter lag-time intervals. 87
- Figure 4.8. SEM images and associated size distribution profiles of the PS particles prepared under different reaction times of (a, b) 2, (c, d) 4, (e, f) 10, (g, h) 12, and (i, j) 14 h. Other reaction parameters were kept in constant: acetone/water and VA-044 initiator/styrene mass ratio, 1.04 and 0.055, respectively, reaction temperature, 60°C. 89
- Figure 4.9. SEM images of hollow silica particles prepared with different PS diameter of: (a) 272, (b) 163, (c) 88, (d) 35, and (e) 31 nm. The molar ratio of NH₄OH/MeOH and TMOS concentration were kept at 0.025 and 0.04 mol L⁻¹, respectively. 90

List of Tables

Table 1.1.	Various morphology of hollow silica particles and their properties.	3
Table 1.2.	Characteristics and limitations of hard and soft template synthesis	6
Table 1.3.	Various hard templates for fabrication of hollow silica	6
Table 1.4.	Thermal conductivity (k) values of commercial insulation materials.	9
Table 1.5.	Thermal conductivity of polymers.	11
Table 1.6.	An overview of recent research articles on the various synthesized mesoporous silica particles and their physical properties.	14
Table 2.1.	Comparison of the required energy for the distillation of alcohols (MeOH and EtOH) generated from TMOS and TEOS as by-products.	27
Table 2.2.	Synthesis condition of PS particle with controllable sizes.	28
Table 2.3.	Properties data of MeOH and water.	31
Table 2.4.	Overall material balances (MeOH-water system)	31
Table 2.5.	Component balances in distillate product (MeOH-water system).	31
Table 2.6.	Component balances of bottom product (MeOH-water system).	32
Table 2.7.	Overall component balances (MeOH-water system).	32
Table 2.8.	Properties data of EtOH and water.	33
Table 2.9.	Overall material balance (EtOH-water system).	33
Table 2.10	Component balances in the distillate product (EtOH-water system).	33

Table 2.11.	Component balances of bottom product (EtOH-water system).	34
Table 2.12	Overall component balances (EtOH-water system).	34
Table 2.13	Synthesis condition of hollow silica particle prepared under various PS particle sizes.	40
Table 2.14	Synthesis condition of hollow silica particles prepared under various TMOS concentrations.	42
Table 2.15	Thermal conductivity of PES/hollow silica composite films.	50
Table 3.1	Type and characteristic phase behaviors of emulsion system of the synthesized MPS particles.	60
Table 3.2	Surface areas and pore properties of the synthesized MPS particle.	69
Table 4.1	Polymerization conditions employed for synthesis of cationic polystyrene particles.	79
Table 4.2	Hansen solubility parameter values of acetone, water and styrene	84
Table 4.3	Synthesis condition of hollow silica particle prepared under different PS particle sizes	91

Chapter 1

Introduction

1.1 Importance of silica material and its growing demand in a wide range of markets

Silica material plays a vital role in a wide range of markets for electronics, polymer, rubber, elastomers, print media, footwear and other applications. With such a diverse range of applications, the demand of silica was increased in many countries. The percentage of major application of silica materials in wide range of markets are shown in **Figure 1.1**.

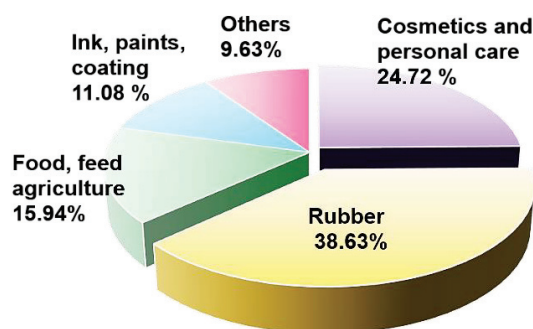


Figure 1.1 Major application of silica material in a wide range of markets.

Precipitated silica was the major product segment in 2016. It is widely used as a performance additive to increase wear resistance and wet grip capabilities in industrial and automotive tires. Fumed silica is exhibiting high growth potential in the overall specialty silica market due to its use as an integral component in paints & coatings [1]. Silica gel is a cost-effective substitute for silica types and is preferred by small and medium customers due to its easy availability in market. Owing to the large number of uses it is unsurprising that silica production has become a significant industry. In 2012, commercial silica production had a market value of approximately 3.6 billion US dollars with an estimated production rate of 2.4 million tons globally [2]. According to a report by The Freedonia Group [3], global demand for specialty silica materials is expected to continue to increase, reaching a production rate of approximately 2.9 million tons by 2018.

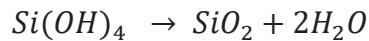
For the wide applications, the commercial marketplace required silica nanoparticle to be produced cheaply and uniformly, with an ability to tailor the properties of the product. For most application, silica nanoparticle can be produced through various chemical synthesis. Sol-gel processing methods based on the *Stöber* method are generally used to produce silica

nanoparticles by hydrolysis and condensation reactions. A silicate precursor is required, which typically takes the form of a silicon alkoxide, such as tetraethyl orthosilicate (TEOS). Silicon alkoxides hydrolyze under both acidic and basic conditions, after which condensation occurs and Si-O-Si bonds start to form, creating a sol of dispersed nanoparticles. One advantage of these method is the ability to control particle size, distribution, and morphology by systematic variation of reaction parameters [4]. The *Stöber* method has been applied widely, and subsequently particles with diameters ranging from tens of nanometers to a few microns have been obtained. General formation of silica particles through hydrolysis and condensation of TEOS based on the Stöber process, written as follows:

I. Hydrolysis reaction:



II. Condensation reaction:



The size of silica nanoparticles produced from the *Stöber* method is mainly controlled by the relative contribution from nucleation and growth of particles. These phenomena are themselves dependent on the hydrolysis and condensation of TEOS, controlled by changing parameter reaction conditions.

1.2 Hollow silica, properties and its applications

Hollow silica is a special type of novel inorganic material with one or more cavities inside. The intrinsic properties of micro/nano hollow structures, such as large surface area, low density, abundant inner void space, high mechanical strength, permeability, relatively low refractive index, thermal and chemical stability, make the hollow silica becomes good candidates for wide applications. For example, the void space inside the hollow shell could be used as micro-nanocontainers or reactors, when filled with different materials, either inside the hollow void space, they could serve as anodes for lithium ion batteries or carriers for drug delivery [5]. Depending on the different application areas which could be classified into the following categories: for energy storage, catalyst, biomedical, cosmetics, heat insulator, Uv-protector, biosensor, as shown in **Figure 1.2**.

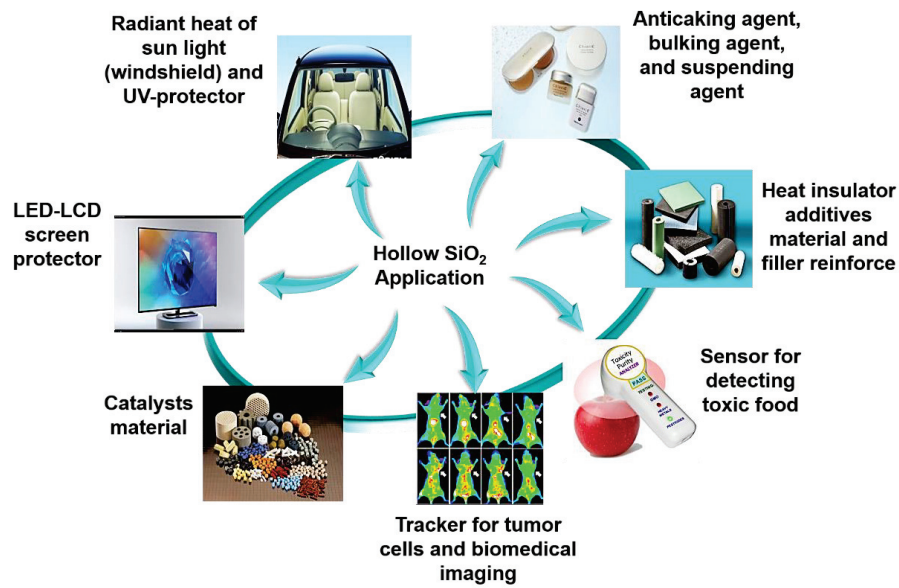





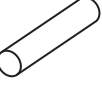
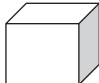


Figure 1.2 Hollow silica in wide range applications.

For over the last decade, hollow nanostructures with a controlled pore volume and shell thickness have emerged as an important class of nanomaterials. Hollow silica nanoparticles compose of hollow interiors and solid shells. This nanostructure can be categorized into various groups from the different perspectives. For examples, there could be hollow spheres, tubes, fibers, cubes etc. reflecting different overall shapes. Some common hollow silica morphologies and their special performance are shown in **Table 1.1**.

Table 1.1 Various morphology of hollow silica particles and their properties

Type	Hollow silica morphology	Type of hollow silica	Unique properties
(a)		Hollow silica spheres with disordered pores	Excellent adsorption and penetration properties
(b)		Hollow silica spheres with well-ordered cylindrical channels	High specific surface area
(c)		Non-porous hollow silica spheres	Avoid mass transfer and improve the surface smoothness and dispersion uniformity
(d)		Multi-shelled hollow silica spheres	Multiply the specific area of the hollow silica spheres and potential to enhance their optical properties
(e)		Silica spheres with multi hollow cores	Promising for sustained release
(f)		One-dimensional hollow silica nanostructures	Large high-aspect ratio, surface area and accessible both inside and outside surfaces

(g)		Hollow silica cubes	Higher specific surface area than hollow spheres of the same volume
-----	---	---------------------	---

Microporous Mesoporous Mater., 227(121-136), 2016

With pores in the shell is a prominent feature of hollow silica since the shell is usually assembled from small silica particles. Theoretically, additives (e.g. surfactants) are often necessary to adjust interactions between templates and the hydrolyzed precursor during the hollow silica preparation. These additives distributed around template also serve as porogen, and the porosity can be adjusted by varying their amounts. Porosity will directly impact the specific surface area and thus the adsorption and penetration performance of hollow silica. Hollow silica spheres with different shell structure were prepared by controlling the pH value of reaction system and the reaction time. The obtained hollow silica spheres were categorized into three types: (A) silica shell is relatively thin and spherical shape of the stacked particulates is clearly identified in the shell, (B) silica shell is similarly thin to type A, but shape of the stacked particulates is identified as half round shape, and (C) silica shell is thick and the stacked particulates are not recognized in the shell [6].

The design of shell structures of hollow silica nanoparticles, including diameter, shape, thickness, surface roughness, morphology, and pore size, is precisely controlled by numerous synthesis processes. Therefore, many approaches have been exploited to synthesize hollow silica nanoparticles with respect to mesostructure shells, which exhibit unique properties of both macroporous and mesoporous structures in one single piece. The well-known approaches are sol-gel and template methods.

1.2.1 Template synthesis of hollow silica

Compared with sol-gel method, the template method has attracted much attention because the diameter and shape of hollow silica nanoparticles are simply controlled by those of used templates. It can also design shell thickness of the hollow silica nanoparticles by ratio of silica source and template, reaction time, etc [7]. Therefore, both hollow interior size and shell thickness of hollow silica nanoparticles being two independent variables in optical designs of the optical displays can be tuned by the choices from the template method. Despite the increasing number of reports on self-templating or other novel routes for preparing hollow silica, most fabrication approaches still rely on the conventional template method. Template synthesis is an easy strategy to regulate the final morphology of hollow silica with the aid of heterogeneous template [8]. Three steps, as illustrated in **Figure 1.3**, namely template

preparation, shell formation and template removal are usually indispensable in the template synthesis of hollow silica.

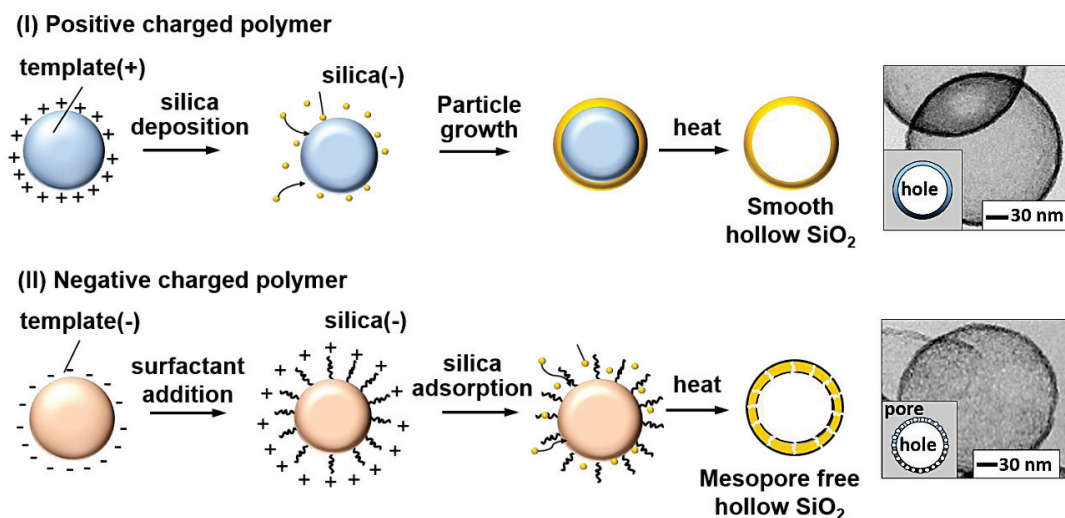


Figure 1.3 General formation of hollow silica by templating method.

By coating of silica onto template surface, the template/silica composites are produced. Hollow silica is then created simply by removing the heterogeneous template core. The advantages of this method lie in its economy, efficiency and especially the structure parameters controllability of products. Moreover, it doesn't require any expensive equipment or uncommon materials. Optimizing the reaction conditions to tailor the morphology, size and pore-structure of hollow silica has been another focus in hollow materials developments. However, this is not a simple matter for inorganic silica itself, due to the lack of structural characteristic as organic materials. By understanding the advantages of template synthesis, it is suggested that template synthesis is the most suitable approaches to precisely control the structures and morphologies of hollow silica, simply by selecting templates with different forms, or changing the experimental parameters. So far, a series of hollow silica with different morphologies have been synthesized, each with its own unique properties and potential applications.

In terms of physical nature, templates can be further divided into hard templates and soft templates. Hard templates usually have definite shape with structure rigidity. Many substances, including polymeric, inorganic, biological, and metallic components can be used as hard templates [9]. Comparatively, soft templates are prone to deformation during the silica coating process. Emulsion droplets, polymer aggregates and surfactant micelles are common soft templates. There are many differences between hard and soft template method, especially in the template formation and/or removal process and the product morphology. For the

comparison of these two methods, the characteristics and limitation of them are listed in **Table 1.2**

Table 1.2 Characteristics and limitations of hard and soft template synthesis

Template	Characteristic	Limitation
Hard template	narrow size distribution, uniform product morphology,	time-consuming, multistep process, the template is difficult to remove
Soft template	simple method, the template is easy to prepare and remove	irregular appearance, wide particle size distribution, poor structural stability and mono-dispersity

Microporous Mesoporous Mater., 227(121-136), 2016.

1.2.2 Hard template synthesis

Over the past several decades, hard template directed approaches have been the most commonly used methods for the preparation of hollow nanostructures. Hard templates are advantageous for their narrow size distribution and availability in a wide range of sizes or morphology, which can provide the shell formation and predetermine the final structure precisely. However, hard templates require a multistep synthetic process as well as a difficult removal process by either thermal or chemical means, which is time-consuming, laborious and prone to cause pollution of organic solvents. Various hard template materials and how to remove are summarized in **Table 1.3**.

Table 1.3 Various hard templates for fabrication of hollow silica

Template	Template shape	Template preparation	Template removal	Literature Reference
Polystyrene	spherical	soap-free emulsion polymerization	calcinated at 550°C	[10]
			dissolved in tetrahydrofuran	[11]
			dissolved in basic-alcohol medium during silica coating	[12]
PS-co-PVP	spherical	Emulsion polymerization	calcinated at 500-600°C	[13]
PAA	spherical	-	washed with water	[14]
PMMA	spherical	soap-free emulsion polymerization	calcinated at 550°C	[15]
CaCO ₃	needle-like	-	washed in acetic acid	[16]
C (carbon)	spherical	pyrolysis of acetylene	calcinated at 550°C	[17]
MWCNT	tubular	thermal Chemical vapor deposition	calcinated at 800°C	[18]
ZnO	ribbon-like	a solution route	etching with Hydrochloric acid	[19]
	flower-like	hydrothermal reaction		
	spherical	zinc acetate decomposition		

Microporous Mesoporous Mater., 227(121-136), 2016.

Although the hard-templating methods are effective in the synthesis of hollow structures, their drawbacks are obvious. The first problem comes from the availability of the templates. It is very difficult to find templates that have the required size, shape, and surface property for growing hollow spheres from targeted materials. In addition, the production cost of the template particles is high so that most of these methods are limited to small scale synthesis. As mentioned previously, the multi-step procedures typically involved in the templating methods also prevent scale-up of such methods for practical applications. The frequent occurrence of homogeneous nucleation of the growing species also complicates the coating process, making it difficult to control the quality and the reproducibility of products.

1.2.3 Soft template synthesis

The soft template synthesis is another simple and general method for obtaining hollow particles. Some hollow particles with nanometer to micrometer diameter have been successfully fabricated using double emulsion process usually composed of water-in-oil-in-water ($W_1/O/W_2$). The soft templates typically include structures formed by surfactants, long-chain polymers, which are usually amphiphilic molecules that contain a hydrophilic head and a hydrophobic chain. Under certain conditions, these materials self-assemble into well-defined aggregating entities such as normal and reverse micelles, emulsions, vesicles, or liquid crystal phases, which restrict and direct the growth of guest structures. Precursor species react in the confined space or on the outer surface of the soft assemblies, producing bubble-like or tube-like structures that mimic the original shape of the templates [20]. Emulsions, including both oil-in-water (O/W) and water-in-oil (W/O) types, are most commonly used soft templates.

The soft templating approaches show a few intrinsic advantages over the hard-templating methods for preparing hollow nanostructures. For instance, the application of hollow structures in fields such as drug delivery, gas storage and catalysis requires facile access to the hollow interior space. With soft templates, one can obtain hollow structures with porous shells, making it convenient to refill the hollow interior with functional species or to encapsulate guest molecules. Comparing to hard templating, soft templating is often limited by the difficulty in controlling the uniformity of the products. In many cases, it is also challenging to scale up the soft templating methods due to the complication associated with the self-assembly of templates and shell growth processes.

1.2.4 Utilization of hollow silica spheres for thermal insulation purposes

Insulation materials play a critical role in the effort made by governments to meet global and national energy efficient targets. A wide range of insulation materials is available, however only a few match with the requirements of modern fish hold construction. Selection of insulation material should be based on initial cost, effectiveness, durability, the adaptation of its form/shape to that of the fish hold and installation method available in each of the areas [21]. From an economic point of view, the best insulation materials are required to have the following properties below:

- a) **Thermal conductivity.** The best thermal insulators have the lowest thermal conductivity. This is the property of a material that measures how well it can conduct heat through its mass. The lower the conductivity measure, the less well a material is able to conduct heat, thus enabling it to trap heat or protect contents from outside heat.
- b) **Heat Resistance.** Thermal insulators should also be resistant to heat, since they will likely be subject to heat on their surfaces because of the inability of heat to move through them. A thermal insulator without a high heat resistance quotient runs the risk of melting or burning.
- c) **Air permeability.** Air permeability is the property of a material to allow air to pass through its weave or pores. It is often attributed to materials such as those used in the manufacture of clothing. High air permeability means a lower level of thermal conductivity.
- d) **Thermo-insulating materials.** Based mainly on thermal conductivity, some of the best and most common thermal insulation materials include fiberglass, which is made of spun threads of melted and fluffed glass, and foam, which has pockets of gas that do not conduct heat well.

1.2.5 Thermal conductivity of insulation material

Thermal conductivity is a measure of the quantity of thermal energy which will flow through a substance. The units of measure for conductivity must quantify the amount of energy transferred in each amount of time, across a measured thickness of material and temperature difference. The concepts of thermal conductivity can be derived from Fourier's law of heat [22]. This law states that the time rate of heat transfer through a material is proportional to the negative temperature gradient and to the area, at right angles to that gradient, through which heat is flowing (Ws). Total heat flow rate through each of the flux meters is given by:

$$dQ = -k \frac{\partial T}{\partial x} x dA x dt \quad (1)$$

Where Q is the heat flux, $\frac{\partial T}{\partial x}$ is the temperature gradient in the x direction, A is the cross-sectional area of material transferring heat and ΔT is the difference in temperature between one side of the material and the other. These factors are visually shown in the **Figure 1.4** below.

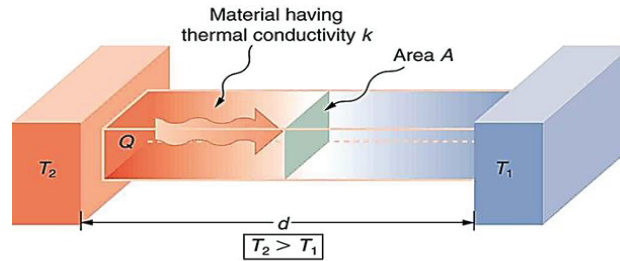


Figure 1.4 Thermal conductivity depends on the temperature gradient, cross section, path length, and the properties of materials [22].

k [W mK^{-1}] is the coefficient which is referred to as the thermal conductivity. It can sometimes be referred to as the k -value or the λ -value. It is the material specific property. In simple term this is a measure of the capacity of a material to conduct heat through its mass. Different insulating materials and other types of materials have specific thermal conductivity values that can be used to measure their insulating effectiveness. Meanwhile, the thermal resistance is determined using:

$$R_m = \frac{\Delta T}{Q}$$

Where Q is the mean value from the upper and lower heat flux meter and ΔT is the temperature difference from measurement, calculated based on the extrapolation of the least squares fit of the data to the contacting surfaces of the flux meter. Some k -values of insulation material that are used in building for thermal insulation purpose are shown in below **Table 1.4**.

Table 1.4. Thermal conductivity (k) values of commercial insulation materials

Insulation materials	Thermal conductivity (λ) [$\text{W m}^{-1} \text{K}^{-1}$]	Thermal resistance (R) value per inch (2.54 cm)	Advantages	Disadvantages
Cellulose	0.030~0.040	2.63	provides a green, efficient, non-toxic, affordable thermal insulation, less conductive heat loss and better protection against air infiltration than other fibers (performance 38 %higher than glass wool), low embodied energy as it takes up to 20 times less energy to manufacture than other fibers, low cost raw material as 75 to 80% recycled content (fire resistant provided by chemicals and dense structure)	necessary to treat the cellulose using chemicals to make it permanent fire and insect-resistant, and is applied as loose-fill or wet-sprayed through a machine.
Glass mineral wool	0.031~0.044	3.7	low cost, ease of installation	readily absorbs water or other fluids, loses insulating value when wet
Expanded polystyrene	0.030~0.038	3.75~4.0	reasonable R-value, lower cost than smooth surfaces sheets	cannot be used with fiberglass, resins unless protected, easily damaged
Polyurethane Foam	0.023~0.032	6.25	very good R-value, can be used with fiberglass resins	not always easily available and relatively expensive
SiO ₂ materials (aerogel)	0.014~0.015	7.0	very good R-value, can be used with fiberglass resins, relative ease of application	requires very careful volume calculations, requires special spray equipment

Food and Agriculture Organization of the United Nations, 2003 [23].

As shown in **Table 1.4**, silica material is recognized as leading insulation materials that have the lowest (k) compared with other insulation materials. Beside the low thermal conductivity, the other most important characteristic of silica materials is heat resistance. This material does not melt even at very high temperature and not release any kind of toxic gases for conventional thermal insulation systems [24].

1.2.6 Polymer based thermally conductive composite film

With the growing demand for thinner and smaller product that are integrated to ensure portability, an increasing number of studies have investigated the efficient thermal control of integrated compact-sized devices. Accordingly, considerable attention is being paid to thermally conductive polymer composites that are easy to fabricate in thin forms. Polymer based thermally conductive composite film has much potential than the traditional thermally

conductive metals in terms of the good resistance to corrosion, stretchable, and electrically insulating, for their purposes (see **Figure 1.5**).

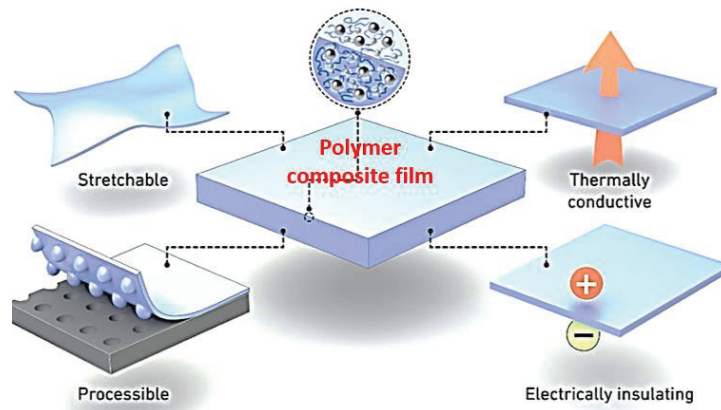


Figure 1.5 Polymer based thermally conductive composite film [25]

Generally, polymers exhibit a low thermal conductivity because of their relatively low atomic density, weak interactions or chemical bonding, and complex structures. The thermal conductivity values of some polymers are listed in **Table 1.5**

Table 1.5 Thermal conductivity of polymers

Polymer	Thermal conductivity (λ) [W m ⁻¹ K ⁻¹]
Low density polyethylene	0.28~0.32
High density polyethylene	0.38~0.58
Epoxy resin	0.17~0.21
Polypropylene	0.18~0.24
Phenol resin	0.24~0.29
Polyethersulfone (PES)	0.28~0.30

Appl. Polym. Sci., 49(9), 1625-1634, 1993.

Incorporation of fillers in electrical insulation polymers is a common approach to improve electrical, mechanical, and thermal properties. When we design thermally conductive polymer composites, a holistic approach to satisfy all the application requirements is needed. It is not sufficient just to select appropriate polymers and fillers (size, shape, type, hybrid filler).

1.2.7 Nanotechnology and thermal insulation

Nanotechnology can be applied as a scientific tool to make high performance thermal insulation materials. The normal focus in nanotechnology is to control matter, typical particles, of dimensions between 0.1 nm and 100 nm, i.e. at an atomic and molecular scale. However, for nanotechnology applied for making thermal insulation materials, the focus is shifted from particles to pores in the nano-range [26]. These aspects are visualized in **Figure 1.6**.

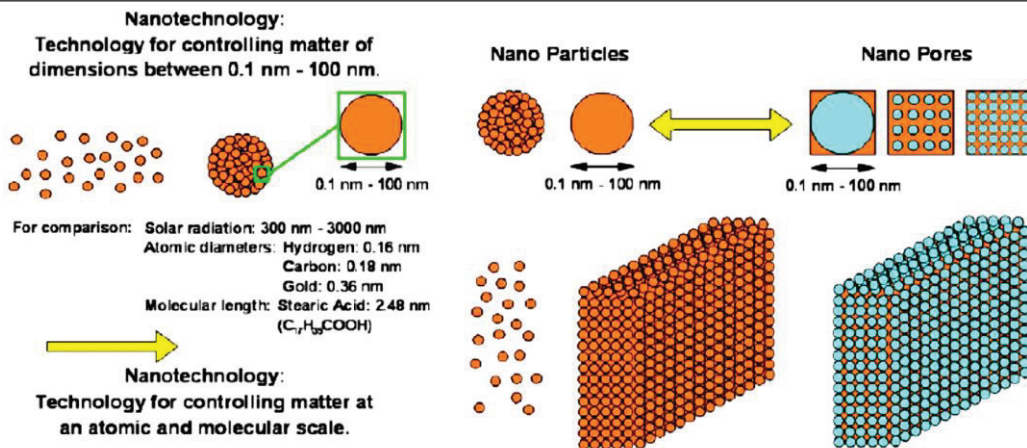


Figure 1.6 Nanotechnology and its application on high performance thermal insulation materials

The morphology (orientation of fillers and polymers, ordered structure, filler arrangement/packing) and the interaction (filler surface treatment) of polymers and fillers also need to be carefully understood and controlled. Furthermore, not only the thermal conductivity, but also other properties and process ability need to be considered and balanced. For insulating material, hollow silica particles are a newly developing material with the special properties of low density, thermal insulation, and distinct optical activity. One of the most prominent applications of hollow silica is their ability to attain homogenous filler in advanced composite materials. The incorporation of silica nanoparticle in polymer films not only enhances mechanical properties of the film, but also reduce the thermal degradation at high temperature. Therefore, it can improve the insulation/heat barrier properties of the composite film [27].

1.3 Porous silica, properties and its applications

The International Union of Pure and Applied Chemistry (IUPAC) classifies porous silica materials into three types depending on their pore sizes: microporous materials with pore sizes below 2 nm, mesoporous materials with pore sizes between 2 and 50 nm, and macroporous materials with pore sizes larger than 50 nm [25]. Mesoporous silica is inorganic materials synthesized in the presence of surfactants as templates through the hydrolysis and condensation of silica species from various sources (i.e., sodium silicate, tetralkoxides such as TEOS, and/or TMOS). The synthesis pathway of the formation mesoporous silica material through surfactant self-assembly process has been proposed in previous reports, as shown in **Figure 1.7**.

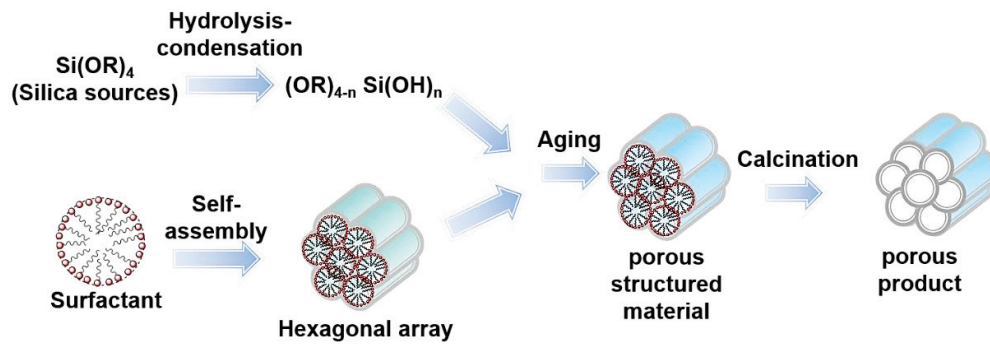


Figure 1.7. Synthesis pathway of the porous silica formation

The control of particle size and morphology of mesoporous silica can be attained in different ways, with the fundamental variables to control being the relative rates of hydrolysis and condensation of the silica source, the interactions between the growing silica polymer and the assembled templates. Mesoporous silica has also many useful characteristics [26], including high surface area, controllable morphology, feasible surface modifications, and biocompatibility, which are promising for various applications, such as catalysis, adsorption, separation, storage, optics, photochemistry, biomedicine, etc (see **Figure 1.8**).

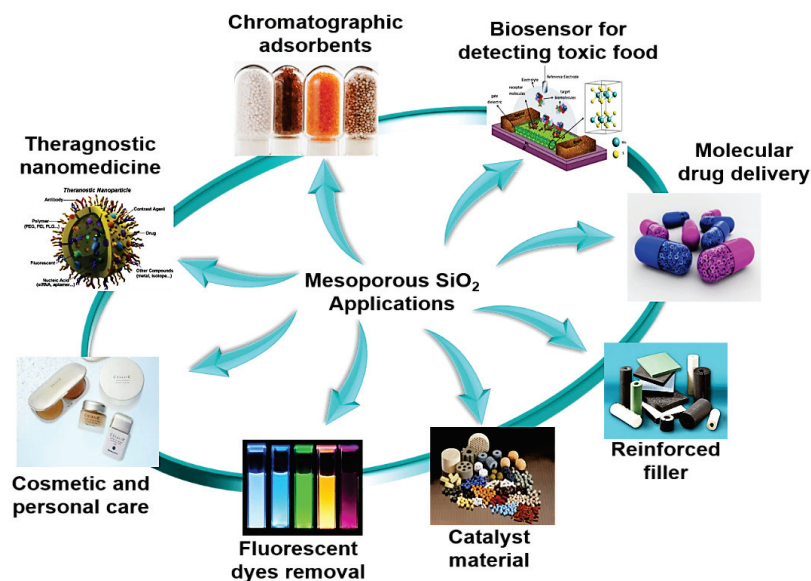


Figure 1.8. Mesoporous silica in wide range applications

1.3.1 Synthesis of porous silica via emulsion process

Emulsion is one of the recent and ideal techniques for the preparation of mesoporous silica with well controlled particle size, shape, spatial arrangement, surface and pore properties. An emulsion is a two-phase system consisting of water droplets dispersed in an oil phase or of oil droplets dispersed in an aqueous phase. The former type is often referred to as water-in-oil (W/O) and the latter type to oil-in-water (O/W). To form an emulsion, a suitable surfactant (emulsifier) is generally required to stabilize the droplets dispersed in the continuous phase.

Emulsion templating takes advantage of the fact that oil droplets compared to solid particulate templates are (i) highly deformable to allow the inorganic gel to accommodate large shrinkages and thus prevents cracking during drying, (ii) can yield architectures on a scale ranging from nano to micron sizes, and (iii) the emulsion droplets are easily removable by evaporation, extraction or calcination [27]. Compared to the applied hard templating approach, the combination of using mesostructured directing agents together with an emulsion has the advantage that the emulsion droplet size can be adjusted by changing the emulsification conditions and the use of block copolymer species, which self-assemble to a large extent independently of the emulsion formation, allows for tailoring the macro-mesopore size.

Table 1.6 An overview of recent research articles on the various synthesized mesoporous silica particles and their physical properties

Synthesis method	Silica source	Morphology type	Particle size (nm)	Pore size (nm)	Pore volume (cm ³ g ⁻¹)	BET surface area (m ² g ⁻¹)	Literature reference
Micro-emulsion	TEOS	center/radial-like structure	250~450	4.6	0.25	641	[28]
	TEOS	fibrous-MSN	400	<20		255	[29]
	TEOS	wrinkle/worm-like structure	300	2~4	<15	520	[30]
Ethyl-ether emulsion	TEOS	dendritic-MSN	400~1300	3.0	<60	803	[31]
	TEOS	hierarchical-MSN	150~220	2.7	5~50	1078	[32]
	TEOS	dendrimer-MSN	150~250	4.5	9~117	747	[33]
	TEOS	chrysanthemum-like structure	230	4.7	10~20	642	[34]
Styrene emulsion	TEOS	center/radial-like structure	20	4	1.04	585	[35]
	TEOS	center/radial-like structure	60	9	1.36	628	[36]
	TEOS	center/radial-like structure	90	15	1.51	694	[37]
Weak template	TEOS	MSN-inner pore	74±8	20	2.13	435	[38]
Phenyl-decorated SiO ₂	TEOS	MSN-inner pore	40~70	<6	1.5	953	[39]

Small, 2015, 11(4), 392-413.

1.3.2 Emulsion and classification of its phase behavior

Emulsion is colloidal dispersions in which two liquids initially immiscible (typically water and oil) coexist in one phase due to the presence of monolayer of surfactant molecules

with balanced hydrophilic and hydrophobic properties. Phase behavior studies of emulsion means of equilibrium phase diagrams of polar solvent/surfactant/non-polar solvent systems provide essential information on emulsion formation and structure. Winsor et.al have developed a classification scheme for emulsions (micro and macro). Oil-in-water (O/W) emulsions are droplets of oil surrounded by a surfactant (and possibly co-surfactant) that forms the internal phase distributed in water, which is the continuous phase, Winsor-I type. In equilibrium phase system, the emulsion system with excess water phase is denoted as Winsor-II type. The O/W type emulsion has generally a larger interaction volume than the W/O emulsion. Water-in-oil emulsions are made up of droplets of water surrounded by an oil continuous phase. These are generally known as a reverse-micelles. The middle phase bicontinuous emulsion in equilibrium with and excess oil phase at the top and excess water phase at the bottom have been classified as Winsor-III type. While, Winsor IV systems are formed by altering the curvature of interface with the help of different factors such as salinity, temperature, etc. **Figure 1.9** shows the classification of emulsion type based on WINSOR system.

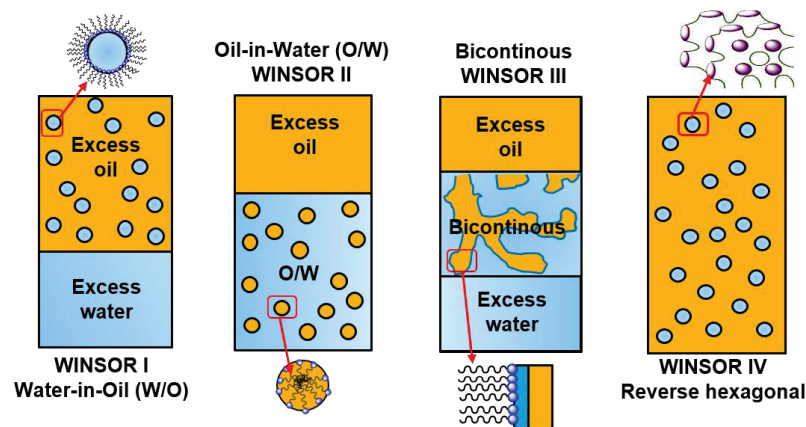


Figure 1.9 Classification of emulsion equilibrium based on WINSOR system

Type I is surfactant-rich oil phase (the upper phase) that co-exist with surfactant-poor water phase (**Winsor I**), type II indicates surfactant-rich water phase (lower phase) that co-exists with surfactant-poor oil phase (**Winsor II**), type III represents the surfactant-rich middle phase which co-exist with both water (lower) and oil (upper) surfactant-poor phases (**Winsor III**) and type IV is a single phase homogenous mixture (**Winsor IV**). Based upon the composition, these can be of various types of WINSOR system. water-in-oil (W/O) or oil-in-water (O/W) type, lamellar or bicontinuous, hexagonal and reverse hexagonal [40].

1.3.3 Dynamic polystyrene template in oil/water emulsion system

Nandyanto et. al have achieved the synthesis of dendritic spherical mesoporous with tunable outer particle diameters (20-80 nm) and pore sizes (4-15 nm) in a novel oil in- water emulsion system using a special dynamic polystyrene template. In the reaction system, octane as an oil phase, styrene monomer as a potential dynamic template, L-lysine as a base catalyst, TEOS as a silica source, and 2,2'-azobis (2-methylpropionamide) dihydrochloride (AIBA) as an initiator, and CTAB (as surfactant) aqueous solution were mixed. The possible formation mechanism involves two simultaneous dynamic reactions in one droplet emulsion, as illustrated in **Figure 1.10**.

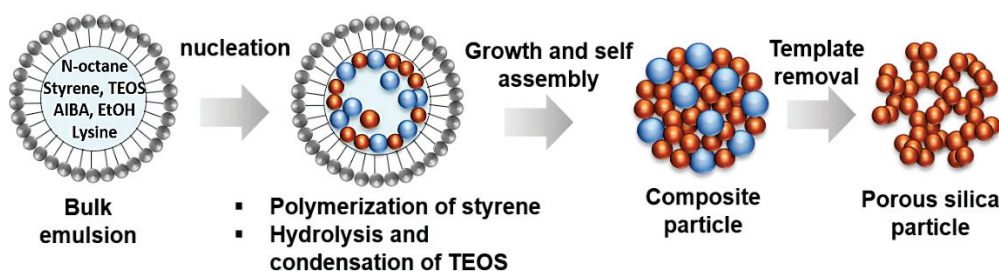


Figure 1.10 Schematic of formation mechanism of mesoporous silica via dynamic polystyrene template through O/W emulsion process proposed by Nandyanto et. al.

The possible formation mechanism of mesoporous silica was described as follows. The dynamic hydrolysis and condensation of TEOS will gradually generate the silicate species and form the nucleation seeds, while the dynamic polymerization of styrene monomer will gradually produce polystyrene (PS) at the same time. The simultaneous formation and self-assembly of silica and PS components in one nanodroplet give rise to the formation of special composite structures of silica/PS/CTAB. Mesoporous silica particles are finally obtained by calcination to remove the organic components (PS and CTAB).

More and more attention still attracted towards the synthesis of dendritic mesoporous silica through dynamic polystyrene template in O/W emulsion system. In recent year, Gustafsson et. al have later showed that the mechanism suggested by Nandyanto et.al., for the formation of the very small particles with relatively large pores is probably not correct [41]. Particles with similar size and morphology were obtained also when styrene was removed from the formulation, which indicated that polymerization of styrene did not play a role for the formation of the porous structure. It was also demonstrated that a basic amino acid, such as lysine, was not needed. The formation mechanism of particle was proposed as follows (See **Figure 1.11**)

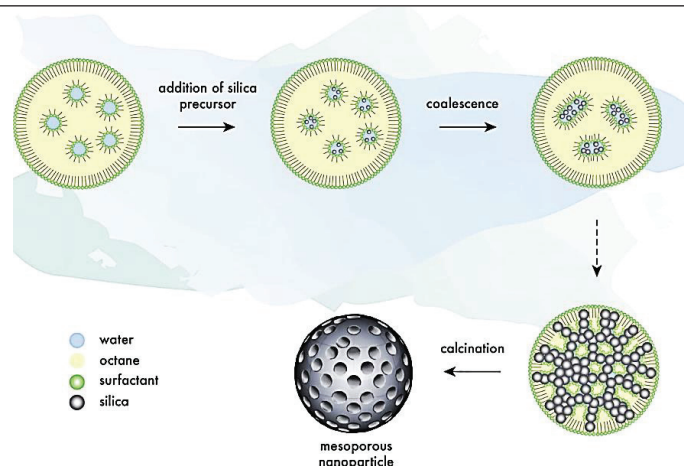


Figure 1.11 Schematic of formation mechanism of mesoporous silica through O/W emulsion process proposed by Gustafsson et. al.

The reaction medium could be simplified to an oil phase containing only TEOS and octane, an emulsifier, and ethanolamine as base to catalyze hydrolysis of TEOS. The hydrolysis of TEOS, which is solubilized in the oil droplets, starts at the interface between oil and water and that interface is very large due to the many small water droplets present in the oil. An oil phase in an emulsion is usually not plain oil but rather a W/O microemulsion. It is well-known that surfactants solubilize water into oil forming a W/O microemulsion, also sometimes called a reversed micellar system. This means that the drops of an O/W emulsion usually do not contain only the oil component, they also contain a varying amount of very small water droplets. The continuous water phase of an O/W emulsion is not pure water. The water phase is a micellar solution of the surfactant and some oil is usually solubilized into the micelles. This is in principle the same transition as is commonly known as a transition from a water-in-oil microemulsion into a bicontinuous microemulsion. The end result will be long narrow silica threads protruding through what remains of the oil drops when all the TEOS has been consumed. After removing the organic material, (i.e. n-octane, surfactant and organic base), the mesoporous structure is obtained.

1.4 Cationic polystyrene nanoparticle and its application

Cationic polymer latex particles not only exhibit the common features of general polymer latex particles such as small size and high specific surface area, but also have some unique properties like positive charge on their surfaces, good mechanical and chemical stability, low surface tension, high hydrophobicity, etc [43]. Consequently, cationic polymer latex particles are employed in a wide range of fields including drug delivery, chromatographic separation, enzyme encapsulation, medical diagnosis and many others. For example, in

papermaking and wastewater treatment, cationic latex particles can be used as flocculants and lead to higher treatment efficiency than Compared with anionic polymer latex particles, cationic polymer shows their advantages in anionic and non-ionic polymer latex particles. specific applications. Relative to anionic latex particles, cationic polymer particles attract more attention and are more widely applied. Because of their unique rheological behavior polymer latexes are widely used as thickeners in foods and cosmetics. However, cationic polymer latexes are more effective for controlling the stability of colloidal dispersions than anionic polymer latexes because of absorption of anionic surfactants. Numerous techniques are available for the preparation of the polymeric nanoparticles and mainly top-down and bottom up processes (Figure 1.12)

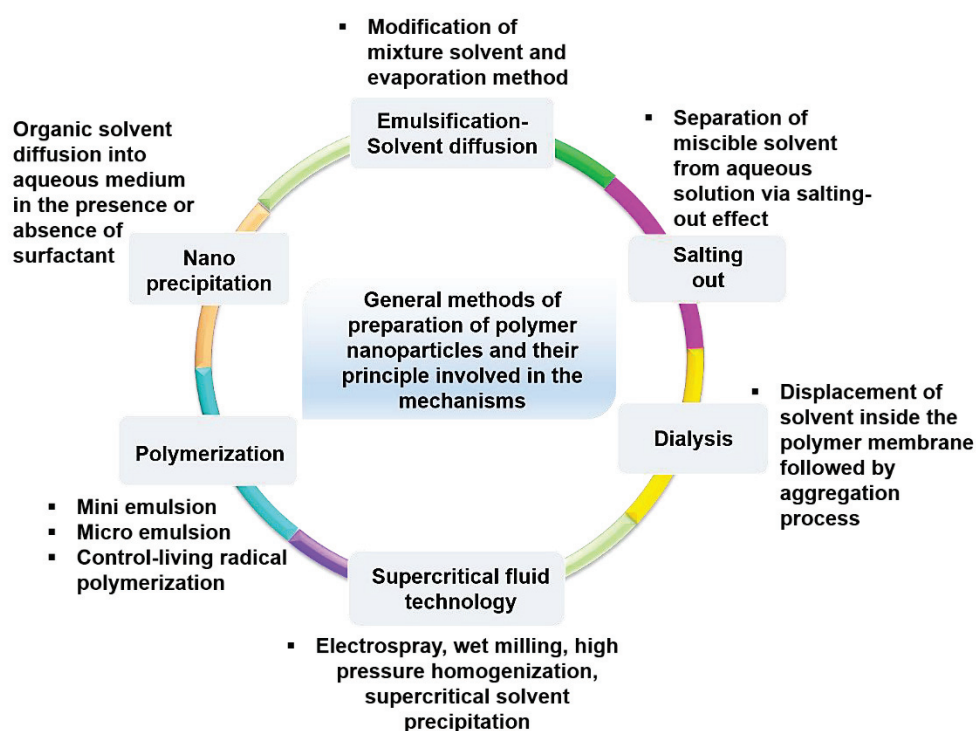


Figure 1.12. General methods of preparation of polymeric nanoparticles and their principle involved in the mechanisms.

Polystyrene latex nanoparticle is used in various applications involving drug delivery systems and personal care. The incorporation of functional materials into the polymer particles and the decreased size of the polymer particles are effective in some cases. For instance, 30-nm-sized polymeric micelles can penetrate well and transport more functional materials such as drug into the cells in comparison with larger micelles [44]. Thus, the less than 30-nm-sized polymer particles including functional materials are more promising. For the preparation of the polymer particles having the average size of 30 nm or less, several methods are used such as micro-emulsion polymerization and mini-emulsion polymerization [45]. Micro-emulsion polymerization often requires the larger amount of surfactant than the amount of added

monomer to obtain smaller polymer particles, which is not suitable for some application. Mini-emulsion polymerization needs strong agitation such as ultrasonication and high-pressure homogenization.

Drawbacks in polymerization techniques are evolving noxious factors such as toxic, reactive residues, un-reacted monomers, the risk of a chemical reaction and the formation of unwanted oligomers [46], and these drawbacks are overcome by using preformed polymers for the polymerization process. Generally, the drug loaded nanoparticles were prepared by dissolving the drug and polymer into the water-immiscible organic solvents and producing a nano-emulsion, as an example by probe-sonication method. The organic solvent is removed by using elevated temperature or reduced pressure [47], as an example of rotary evaporation method, and the nanoparticle is washed and collected by centrifugation. Followed by various changes and improvements of the emulsification techniques have been reported [48]. For example, the sonication process is a crucial step in the preparation of the sensitive drug loaded nano-emulsion, and the sonication process can increase the temperature, that leads to inactivate the active ingredients. To avoid the problems researchers utilized an on/off cycle to maintain a low temperature. Other examples of general methods to prepare the drug polymer nanoparticle are described in the **Figure 1.12**. The biodegradable polymeric nanoparticles are commonly prepared by five different techniques such as emulsification-solvent evaporation, solvent displacement, salting-out, emulsification-solvent diffusion and double emulsion solvent evaporation. The synthesizing methods include salting-out method, it is based on the separation of a water miscible solvent from aqueous solution through the salting out effect, solvent displacement method, phase separation method, evaporation precipitation, antisolvent precipitation and electrospray methods [49]. Other methods have also been developed for the polymer particle size reduction (increase in the surface) to the nanometer size range. For size-reduction, supercritical technology, high pressure homogenization or wet bead milling is frequently used technique to produce reduced size polymer nanoparticle [50].

1.5 Objective and outline of the dissertation

The main objective of this dissertation is concerned with the development of synthesis method to prepare of hollow and porous silica particles using tetramethyl-orthosilicate (TMOS) instead of tetraethyl-orthosilicate (TEOS) as silica source through organic-template assisted wet-chemical process. The use of TMOS rather than more typical TEOS has several potential advantages for practical applications, including fast reaction which enables the use of smaller-

scale equipment and reduced energy cost. The role of polystyrene as a template particle along with hydrolysis/condensation of TMOS in deciding the final silica structure is described. Several synthesis parameters have also been carried out to investigate the effect of particles morphology. The brief descriptions of each chapter are shown below.

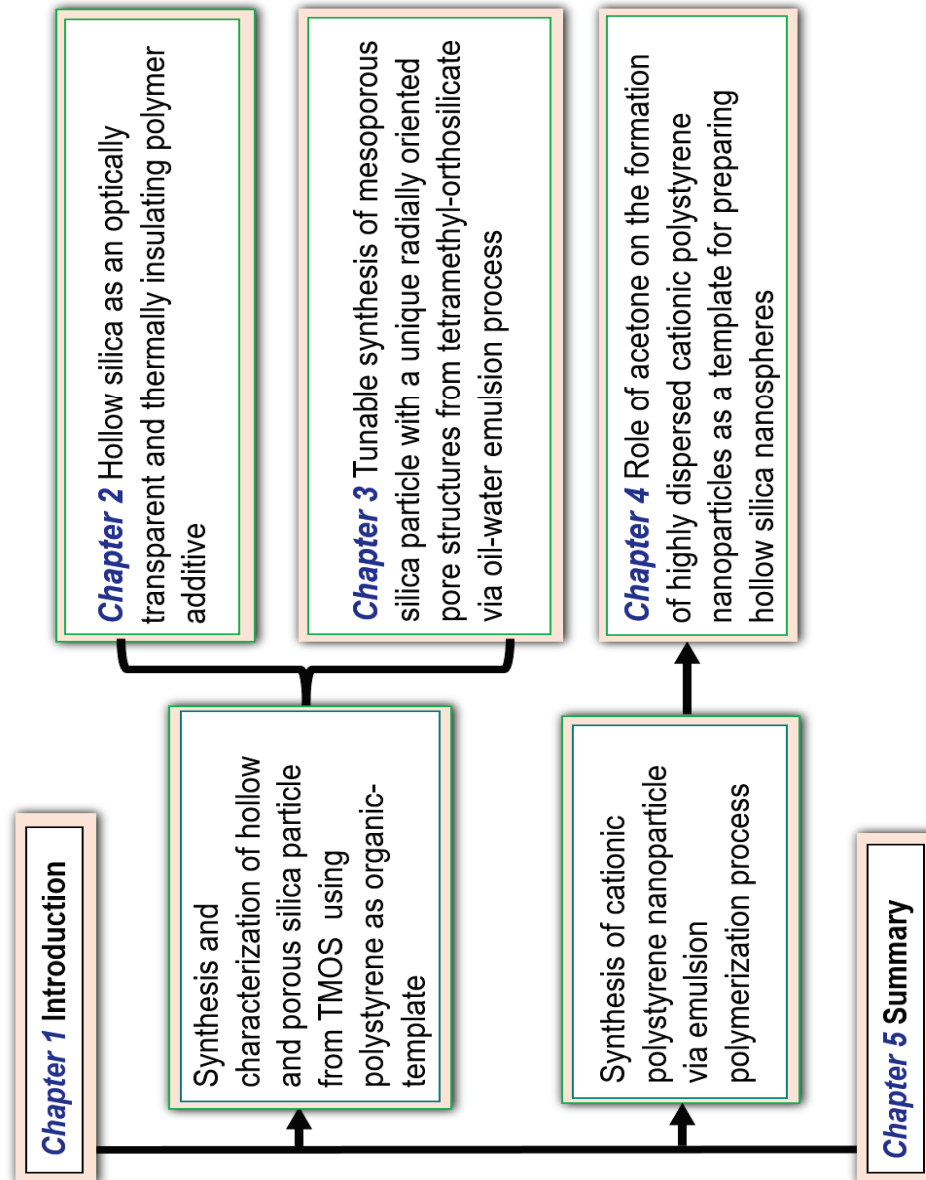


Figure 1.13 Organization and structure of chapters in the present dissertation.

Chapter 1 describes the background and the motivation of the current research. Basic explanation and review of previous researches on the synthesis and application of hollow and porous silica fine particles were also provided.

An improved synthesis route of hollow silica particles using TMOS and their applications as an optically and thermally insulating polymer additive are explained in **Chapter 2**. The results showed that as synthesized particles were successfully implemented into polymer films and permitted maintaining optical transparency while significantly improving the heat

barrier properties of composite film. The shell-thickness of particle was controlled from 6.2 to 17.4 nm by increasing TMOS concentration and the diameter of particle from 95 to 430 nm through use of the different sizes of polystyrene particles. Hollow silica particle with the shell-thickness about 6.2 nm displayed a high light transmittance intensity up to 95%. Polyethersulfone (PES)/hollow silica composite films (35±5 μm thick) exhibited a much lower thermal conductivity (0.03±0.005 W m·K⁻¹) than pure polymer films. The prepared particle has promising for cost and energy effective optical devices requiring thermal insulation.

Chapter 3 describes the synthesis of submicron sized spherical mesoporous silica particles using TMOS via an oil-water (O/W) emulsion process. The results showed that controlling water-surfactant-oil ratios in emulsion system leads to the formation of radially oriented structured of mesoporous silica with high specific surface area (up to 800 m² g⁻¹) and large pore (20 nm) that will be most attractive for applications in catalysis and biomaterials. The characterization of the particles and how their morphology depends on the emulsions formed were detail studied. Additionally, the discussion of proposed mechanisms was also presented.

Chapter 4, a modified emulsion polymerisation synthesis route for preparing highly dispersed cationic polystyrene nanoparticles is described. The combined use of 2,2'-azobis[2-(2-imidazolin-2-yl) propane] di-hydrochloride (VA-044) as the initiator and acetone-water as the solvent medium afforded successful synthesis of cationic PS particles as small as 31 nm in diameter. This study provides important insights and a new methodology for further research and application, especially for synthesis and design of nanostructure materials.

Chapter 5 contains the summary and conclusions of all chapters and direction for further research.

1.6 References

1. E. D. E. R. Hyde, A. Seyfaee, F. Neville, R. Moreno-Atanasio. Colloidal Silica Particle Synthesis and Future Industrial Manufacturing Pathways: A Review, *Ind. Eng. Chem. Res.*, 55(33), 8891-8913, **2016**.
2. C. Drummond, R. McCann, S. V. A. Patwardhan. Feasibility Study of the Biologically Inspired Green Manufacturing of Precipitated Silica. *Chem. Eng. J.* 244, 483-492, **2014**.
3. The Freedonia Group. World Speciality Silicas: Demand and Sales Forecasts, Market Share, Market Size, Market Leaders. *The Freedonia Group: Cleveland*, **2014**.

4. H. K. Schmidt, H. Scholze, A. Kaiser. Principles of hydrolysis and condensation reaction of alkoxy silanes. Part I: Basic investigations on hydrolysis, condensation and densification. *J. Non-Cryst. Solids*, 63, 1-11, **1984**.
5. T. N. M. Bernards, M. J. Van Bommel, A. H. Boonstra. Hydrolysis-condensation processes of the tetra-alkoxy silanes TPOS, TEOS and TMOS in some alcoholic solvents. *J. Non-Cryst. Solids*, 134, 1-13, **1991**.
6. X. Fang, X. Zhao, W. Fang, C. Chen, N. Zheng. Self-templating synthesis of hollow mesoporous silica and their applications in catalysis and drug delivery. *Nanoscale*, 5, 2205-2218, **2013**.
7. Y. Bao, C. Shi, T. Wang, X. Li, J. Ma. Recent progress in hollow silica: Template synthesis, morphologies and applications. *Microporous Mesoporous Mater.*, 227, 121-136, **2016**.
8. H. S. Hwang, J. H. Bae, I. Park, J. M. Park, K. T. Lim. Fabrication of hollow silica particles using copolymeric spheres prepared in supercritical carbon dioxide. *J. Supercrit. Fluids*, 50(3), 292-296, **2009**.
9. M. N. Tan, Y. S. Park. Synthesis of stable hollow silica nanospheres. *J. Ind. Eng. Chem.*, 15(3), 365-369, **2009**.
10. Z. Chen, S. Li, F. Xue, G. Sun, C. Luo, J. Chen, Q. Xu. A simple and efficient route to prepare inorganic hollow microspheres using polymer particles as template in supercritical fluids. *Colloid Surf. A*, 355, 45-52, **2010**.
11. C. Ge, D. Zhang, A. Wang, H. Yin, M. Ren, Y. Liu, T. Jiang, L. Yu. Synthesis of porous hollow silica spheres using polystyrene-methyl acrylic acid latex template at different temperatures. *J. Phys. Chem. Solids*, 70, 1432-1437, **2009**.
12. Z. Deng, M. Chen, S. Zhou, B. You, L. Wu. A Novel Method for the Fabrication of Monodisperse Hollow Silica Spheres. *Langmuir*, 22, 6403-6407, **2006**.
13. H. Fan, Z. Lei, J. H. Pan, X. S. Zhao. Sol-gel synthesis, microstructure and adsorption properties of hollow silica spheres. *Mater Lett.*, 65, 1811-1814, **2011**.
14. H. Hu, H. Zhou, J. Liang, L. An, A. Dai, X. Li, H. Yang, S. Yang, H. Wu, J. Facile synthesis of amino-functionalized hollow silica microspheres and their potential application for ultrasound imaging. *J. Colloid Interf. Sci.*, 358, 392-398, **2011**.
15. H. S. Hwang, S. B. Lee, I. Park. Polyelectrolyte Controlled Large-Scale Synthesis of Hollow Silica Spheres with Tunable Sizes and Wall Thicknesses. *Mater Lett.*, 64, 2159-2162, **2010**.
16. H. Pu, X. Zhang, J. Yuan, Z. Yang. A facile method for the fabrication of vinyl functionalized hollow silica spheres. *J. Colloid Interf. Sci.*, 331, 389-393, **2009**.

17. S. Gai, P. Yang, P. Ma, L. Wang, C. Li, M. Zhang, L. Jun. Uniform and size-tunable mesoporous silica with fibrous morphology for drug delivery. *Dalton Trans.*, 41(15), 4511, **2012**.
18. V. Polshettiwar, D. Cha, X. Zhang, J. M. Basset. High-Surface-Area Silica Nanospheres (KCC-1) with a Fibrous Morphology. *Angew. Chem. Int. Ed.*, 49(50), 9652-9656, **2010**.
19. D. S. Moon, J. K. Lee. Tunable Synthesis of Hierarchical Mesoporous Silica Nanoparticles with Radial Wrinkle Structure. *Langmuir*, 28(33), 12341-12347, **2012**.
20. G. Wei, Y. Liu, X. Zhang, F. Yu, X. Du. Thermal conductivities study on silica aerogel and its composite insulation materials. *Int. J. Heat Mass Transf.*, 54(11-12), 2355-2366, **2011**.
21. D. W. Park, S. E. Shim. A review on thermal conductivity of polymer composites using carbon-based fillers: carbon nanotubes and carbon fibers. *Carbon Lett.*, 11(4), 347-356, **2010**.
22. D. D. L. Chung. Materials for thermal conduction. *Appl. Therm. Eng.*, 21(16), 1593-1605, **2001**.
23. I. A. Tsekmes, R. Kochetov, P. H. F. Morshuis, J. J. Smit. Thermal conductivity of polymeric composites. *IEEE International Conference on Solid Dielectrics*, 678-681, **2013**.
24. Z. Han, A. Fina. Thermal conductivity of carbon nanotubes and their polymer nanocomposites: A Review. *Progr. Polym. Sci.*, 36(7), 914-944, **2011**.
25. Y. Agari, A. Ueda, S. Nagai. Thermal conductivity of a polymer composite. *J. Appl. Polym. Sci.*, 49(9), 1625-1634, **1993**.
26. L. Ernawati, T. Ogi, R. Balgis, K. Okuyama, M. Stucki, S. C. Hess, W. J. Stark. Hollow Silica as an Optically Transparent and Thermally Insulating Polymer Additive. *Langmuir*, 32(1), 338-345, **2016**.
27. X. Du, J. He. Fine-Tuning of Silica Nanosphere Structure by Simple Regulation of the Volume Ratio of Co-solvents. *Langmuir*, 26(12), 10057-10062, **2010**.
28. H. Lin, K. Cui, Y. Yao, Q. Cai, Q. Feng, H. Li. A simple route for preparing radiolarian-like mesoporous silica from water-diethyl ether binary solvent system. *Chem. Lett.*, 34(7), 918-919, **2005**.
29. X. Du, B. Shi, J. Liang, J. Bi, S. Dai, S. Z. Qiao. Developing Functionalized Dendrimer-Like Silica Nanoparticles with Hierarchical Pores as Advanced Delivery Nanocarriers. *Adv. Mater.*, 25(41), 5981-5985, **2013**.
30. K. Zhang, L. L. Xu, J. G. Jiang, N. Calin, K. F. Lam, S. J. Zhang, H. W. Wu, G. D. Wu, B. Albela, L. Bonneviot, P. Wu. Facile Large-Scale Synthesis of Monodisperse Mesoporous

- Silica Nanospheres with Tunable Pore Structure. *J. Am. Chem. Soc.*, 135(7), 2427-2430, **2013**.
31. W. C. Yoo, A. Stein. Solvent Effects on Morphologies of Mesoporous Silica Spheres Prepared by Pseudomorphic Transformations. *Chem. Mater.*, 23(7), 1761-1767, 2011.
32. Y. Zhang, Z. Zhi, T. Jiang, J. Zhang, Z. Wang, S. Wang. Spherical mesoporous silica nanoparticles for loading and release of the poorly water-soluble drug telmisartan. *J. Controlled Release*, 145(3), 257-263, **2010**.
33. H. Zhang, Z. Li, P. Xu, R. Wu, Z. Jiao. A facile two step synthesis of novel chrysanthemum-like mesoporous silica nanoparticles for controlled pyrene release. *Chem. Commun.*, 46(36), 6783, **2010**.
34. A. J. Paula, L. A. Montoro, A. G. S. Filho, O. L. Alves. Towards long-term colloidal stability of silica-based nanocarriers for hydrophobic molecules: beyond the Stöber method. *Chem. Commun.*, 48(4), 591-593, **2012**.
35. S. C. Hess, A. X. Kohll, R. A. Raso, C. M. Schumacher, R. N. Grass, W. J. Stark. Template-Particle Stabilized Bicontinuous Emulsion Yielding Controlled Assembly of Hierarchical High-Flux Filtration Membranes. *ACS Appl. Mater. Interfaces*, 7, 611-617, **2014**.
36. Q. Cai, Y. Geng, X. Zhao, K. Cui, Q. Sun, X. Chen, Q. Feng, H. Li, E. G. Vrieling. Morphological classification of mesoporous silicas synthesized in a binary water-ether solvent system. *Microporous Mesoporous Mater.*, 108 (1-3), 123-135, **2008**.
37. T. Nallamilli, B. P. Binks, E. Mani, M. G. Basavaraj. Stabilization of Pickering Emulsions with Oppositely Charged Latex Particles: Influence of Various Parameters and Particle Arrangement around Droplets. *Langmuir*, 31(41), 11200-11208, **2015**.
38. X. Du, X. Li, H. Huang, J. He, X. Zhang. Dendrimer-like hybrid particles with tunable hierarchical pores. *Nanoscale*. 7(14), 6173-6184, **2015**.
39. H. Yamada, H. Ujiie, C. Urata, E. Yamamoto, Y. Yamauchi, K. Kuroda. A multifunctional role of trialkylbenzenes for the preparation of aqueous colloidal mesostructured-mesoporous silica nanoparticles with controlled pore size, particle diameter, and morphology. *Nanoscale.*, 7(46), 19557-19567, **2015**.
40. P. A. Winsor. Hydrotrophy, solubilisation and related emulsification processes. *Trans. Faraday Soc.* **1948**, 44, 376-398.
41. A. B. D., Nandiyanto, S. G. Kim, F. Iskandar, K. Okuyama. Synthesis of spherical mesoporous silica nanoparticles with nanometer-size controllable pores and outer diameters. *Microporous Mesoporous Mater.*, 120(3), 447-453, **2009**.

42. H. Gustafsson, S. Isaksson, A. Altskar, K. Holmberg. Mesoporous silica nanoparticles with controllable morphology prepared from oil-in-water emulsions. *J. Colloid Interface Sci.*, 467(4), 253-260, **2016**.
43. Z. Liu, H. Xiao, N. Wiseman. Emulsifier-free emulsion copolymerization of styrene with quaternary ammonium cationic monomers. *J. Appl. Polym. Sci.*, 76(7), 1129-1140, **2000**.
44. X. Du, S. Z. Qiao. Dendritic Silica Particles with Center-Radial Pore Channels: Promising Platforms for Catalysis and Biomedical Applications. *Small.*, 11(4), 392-413, **2015**.
45. V. Shubin. Adsorption of cationic polymer onto negatively charged surfaces in the presence of anionic surfactant, *Langmuir*, 10(4), 1093-1100, **1994**.
46. Q. Liu, Y. Li, Y. Duan, H. Zhou. Research progress on the preparation and application of monodisperse cationic polymer latex particles, *Polym. Int.*, 61(11), 1593-1602, **2012**.
47. D. Guerrero, E. Allemann, E. Doelker, H. Fessi. Preparation and Characterization of Nanocapsules from Preformed Polymers by a New Process based on Emulsification-Diffusion Technique. *Pharmaceutical Research*, 15(7) 1056-1062, **1998**.
48. J. C. Leroux, E. Allemann, E. Doelker, R. Gurny. New Approach for the Preparation of Nanoparticles by an Emulsification-Diffusion Method. *European Journal of Pharmaceutics and Biopharmaceutics*, 41(3) 14-18, **1995**.
49. E. Allemann, R. Gurny, E. Doelker. Preparation of Aqueous Polymeric Nanodispersions by a Reversible Salting-Out Process: Influence of Process Parameters on Particle Size. *J. Pharmaceutics*, 87(1-3) 247-253, **1992**.
50. J. W. Tom, P. G. Debenedetti. Particle Formation with Supercritical Fluids-A Review. *J. Aerosol Science*, 22(5) 555-584, **1991**.

Chapter 2

Hollow Silica as an Optically and Thermally Insulating Polymer Additive

2.1 Introduction

Hollow nanostructured particles have been extensively studied as important nanomaterials. Recently, hollow silica particles have attracted great attention due to its unique structural properties and possible applications efficient catalysts, in optical devices, drug delivery carriers, thermal and electrical insulators [1-8]. Among various methods for preparation of hollow silica particles, the templating method offers one of the most attractive and efficient approaches because of convenience and facile access to starting materials [9-14].

Hollow silica is normally prepared in two steps: First, a core-shell (template-silica) structured particle is prepared and followed by removal of the inner template. Several groups have made significant advances to control the size and shell-thickness [15-17], and mainly used tetraethyl-ortho silicate (TEOS) as a starting material [18-20]. Reliable preparation of larger amounts of hollow silica and proper control is difficult due to (i) agglomeration of particles at any step; (ii) irregular shapes as a result of non-uniform silica deposition; (iii) detachment of shell material and/or formation of separated (solid) particles; and (iv) control of the hydrolysis and condensation reaction rate [21-23]. Therefore, the synthesis of hollow silica particle with controllable size and shell-thickness has remained a great challenge for the growth and expansion of industrial applications.

In this chapter, a presumably minor modification of the process to prepare hollow silica particle by switching to the methyl ortho silicate instead of the broadly used ethyl ortho silicate was studied. This apparently simple change, however, has far reaching consequences, both on the hollow silica quality and economics of production. We then investigated the resulting hollow silica as an optically transparent and insulating with polymer additive.

Our motivation to investigate the smaller methyl derivative of silicic acid came

from two observations: The methoxy residue (Me-O-Si) usually hydrolyzes faster than the ethoxy residue (Et-O-Si). Faster reaction rates typically permit use of smaller equipment in production, which significantly reduces costs. Second, in large scale operation, the by-product ethanol (EtOH, from TEOS) or methanol (MeOH; present work, from tetramethyl-ortho silicate, TMOS) would be recycled. The here proposed simple switch from the ethyl to the methyl ester of silicic acid profoundly alters the amount of recycle streams and consequently, energy and equipment costs, as shown in **Table 1**.

Table 2.1 Comparison of the required energy for the distillation of alcohols (MeOH and EtOH) generated from TMOS and TEOS as by-products.

Silica source	Generation of alcohol* (i.e MeOH and EtOH) [kg h ⁻¹]	Reflux ratio	Required energy for alcohol distillation [kJ h ⁻¹]	Difference of required energy [MJ year ⁻¹]
TMOS	2133	0.14	2939	51163
TEOS	3067	2.44	10045	

*Production of 1 ton h⁻¹ of hollow silica particles was assumed in this calculation.

Experimental tests confirmed that the production rate of silica particle from TMOS is about 2 times higher than that of TEOS at the same concentration of TMOS and TEOS (0.08 mol L⁻¹), respectively. This is in line with earlier reported hydrolysis rates of TMOS and TEOS in an ionic liquid [24-26]. Compared to the other tetra-alkoxysilane groups (e.g. propyl, butyl, isopropyl), TMOS has the highest reactivity [27,28]. Unfortunately, a fast reaction is more difficult to control. Synthesis of hollow silica particles by using TMOS as silica precursor and polymeric micelle of poly (styrene-*b*-2-vinylpyridine-*b*-ethylene oxide) as a template has been reported by Nakashima et al. [29]. Different from previous work, here, PS particles are selected as a template for preparing hollow silica particles because of their excellent monodispersity, uniformly, narrow size distribution, and easy preparation [30-34]. MeOH was used as a co-solvent for controlling the hydrolysis and condensation of TMOS. Interestingly, we found that high MeOH concentration could serve as a co-solvent and permitted feasible formation of hollow silica.

2.2 Experimental

2.2.1 Raw materials

Styrene (99%, Kanto-Chemical, Japan) as a monomer and 2,2'-azobiz (2-

methylpropionamide)-dihydrochloride (AIBA, Sigma-Aldrich, US) as an initiator were used to prepare PS particles. Tetramethyl-orthosilicate (TMOS 99%, Sigma-Aldrich, USA) was used as silica source. Ammonia solution (NH₄OH 28%, Kanto Chemical, Japan) was used as a basic catalyst solution for silica formation, and high-purity methanol (MeOH 99.8%, Kanto-Chemical, Japan) as a co-solvent. Polyether-sulfone (PES) (Veradec, A-201) was used as a matrix of silica composite film and dimethylacetamide (DMAc) (Sigma Aldrich, US) was used as a solvent for PES.

2.2.2 Synthesis of PS particle

PS particles were synthesized through free-radical polymerization of the styrene as monomer and AIBA as initiator as described in detail earlier [11,12]. To produce PS particles with different diameter and surface charge, the concentration of styrene and AIBA, and reaction temperature were varied independently. All experimental conditions are summarized in **Table 2.2**.

Table 2.2 Synthesis condition of PS particle with controllable sizes

sample	styrene conc. [wt%]	AIBA conc. [wt%]	reaction time [h]	reaction temp. [°C]	PS size [nm]	zeta potential [mV]
(a)	0.16	0.004	6	90	aggregated	+23.2
(b)	0.20	0.004	6	90	53	+26.9
(c)	0.40	0.004	6	90	79	+31.4
(d)	1.00	0.004	6	80	116	+40.9
(e)	2.00	0.020	6	80	185	+41.5
(f)	4.00	0.040	12	80	377	+47.1

Total amount of precursor solution 250 ml and rotation speed in the reactor at 700 rpm were fixed.

2.2.3 Synthesis of hollow silica particle

At first, the prepared PS particles were mixed with MeOH-water solution as a solvent under vigorous stirring of 400 rpm in a 100 ml two-necked glass reactor system. After 15 min of stirring, TMOS and NH₄OH were added. The reaction was vigorously stirred for 3 h, and the temperature maintained at 35°C. The resultant, silica-coated PS particles, were isolated by centrifugation at 7000 rpm for 5 min then washed by using ethanol. As a last step, calcination at 550°C for 2 h was maintained to remove the PS template and yielded hollow silica particle. Hollow silica particles were then re-dispersed in water prior to characterization. To control the average diameter and shell-thickness of

hollow silica particles, the sizes of PS particles and the concentrations of TMOS were varied from 72 to 380 nm and 0.025 to 0.1 mol L⁻¹, respectively. Here, the molar ratio of NH₄OH/MeOH was kept at 0.065 for all of the prepared samples. Therefore, the molar ratios of NH₄OH/TMOS became varied from 0.068 to 0.017.

2.2.4 Preparation of PES/hollow silica composite film

PES/hollow silica composite film was prepared according to previous work [35], after preparation of a dispersion, film coating and drying. Firstly, 0.05 g of hollow silica particles were mixed in 20 g of dimethyl-acetamide (DMAc) and this solution was mixed by ultrasonic homogenizer with 5 min. 2 g of PES pellet was added to this hollow silica DMAc solution and vigorously stirred for overnight at room temperature. PES/hollow silica composite films were prepared using a spiral film applicator (Zehntner, ZAA-2300, 150 μm spiral). The prepared composite films then were dried in a ventilated oven and kept at 100°C for 10 min to remove the solvent contained.

2.2.5 Characterizations

The size, morphology and distribution of the hollow silica particles were characterized using a scanning-(SEM, Hitachi S-5000, operated at 20 kV, Japan) and a transmission-electron microscopy (TEM, JEM-3000F, JEOL, operated at 300 kV, Japan). The morphology, average diameter and standard deviation of PS particles were obtained using SEM. More than 200 particles ($\Sigma n_i = 200$) were statistically counted from SEM and TEM observations. The functional groups and chemical composition of the prepared samples were identified using Fourier-transform infrared spectroscopy in the range 500-4000 cm⁻¹ (FT-IR, Shimadzu, IR-Affinity-1S, JIS C6802, operated at 150 V, Japan). The surface charge of PS particle was measured using a zeta potential analyzer (Malvern Zetasizer, Nano ZS, UK). Nitrogen adsorption and desorption analysis (BELSORP 28SA, Bel Japan, Japan) was used to determine the specific surface area and pore size. BET analysis was carried out at a relative pressure (P/P_0) of approximately 0.6 to 1 at 77 K, where P_0 is the saturation pressure of N₂. Each of samples was tested at least twice. The optical transmittance properties of hollow silica particles suspension (length of light path~1 cm) were analyzed using a UV-vis spectrophotometer (UV-3150, Shimadzu, Japan). The transmittance spectra of the sample were obtained through the cells prepared by mixture 0.01 g of hollow silica particle in 10 ml of ultra-pure water. All measured

samples were observed in the wavelength region at 300 to 800 nm. The thermal conductivity was measured with two thermocouples and a heat flux sensor (green TEG, g SKIN® KIT-2615C). Top (30°C) and bottom (29.9°C) temperature of the setup were kept constant by two individual water baths. The actual temperature difference was recorded by thermocouples (ΔT , K) and the sensor measured the resulting heat flux (ϕ_q ; $W m^{-2}$) through the sample. The thermal conductivity for the sample (λ_s) was obtained by dividing the layer thickness (d_s) through the difference between the thermal resistance of the setup (R_{setup}) and the measured total thermal resistance (R_m):

$$R_m = \frac{\Delta T}{\phi_q} \quad (1)$$

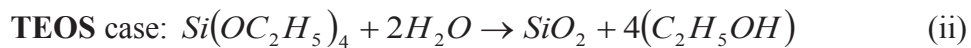
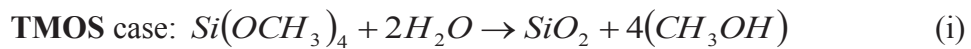
$$\lambda_s = \frac{d_s}{R_m - R_{setup}} \quad (2)$$

Measurements per sample were repeated three times at a steady state period of at least 30 min each.

2.3 Results and discussions

2.3.1 Theoretical calculation of different required energy between TEOS and TMOS as silica source for hollow silica production

To describe the difference of the required energies for the producing of hollow silica particles from TMOS and TEOS, we focused on the energy for the methanol (MeOH) and ethanol (EtOH) distillation, which are generated as by-products of hollow silica as the following overall mechanism of reaction:



To simplify the energy calculation, we made several assumptions: (i) molar enthalpies of vaporizations (latent heats (λ)) assumed to be constant; (ii) the component heat capacity changes and the heat of mixing are negligible compared to the heat of vaporization; (iii) liquid enthalpy (h) and steam enthalpy (H) of each stage are constant; (iv) the distillation column, the condenser and the reboiler are well insulated, so that the heat losses to environment are negligible; (v) the pressure is constant throughout the column, no

pressure drop occurs, and (vi) kinetic and potential energies are negligible. The following target values are taken to solve the energy calculation: (i) the feed liquid fraction is boiling liquid ($q=1$); (ii) the value of typical reflux ratio (R) is 1.5 times of minimum reflux ratio (R_{\min}); (iii) the target concentration of MeOH and EtOH in a distillate product and bottoms product is 95 wt% and 1 wt%, respectively; (iv) 1000 kg/h per unit hollow silica was produced in this system. (v) 1000 kg/h of water was used for the production of the hollow silica particle in this system.

2.3.1.1 Calculation of required energy using TMOS in MeOH-water system

Table 2.3 Properties data of MeOH and water

Properties	MeOH	water
boiling point (K)	338	373
molecular weight (kg kmol^{-1})	32	18
heat of vaporization (kJ mol^{-1})	35.27	40.83

Table 2.4 Overall material balances (MeOH-water system)

feed component	molecular weight [kg kmol^{-1}]	feed composition [wt%]	mass flow rate [kg h^{-1}]	molar feed flow rate [kmol h^{-1}]	mole fraction
MeOH	32	84.2	2133	66.7	0.75
Water	18	15.8	400	22.2	0.25
Total		100	2533	88.9	1.00

Total mass flow rate of feed (MeOH-water) $\rightarrow F = (D + B) = 2533 \text{ kg h}^{-1}$

Mole fraction of feed $\rightarrow x_F = 0.75$

Average molecular weight of feed, $M_F = 28.5$ ($=0.75 \times \text{molecular weight of MeOH} + 0.25 \times \text{molecular weight of water}$)

Table 2.5 Component balances in distillate product (MeOH-water system)

feed component	feed composition [wt %]	mole fraction
MeOH	95	0.1
water	5	0.9
Total	100	1

Average molecular weight of distillate product, $M_D = 30.8$

Table 2.6 Component balances of bottom product (MeOH-water system)

feed component	feed composition [wt %]	mole fraction
MeOH	1	0.006
water	99	0.994
Total	100	1

Average molecular weight of bottom product, $M_w = 18.1$

From the overall mass balances,

The distillate flow rate $\rightarrow D = 2242 \text{ kg h}^{-1} = 73 \text{ kmol h}^{-1}$

The bottoms flow rate $\rightarrow W = 290 \text{ kg h}^{-1} = 16 \text{ kmol h}^{-1}$

Table 2.7 Overall component balances (MeOH-water system)

product component	molar flow rate [kmol h ⁻¹]	average molecular weight g mol ⁻¹	MeOH		
			[kg y ⁻¹]	[wt%]	mole fraction
F	88.9	28.5	2133	84.2	0.75
D	72.8	30.8	2130	95.0	0.91
W	16.1	18.1	2.9	1.0	0.006

Most of the distillation columns are designed to operate between 1.2 and 1.5 times of the minimum reflux ratio, because this is approximately value of minimum operating cost.

The operating reflux ratio can be expressed as the following:

$$R_{actual} = 1.5R_{min}$$

The value of minimum reflux ratio (R_{min}) can be approximated by using *McCabe Thiele* method, as shown in the **Figure 2.1**.

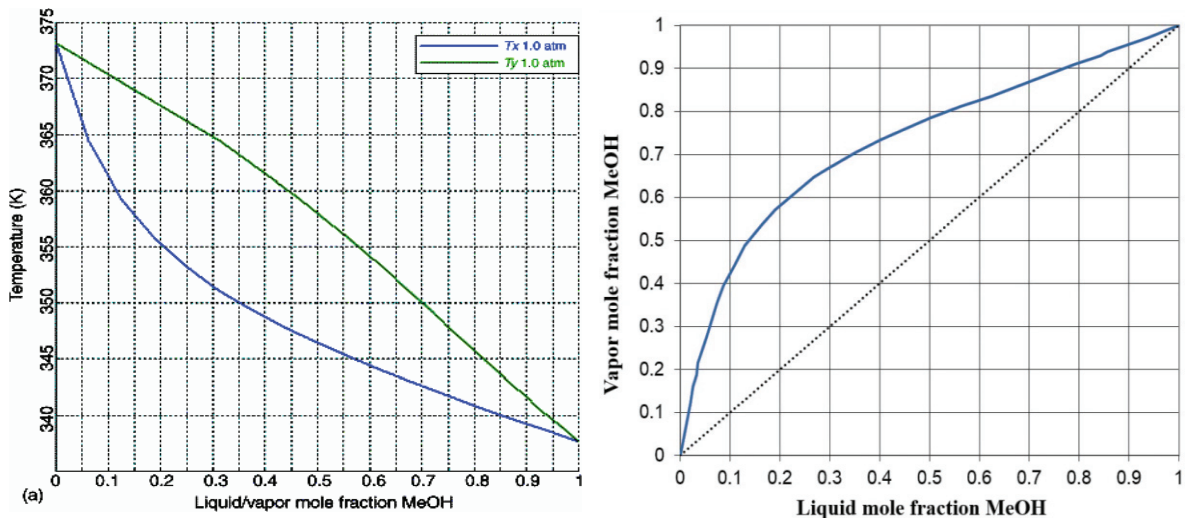


Figure 2.1 Vapor-liquid equilibrium phase-diagram: (a) T-xy plot for MeOH-water, and (b) xy plot diagram for MeOH-water (*Copyright: 2006 John Wiley & Sons, Inc.*).

From the **Figure 2.1**, the value of R_m was measured from the slope, as the following equation:

$$R_m = \frac{x_D - y_F}{y_F - x_F} = \frac{0.91 - 0.90}{0.90 - 0.75} = 0.096$$

Then, the value of R is equal to $\rightarrow R_{actual} = 1.5 R_{min} = 1.5 * 0.096 = 0.14$.

The heat energy that is lost in the condenser can be calculated as:

$$Q_C = \lambda(1 + R)D \rightarrow Q_C = 35.27 \text{ kJ mol}^{-1} * (1 + 0.14) * 72.8 \text{ kmol h}^{-1} = 2939 \text{ kJ h}^{-1}$$

From $Q_C = Q_B$, the heat energy that given by reboiler is also **2939 kJ h⁻¹**

2.3.1.2 Calculation of required energy using TEOS in EtOH-water system

Table 2.8 Properties data of EtOH and water

Properties	EtOH	Water
boiling point (K)	352	373
molecular weight (kgkmol ⁻¹)	46	18
heat of vaporization (kJ mol ⁻¹)	38.6	40.83

Table 2.9 Overall material balance (EtOH-water system)

feed component	molecular weight [kg kmol ⁻¹]	feed composition [wt %]	mass flow rate [kg h ⁻¹]	molar feed flow rate [kmol h ⁻¹]	mole fraction
EtOH	46	88.5	3067	66.7	0.75
Water	18	11.5	400	22.2	0.25
Total		100	3467	88.9	1.00

Total mass flow rate of feed (EtOH-water) $\rightarrow F = (D + B) = 3467 \text{ kg h}^{-1}$

Mole fraction of feed $\rightarrow x_F = 0.75$

Average molecular weight of feed, $M_F = 39.0$

Table 2.10 Component balances in the distillate product (EtOH-water system)

feed component	feed composition [wt %]	mole fraction
EtOH	95	0.88
water	5	0.12
Total	100	1

Average molecular weight of distillate product, $M_D = 42.7$

Table 2.11 Component balances of bottom product (EtOH-water system)

feed component	feed composition [wt %]	mole fraction
EtOH	1	0.004
water	99	0.996
Total	100	1

Average molecular weight of bottom product, $M_w = 18.1$

From the overall mass balances,

The distillate flow rate $\rightarrow D = 3226 \text{ kg h}^{-1} = 75.6 \text{ kmol h}^{-1}$

The bottoms flow rate $\rightarrow W = 241 \text{ kg h}^{-1} = 13.3 \text{ kmol h}^{-1}$

Table 2.12 Overall component balances (EtOH-water system)

product component	molar flow rate [kmol h ⁻¹]	average molecular weight g mol ⁻¹	EtOH composition		
			[kg y ⁻¹]	[wt %]	mole fraction
F	88.9	39.0	3067	88.5	0.75
D	75.6	42.7	3064	95.0	0.88
W	13.3	18.1	2.4	1.0	0.004

The operating reflux ratio can be expressed as the following:

$$R_{actual} = 1.5R_{min}$$

The value of minimum reflux ratio (R_{min}) can be approximated by using *McCabe Thiele* method, as shown in the **Figure 2.2**.

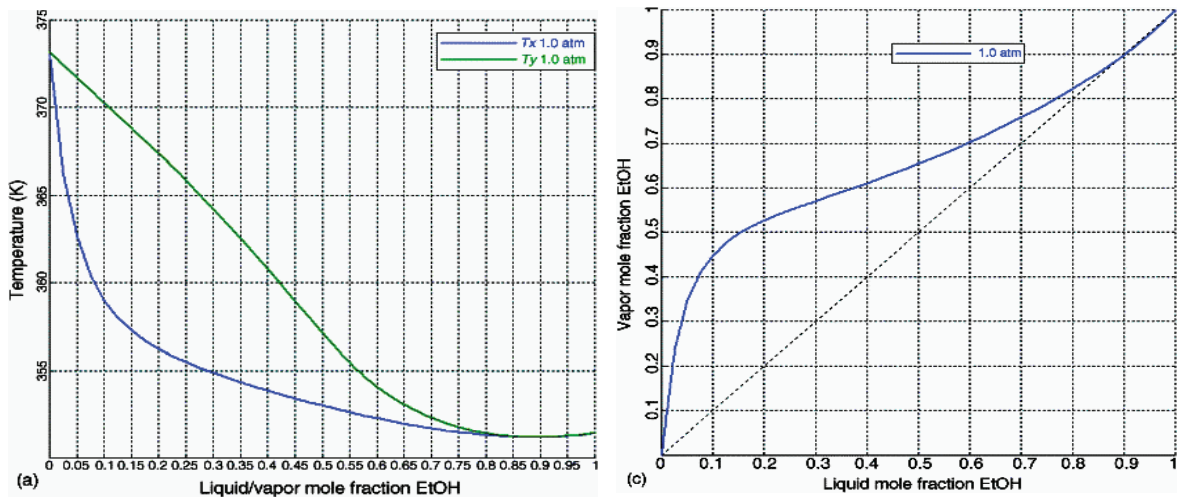


Figure 2.2 Vapor-liquid equilibrium phase-diagram: (a) T-xy plot for EtOH-water, and (b) xy plot diagram for EtOH-water. (Copyright: 2006 John Wiley & Sons, Inc.).

From the **Figure 2.2**, the value of R_m was measured from the slope, as the following equation:

$$R_m = \frac{x_D - y_F}{y_F - x_F} = \frac{0.88 - 0.80}{0.80 - 0.75} = 1.629$$

Then, the value of R is equal to $\rightarrow R_{actual} = 1.5R_{min} = 1.5 * 1.629 = 2.44$

The heat energy that is lost in the condenser:

$$Q_C = \lambda(1 + R)D \rightarrow Q_C = 38.6 \text{ kJ mol}^{-1} * (1 + 2.44) * 75.6 \text{ kmol y}^{-1} = \mathbf{10045 \text{ kJ h}^{-1}}$$

From $Q_C = Q_B$, the heat energy that given by reboiler is also $\mathbf{10045 \text{ kJ h}^{-1}}$.

From the calculation above, the difference of required energy between TEOS and TMOS is around 52000 MJ y^{-1} ($= (10045 - 2939) * 24 \text{ hour} * 300 \text{ days}$). The results show that the heat loss energy ($Q_C = Q_B$) corresponding to the total required energy of TEOS is higher when compared with TMOS. By considering of economically point of view and also in terms of production cost, it can be concluded that TMOS offers the significant advantages over existing alternatives including lower cost to produce hollow silica particle and improve the benefits from the process.

2.3.2 Polystyrene particle with controllable sizes

SEM images of PS particle with different sizes were shown in **Figure 2.3**.

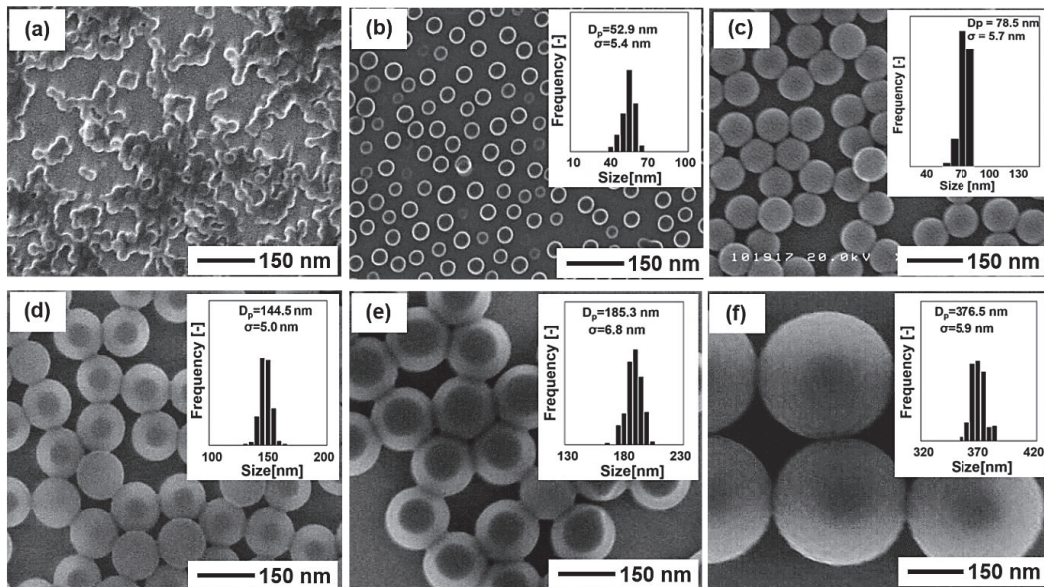


Figure 2.3 SEM images of polystyrene (PS) particles produced at different temperature, and styrene/AIBA concentration: (a-c) at 90°C, using (a) 0.16/0.004, (b) 0.2/0.004, and (c) 0.4/0.004 (wt%); (d-f) at 80°C, using (d) 1.0/0.004, (e) 2.0/0.002, and (f) 4.0/0.004 (wt%), respectively. Detail synthesis condition was summarized in **Table 2.2**.

No formation of spherical PS particles observed at a combination of very low styrene concentration (i.e. 0.16 wt%) and high reaction temperature (90°C) (**Figure 2.3 (a)**). PS particles with an average diameter of 53 and 79 nm were obtained using styrene concentration of 0.2 and 0.4 wt% (constant AIBA concentration of 0.004 wt%, temperature at 90°C (see **Figure 2.3 (b and c)**). The size of PS particle was also increased from 145 to 185 nm when higher styrene concentration was used (1.0 and 2.0 wt%; temperature at 80°C, **Figure 2.3 (d and e)**). Larger PS particle with an average diameter of 380 nm were obtained at very high styrene concentration (i.e. 4.0 wt%), but lower reaction temperature (45°C), as shown in **Figure 2.3 (f)**. Monodispersed PS particles with relatively spherical shape were obtained for most cases. The size and zeta potential values of all prepared PS particles are shown in **Table 2.2**.

2.3.3 Effect of MeOH concentration on the formation of hollow silica

The effect of MeOH concentration on the nucleation rate of TMOS was shown in **Figure 2.4**.

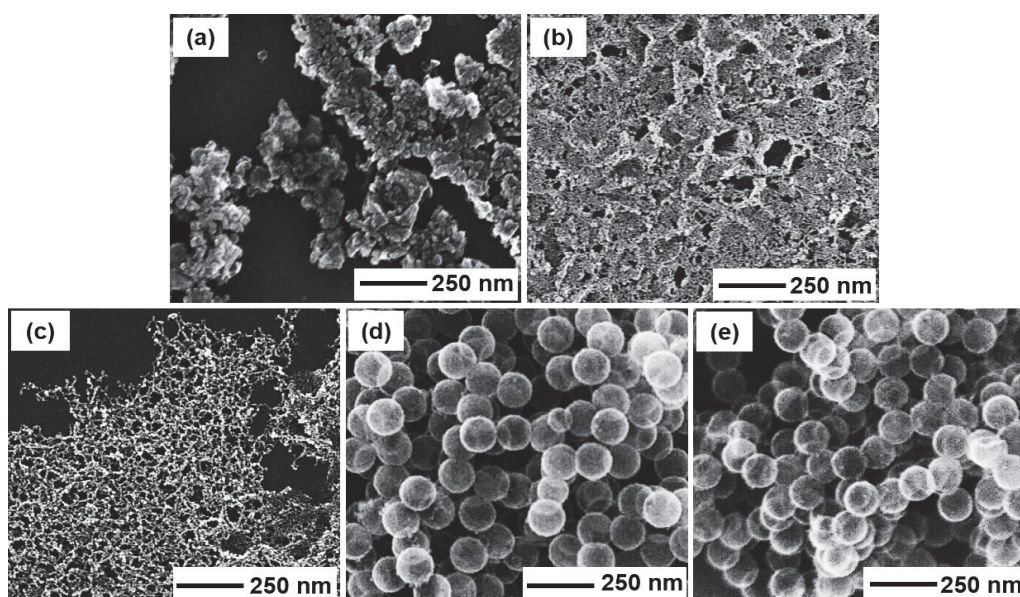


Figure 2.4 SEM images of the prepared hollow silica particles with different MeOH concentrations: (a) 0, (b) 30, (c) 50, (d) 75, and (e) 90 wt%. All the samples were prepared using PS particles of 116 nm in size. Hydrolysis of TMOS under various MeOH concentrations: At low concentration of MeOH, irregular gels and networks of particles are formed, (a-c). At higher concentration of MeOH, polystyrene template particles could

be reliably coated with silica, (d, e).

Highly agglomerated silica particles were observed from the sample prepared without MeOH as shown in **Figure 2.4 (a)**. Here, obviously, TMOS hydrolyzed fast, and intermediately formed Si-OH rapidly continuous reacting. As a result, a high nucleation occurred, so a lot of small, nm-size of silica particles are generated in a short period of time and grow into a large particle. Meanwhile, at a low MeOH concentration (30 and 50 wt%), homogeneous nucleation tends to occur rapidly and leads to the formation of aggregated silica particles (**Figure 2.4 (b and c)**). It might be due to the fast formation of primary silica particles which are electrostatically unstable in water. Interestingly, **Figure 2.4 (d and e)** shows that hollow silica particles were successfully produced at high MeOH concentrations of 75 and 90 wt%, respectively. Here, the formation of Si-OH and nucleation of new silica is sufficiently suppressed. All silica now deposits onto the polymer particles. The hydrolysis and condensation mechanism of TMOS in MeOH-water is illustrated in the **Figure 2.5**.

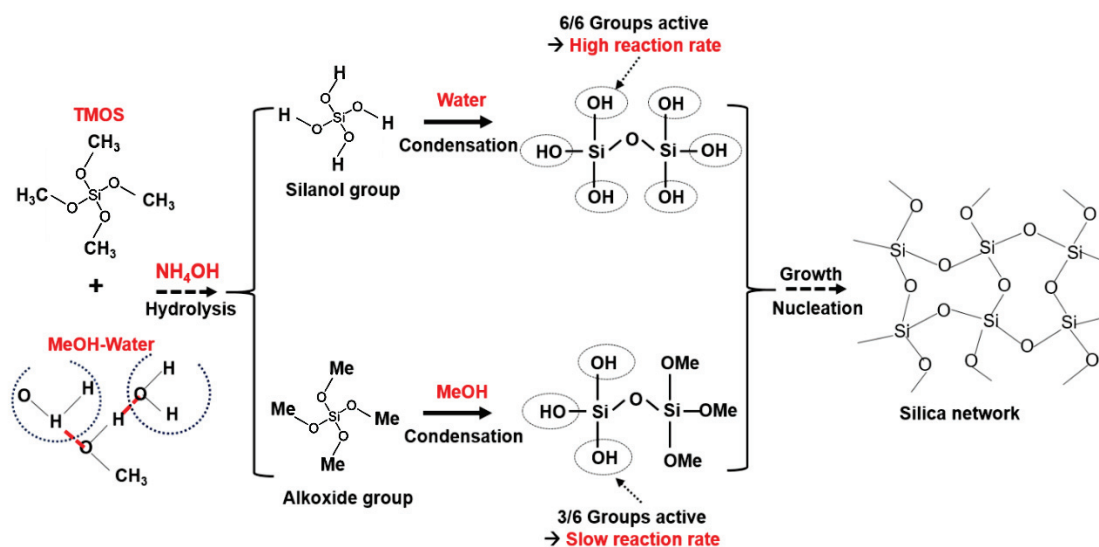


Figure 2.5 Hydrolysis and condensation of TMOS in MeOH-water system. The addition of MeOH or presence of partially hydrolyzed methoxy-silane species (bottom) slow down the overall condensation to silica (right) as $\text{CH}_3\text{-O-Si}$ is less reactive than Si-O-H . The amount of MeOH can be used to control the condensation rate of TMOS for controlled deposition of silica onto a template.

The hydrolysis reaction rate of TMOS is only fast in pure water, generating large numbers of very small silica particles in a short period of time. These very small silica

particles become abundant collide and form highly agglomerated silica particles. The addition of a relatively low concentration of MeOH (i.e. 30 and 50 wt%) reduced the hydrolysis rate of TMOS. In this condition, silica particles growth better and surface growth now completes with nucleation of new silica particles. These primary particles eventually form interconnected silica network structures consisting of large aggregates. The hydrolysis reaction rate of TMOS decreases further when the MeOH concentration was increased up to 75 wt%. Here, MeOH easy substitutes the Si-OH group of hydrolyzing TMOS. The hydrolysis reaction rate of TMOS was even slower at 90 wt% of MeOH concentration where we experimentally observe the formation of PS-silica in the form of core-shell structured particle. While, the deposition as a function of MeOH concentration can be shown in **Figure 2.6**.

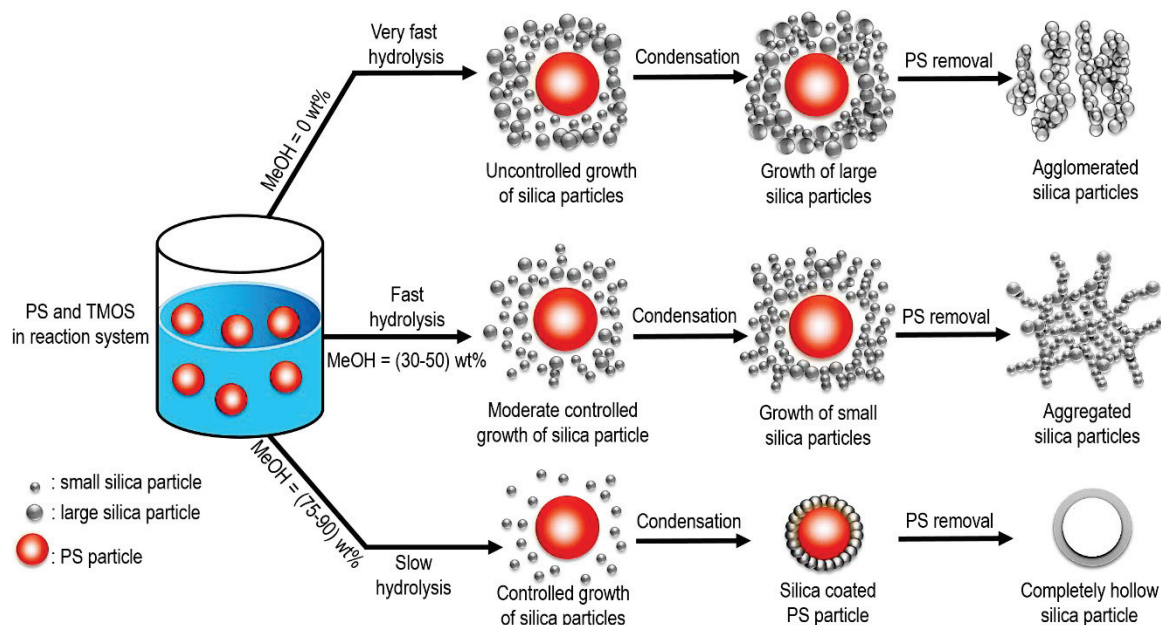


Figure 2.6 Hollow silica is only formed at higher MeOH concentration (bottom) when the reaction rate is sufficiently low to suppress excessive nucleation (formation of free floating, new particles, (top)) and favoring deposition of silica onto surfaces or previously deposited silica nuclei on PS template surfaces. Here, surface growth fills the gaps between the porous shells and eventually leads to solid layers of silica (bottom).

Furthermore, the composite nature of the particles and of the ability to remove the PS phase was provided by FT-IR spectra (the details are given in **Figure 2.7**).

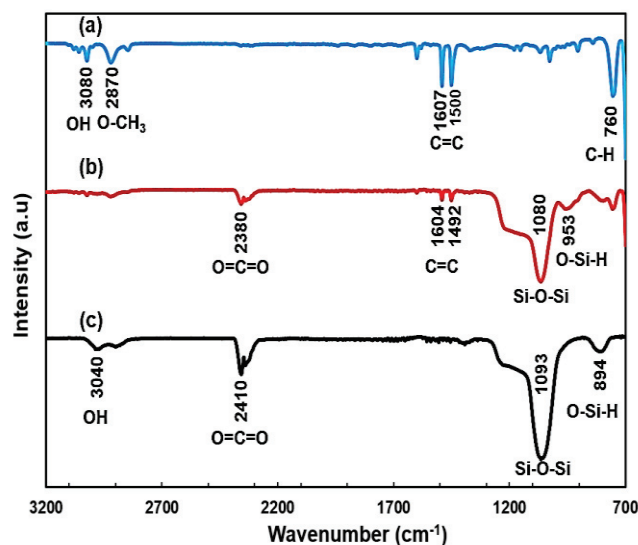


Figure 2.7 Fourier transform-infrared (FT-IR) spectra illustrate how the methoxy species (2870 cm^{-1}) and benzene ring of PS (760 , 1500 , 1607 cm^{-1}) vanish during the reaction, and lead to the formation of silica (Si-O-Si bonds at 1080 and 1093 cm^{-1}): (a) pure PS template particles, (b) silica-coated PS particle before template removal, and (c) hollow silica particle.

The typical pure PS particle absorption bands are observed at 760 cm^{-1} , 1500 - 1670 cm^{-1} , and 2870 - 3080 cm^{-1} , as shown in **Figure 2.7 (a)**. The broad bands at 3080 and 2870 cm^{-1} represent absorption of hydroxyl group (OH) and methoxy groups (O-CH_3), respectively. Two absorption bands at 1500 and 1607 cm^{-1} are corresponding to C=C stretching vibrations and the band at 760 cm^{-1} is assigned to C-H bonding vibration of benzene ring of PS [39, 40]. For the silica-coated PS particle (**Figure 2.7 (b)**), the absorption bands assigned to Si-O-Si stretching vibration appeared at 1080 cm^{-1} , revealing that silica particle were successfully coated on the surface of PS template. Furthermore, two bands at 894 and 1093 cm^{-1} corresponding to O-Si-H and Si-O-Si groups [41], appeared in the FT-IR spectra of the hollow silica particle, as shown in **Figure 2.7 (c)**. The absorption bands of the PS template disappeared in the FTIR spectra for hollow silica particle, indicating that PS template were removed by calcination. Two absorption bands at 2380 and 2410 cm^{-1} appeared in the FT-IR spectra of silica-coated PS particle and hollow silica, respectively, are assigned to O=C=O bonds [42].

2.3.4 Effect of PS particle size on the outer diameter of hollow silica

The size of hollow silica particles can be controlled by changing the size of PS particles, as shown in SEM and TEM images of **Figure 2.8**. Detail experimental conditions were given in **Table 2.13**.

Table 2.13 Synthesis condition of hollow silica particle prepared under various PS particle sizes

PS size [nm]	PS conc. [mg mL ⁻¹]	TMOS conc. [mg mL ⁻¹]	MeOH conc. [mg mL ⁻¹]	Hollow size [nm]
72	0.38	12.4	0.88	95
116	0.57	12.4	0.86	126
185	0.85	12.4	0.86	181
380	0.91	12.4	0.91	393
430	0.91	12.4	0.91	428

- total amount of precursor solution is 81 mL, NH₄OH concentration 0.06 mg mL⁻¹.
- Reaction temperature at 35°C, reaction time 285 min.
- The rate of TMOS addition is 0.05 mL 15 min⁻¹, all were fixed.

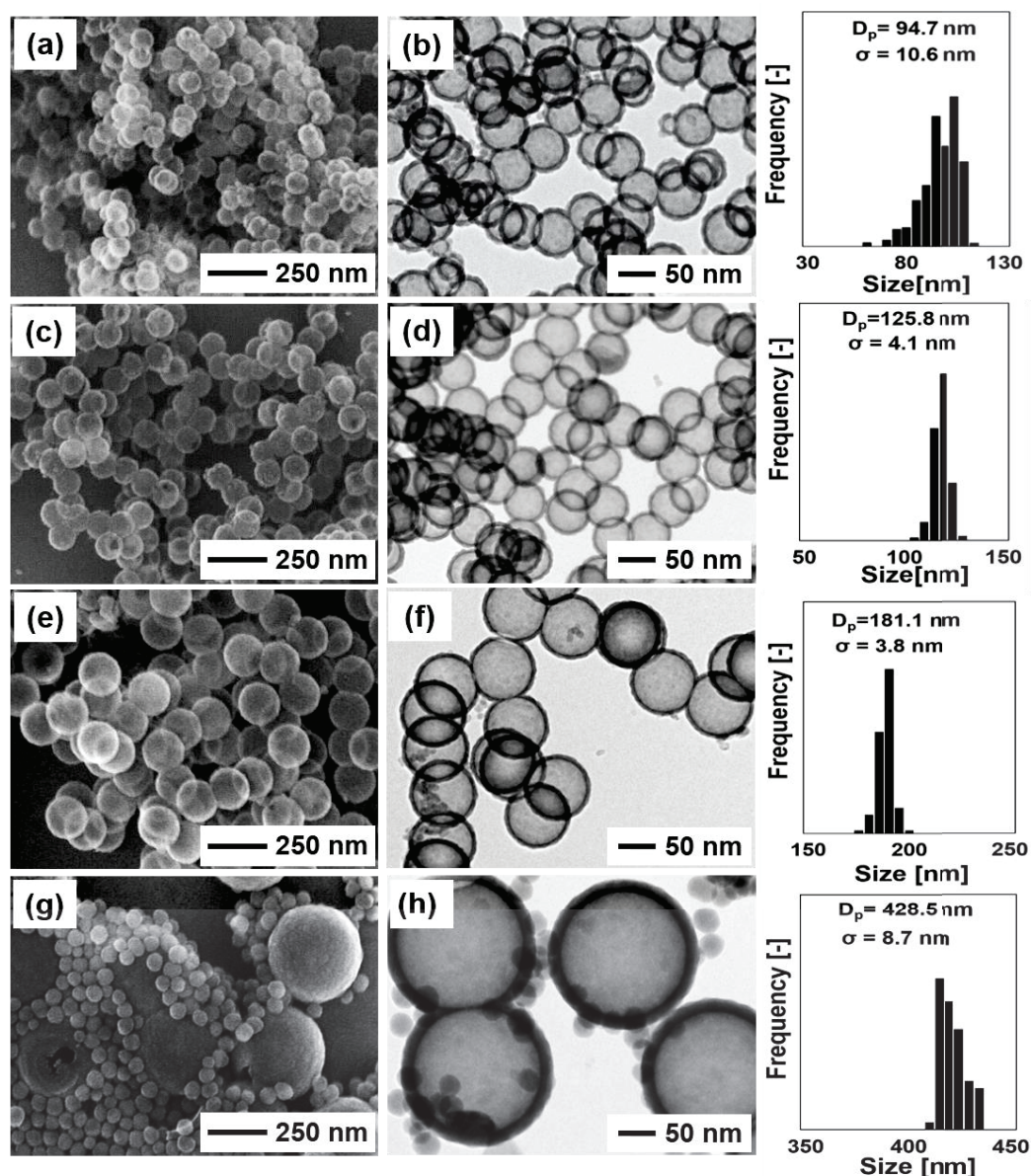


Figure 2.8 SEM and TEM images of hollow silica particles prepared with different PS diameter of: (a, b) 72, (c,d) 116, (e, f) 185, and (g, h) 380 nm. The molar ratio of $\text{NH}_4\text{OH}/\text{MeOH}$ and TMOS concentration were kept at 0.065 and 0.08 molL^{-1} , respectively. The coating process works well up to 180 nm. At 380 nm in size, homogeneous nucleation (i.e. independent of the template) leads to a second population of small particles (bottom) of 20 to 40 nm in size.

Average diameters of hollow silica particle rapidly increased from 95 to 430 nm along with increase in PS particle sizes from 72 to 380 nm. Surprisingly, small silica particles are found in even larger samples (i.e. hollow silica particle with an average

diameter of 430 nm), as shown in **Figure 2.8 (g and h)**. Here, the rapid homogeneous nucleation of free silica nanoparticles was higher than the capture rate of these large PS particles. The ratio of hollow and small silica particles was statistically calculated by

$\left(\frac{\sum_{i=1}^{i=k} n_{iH}}{n_{iS}} = 0.72 \right)$, where n_{iH} and n_{iS} are the counted number of hollow and small particles, respectively.

2.3.5 Effect of TMOS concentration on the shell-thickness of hollow silica

Hollow silica particles with different shell-thickness can be obtained by varying the concentrations of TMOS, as shown in **Figure 2.9 (a-j)** and **Table 2.14**.

Table 2.14 Synthesis condition of hollow silica particles prepared under various TMOS concentrations.

PS size	PS conc.	volume of TMOS addition	TMOS conc.	hollow shell-thickness
[nm]	[mg ml ⁻¹]	[ml]	[mol L ⁻¹]	[nm]
185	0.85	0.3	0.025	6.2
185	0.85	0.5	0.04	7.1
185	0.85	0.75	0.06	10.7
185	0.85	1.00	0.08	13.2
185	0.85	1.5	0.10	17.4

Total amount of precursor solution 81 ml, MeOH concentration 0.87 ml/ml, NH₄OH concentration 0.06 mg/ml, reaction temperature at 35°C, reaction time 285 min (the rate of TMOS addition is 0.05 ml/15 min), all were fixed.

The shell thickness of hollow silica particle increased from 6.2 to 17.4 nm as initial concentrations of TMOS increased from 0.025 to 0.1 mol L⁻¹. This means that the shell-thickness of hollow silica particles can be controlled within a certain range.

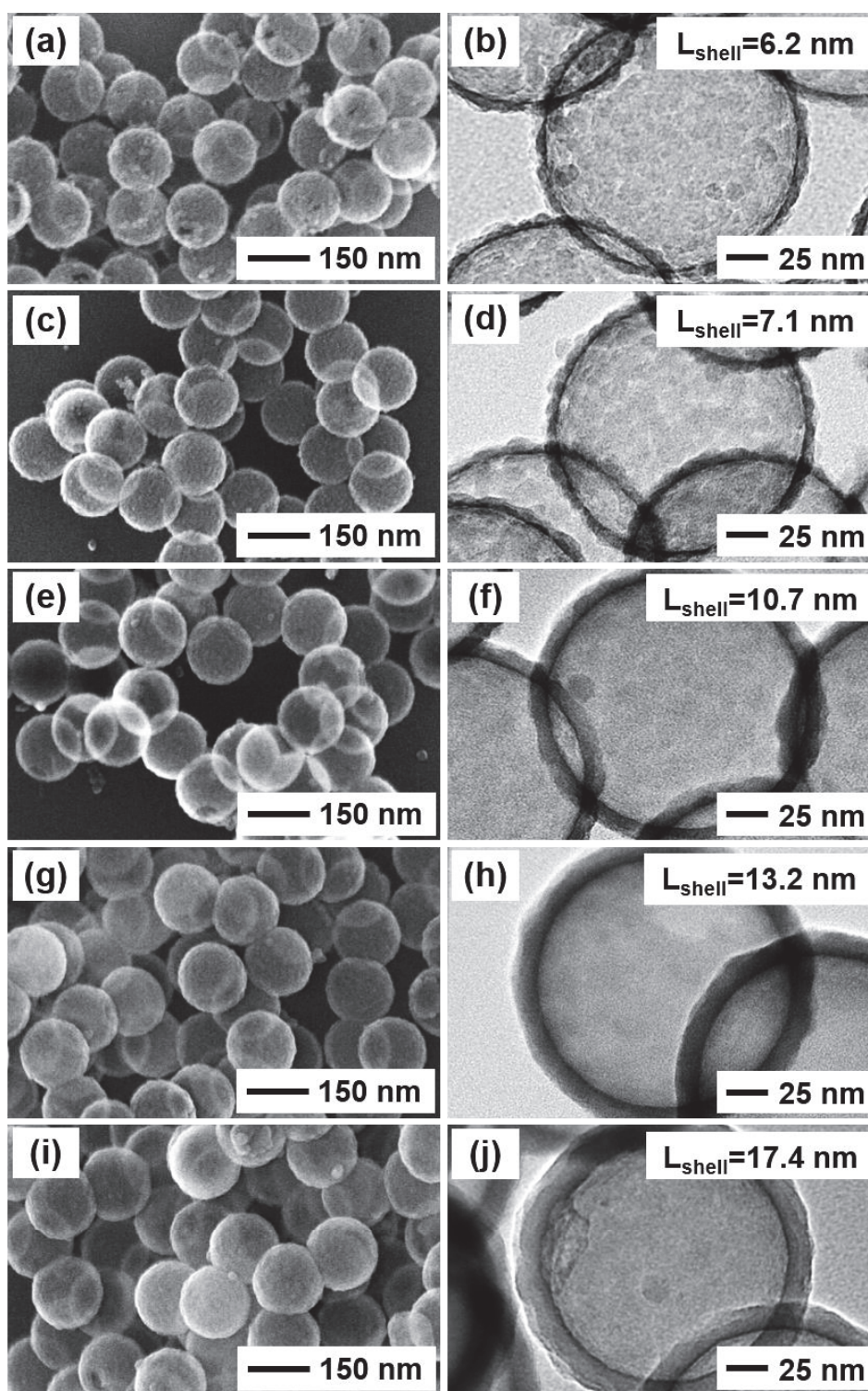


Figure 2.9 The coating formation process becomes visible when using TEM (right side) instead of SEM for increasing shell-thickness. Hollow silica particles were prepared under various TMOS concentrations: (a, b) 0.025, (c, d) 0.04, (e, f) 0.06, (g, h) 0.08, and

(i, j) 0.1 mol L^{-1} . Thin shells (top) appear grainy because of the growth of silica, where first a layer of small silica particles is deposited, and subsequently grows together through surface growth, (i.e. direct deposition of silica onto previously formed silica surfaces (bottom)).

To describe the correlation between an initial TMOS concentration and shell thickness (L) of hollow silica particle, the simple geometry model of the formation of hollow silica particle in core-shell structure are used as shown in **Figure 2.10**. The derivation of equation for the shell-thickness of hollow silica particle, we made several assumptions: (i) the density of the silica shell in all case was same; (ii) a certain volume of TMOS (V_{TMOS}) reacted to produce a certain volume of silica (V_{SiO_2}) uniformly, through the silica shell; (iii) all of TMOS are converted to be silica particles (no agglomerated or free silica particles are produced); (iv) PS particles are covered by silica homogenously; (v) no dissolution of PS particle. The particle composition and amount of silica can be calculated from the diameter and shell.

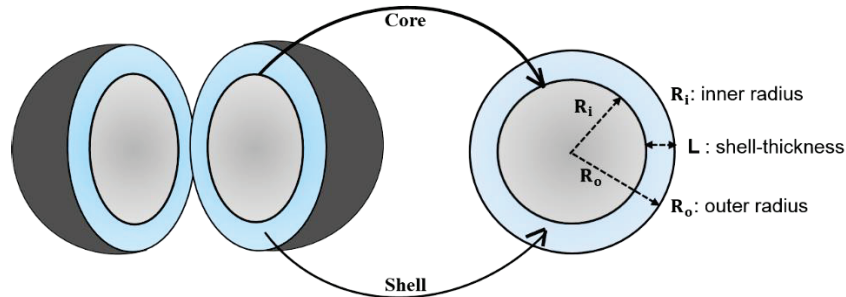


Figure 2.10 Schematic illustration of the geometry of hollow silica sphere

From the **Figure 2.10**, the calculation of shell thickness (L) is given by the following expression:

$$L = R_o - R_i \quad (1)$$

By assuming that the hollow silica particle is produced as spherical particle, a total volume of core-shell structure ($V_{core-shell}$) can be derived as the following equation:

$$V_{core-shell} = V_{core} + V_{shell} \quad (2)$$

With $V_{core-shell} = \frac{4}{3}\pi R_o^3$ and $V_{core} = \frac{4}{3}\pi R_i^3$, where, R_i and R_o is an inner and outer radius of the prepared hollow silica particle, respectively). Thus, the $V_{core-shell}$ can be described as the following equation:

$$V_{core-shell} = \frac{4}{3}\pi R_o^3 = \frac{4}{3}\pi R_i^3 + V_{shell} \quad (3)$$

$$R_o = \frac{3}{4\pi} \left(\frac{4\pi}{3} R_i^3 + V_{shell} \right)^{\frac{1}{3}} \quad (4)$$

R_i and R_o radius of the prepared hollow silica particle are measured from TEM results. Since volume of the shell (V_{shell}) represent of the formation of silica particle coated on the surface of PS particle as a core, it can be expressed as:

$$V_{shell} = \frac{[SiO_2]Mw_{SiO_2}V_{solution}}{\rho_{SiO_2}N} \quad (5)$$

Where $[SiO_2]$ is the concentration of silica, Mw_{SiO_2} is the molecular weight of SiO_2 , and ρ_{SiO_2} is the density of silica. Meanwhile, the number of PS particle (N) can be obtained from the mass ratio of the total mass of PS particle in the precursor and the mass of the single PS particle (calculated by multiplying the volume from the measurement of diameter in the SEM image and the density of PS particle (1.05 g/cm³)). By combining the Eq. (4), (5) and (6), the shell thickness of hollow silica particle (L) can be derived as the following equation:

$$L = \left[\frac{3}{4\pi} \left(\frac{4\pi}{3} R_i^3 + \frac{[SiO_2]Mw_{SiO_2}V_{solution}}{\rho_{SiO_2}N} \right) \right]^{\frac{1}{3}} - R_i \quad (6)$$

To derive the $[SiO_2]$, we focus on the hydrolysis and condensation reaction of TMOS. The hydrolysis reaction rate of TMOS is expected to be proportional to its concentration $[TMOS]$ and hydroxyl ion concentration $[OH^-]$ in the solution, as shown in the following equation:

$$-\frac{d[TMOS]}{dt} = C_h[OH^-][TMOS] \quad (7)$$

Where C_h is the hydrolysis rate constant of TMOS is equal to 0.21 m³mol⁻¹.s⁻¹. This value was determined by fitting Eq. (8) to the experimental of TMOS concentration curves [42, 43]. A $[OH^-]$ is calculated by using:

$$[OH^-] = \sqrt{K_b[NH_4OH]} \quad (8)$$

K_b is the association constant of a weak base of ammonium hydroxide ($pK_b = 5.43$ in methanol-water system) [10]. Since the concentration of ammonium hydroxide $[NH_4OH]$ is constant, the integration of Eq. (8) from initial ($t=0$) to reaction time of ($t=t$) gives the following equation:

$$\int_{[TMOS]_0}^{[TMOS]_t} \frac{d[TMOS]}{[TMOS]} = \ln \frac{[TMOS]}{[TMOS]_0} = -C_h[OH^-] \int_0^t dt \quad (9)$$

$[TMOS]_0$ is the initial concentrations of TMOS at $t=0$ and $[TMOS]$ is the concentration of the TMOS after certain time, respectively. From the Eq. (10), the concentration of the generated silica particle $[SiO_2]$ can be obtained by the following equation:

$$[SiO_2] = [TMOS]_0(1 - \exp(-C_h[OH^-]t)) \quad (10)$$

Since, the concentration of the generated silica $[SiO_2]$ can be solved by following Eq. (11), the equation of the shell-thickness is given by:

$$L = \left[R_i^3 + \frac{3}{4\pi} \left(\frac{[TMOS]_0(1 - \exp(-C_h[OH^-]t))MW_{SiO_2}V_{solution}}{\rho_{SiO_2}N} \right) \right]^{\frac{1}{3}} - R_i \quad (11)$$

Where, R_i is an inner radius of the prepared hollow silica particle, C_h is a hydrolysis rate constant of TMOS, $[OH^-]$ is a hydroxyl ion concentration in the solution, t is a reaction time, $V_{solution}$ is total volume of precursor solution, MW_{SiO_2} and ρ_{SiO_2} are a molecular weight and a density of silica, respectively, and N is number of PS particle.

The experimental results shown are in a good agreement with the theoretical analysis method, as shown in **Figure 2.11 (a)**. These simplified results to make quick prediction of shell-thickness of hollow silica particles. It indicates that this method is greatly valid to estimate the shell-thickness of a thin and thick spherical shell of the prepared hollow silica particles.

2.3.6 Surface area and pore properties of hollow silica

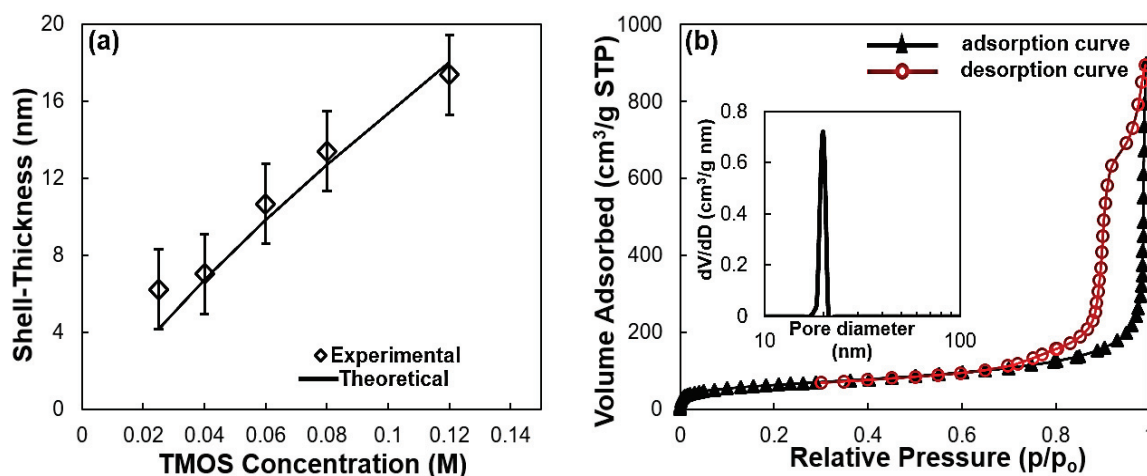


Figure 2.11 (a) Shell-thickness of hollow silica particles can be controlled by changing TMOS concentrations. The layer thickness measured from TEM images well matches with the theoretical values when assuming even distribution of the silica on the surface of PS particle, and (b) Nitrogen (N₂) adsorption-desorption isotherms and BJH pore size distribution plots of hollow silica with 6.2 nm in shell-thickness. Adsorption and desorption volumes show a significant hysteresis, typical for the presence of large cavities in a material.

Representative nitrogen adsorption-desorption isotherms and the corresponding pore volume and size distribution of the hollow silica particles with 6.2 nm in shell-thickness was shown in **Figure 2.11 (b)**. Hollow silica samples with different shell-thickness 13.2 and 7.1 nm were also prepared. The specific surface area of the hollow silica particles was obtained to be 90 m² g⁻¹, when the TMOS concentration of 0.08 mol L⁻¹ was used. In addition, along with the increasing of TMOS concentration 0.04 to 0.025 mol L⁻¹, the specific surface area of hollow silica was increased to 203 m² g⁻¹ and 215 m² g⁻¹, respectively. The pore volume and pore size also increased from 0.45 to 1.25 cm³ g⁻¹ and 19 to 23 nm with decreasing TMOS concentrations. The large pores were obtained due to the formation of voids between the shells of particles.

2.3.7 Optical properties of the prepared hollow silica particle

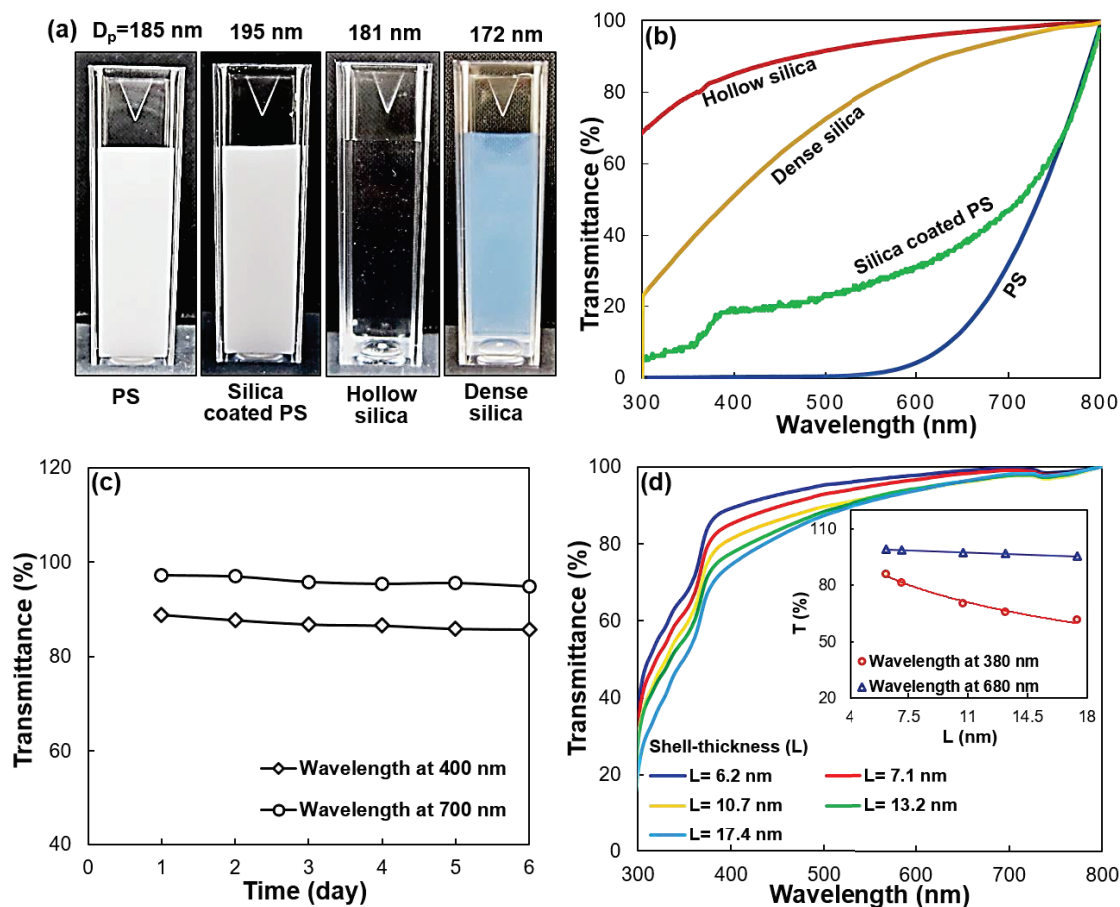


Figure 2.12 (a) Hollow silica is nearly fully transparent and stable over weeks in dispersion. For the comparison, photograph of the samples containing PS, silica-coated PS, hollow and dense silica particles with similar sizes were provided, (b) Optical transmittance light spectra of the samples, (c) Transparent stability of hollow silica particles ($D_p = 181$ nm and $L = 6.2$ nm) as a function of measuring time, and (d) Optical transmittance light spectra of the prepared hollow silica particles with different shell-thickness. Inset of Figure 7(d) shows the correlation between shell-thickness and optical transparency of hollow silica at shorter ($\lambda = 380$ nm) and longer ($\lambda = 680$ nm) wavelength, respectively.

The digital photograph and optical transmittance light spectra of the sample solutions containing PS particle, silica-coated PS particle, dense silica particle, and hollow silica particle prepared at a concentration of 0.1 wt% are shown in **Figure 2.12** (a and b). Hollow silica with diameter of 181 nm was transparent. In contrast, samples containing

dense silica particles with a similar diameter ($D_p \sim 172$ nm) were opalescent. Sample of PS (i.e. 185 nm) and silica-coated PS particles ($D_p \sim 195$ nm) were completely opaque. The dispersion stability and optical properties were measured over 5 days, as shown in **Figure 2.12 (c)**, where the transmittance of the hollow silica remained around 90% in the visible region of 400 and 800 nm, respectively. The correlation between hollow silica particle and their shell-thickness were given in the inset of **Figure 2.12 (d)**. The transmittance intensity mostly decreased at shorter wavelengths ($\lambda = 380$ nm), when the shell-thickness of hollow silica was increased. In contrast, at longer wavelength, the thickness of the shell did not alter significantly on the transmittance intensity. The highest transparency among all of the hollow silica samples is 97.1% at longer wavelength ($\lambda = 680$ nm) and obtained from the prepared particle with the thinner shell of 6.2 nm.

2.3.8 Thermal conductivity of PES/hollow silica composite film

Figure 2.13 (a) shows a digital photograph of a PES/hollow silica composite film containing 2.5 wt% of hollow silica particles. The calculated percent volume of silica particle using the corresponding material densities (i.e. hollow silica: 0.3 g cm^{-3} , PES: 1.37 g cm^{-3}) is around 12 vol%. The film is transparent (i.e. absorption edge: 370 nm) and has a relatively homogeneous thickness (35 μm). The morphology and structures of the composite film at the top and bottom surface were shown in the **Figure 2.13 (b)** and **(c)**. The film surfaces were homogeneous and flat on both sides. Observation of the cross-section (**Figure 2.13 (d)**) confirmed the existence of hollow silica particles. The resulting thermal conductivity of pure PES and PES/hollow silica composites film were summarized in **Table 2.15**.

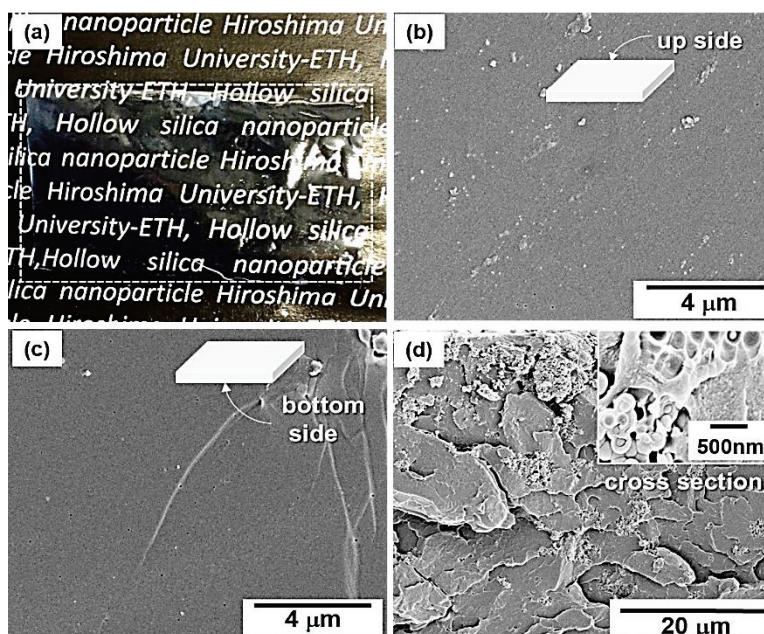


Figure 2.13 (a) Hollow silica particle can be implemented into polymer films. Photograph of the succeed transparent composite film of PES/hollow silica (the film is indicated with the dotted line), the results of SEM images are shown in: (b) view from the top surface, (c) view from the bottom surface, and (d) cross sectional surface and the inset shows high magnification image.

Table 2.15 Thermal conductivity of PES/hollow silica composite films

sample	particle size [nm]	hollow silica/PES mass ratio [wt%]	thickness of composite film [μm] ^a	thermal conductivity of composite film [W m-K ⁻¹] ^b
Polyether-sulfone (PES) only	-	0	33 \pm 1	0.09 \pm 0.02
PES/hollow silica*	200	2.5	35 \pm 5	0.03 \pm 0.005

*Transparent composite film containing 2 g of PES and 0.05 g of hollow silica was tested for three times at a steady state period of at least 30 min. Hollow silica with 181 nm in size was used for film preparation. Additionally, a pure PES also was measured for comparison. The error values of ^a and ^b are calculated by the standard error mean and measured three times.

The resulting thermal conductivity of PES/hollow silica composite film (0.03 \pm 0.005 W m-K⁻¹) is obviously lower than that of pure PES (0.09 \pm 0.02 W m-K⁻¹) film. This result indicates that the hollow silica particles produced from TMOS have a potential to become a cost and energy effective low thermal conductivity additive even in application where transparency is a key material attributed.

2.4 Conclusions

Hollow silica particles from TMOS with controllable size and shell thickness were successfully prepared in MeOH-water system via liquid-phase synthesis using PS particles as a template. The size and shell thickness of hollow silica particles were controlled by changing the size of PS particle and the concentration of TMOS. A high concentration of MeOH (i.e. 75 to 90 wt%) was required to produce hollow silica particles. The measured shell-thickness of hollow silica particles as function of the TMOS concentrations was in a good agreement with theoretical calculation. Hollow silica particle with the shell-thickness of 6.2 nm displayed a high light transmittance intensity of 97.1%, in the wavelength at 680 nm. The thermal conductivity of the PES/hollow silica composite film (silica composition, 2.5 wt%, film thickness, $35 \pm 5 \mu\text{m}$) shows a low value ($0.03 \pm 0.005 \text{ W m-K}^{-1}$) if compared to the pure PES film. These results indicate that the prepared hollow silica particle has a high potential to be used for flexible optical devices, thermal insulator, yet visible-transparent composite film applications.

2.5 References

1. Ariga, K.; Yamauchi, Y.; Rydzek, G.; Ji, Q.; Yonamine, Y.; Wu, K.C.W.; Hill, J.P. Layer-by-layer Nanoarchitectonics: Invention, Innovation, and Evolution. *Chem. Lett.* 43(1), 36-68, **2014**.
2. Malgras, V.; Ji, Q.; Kamachi, Y.; Mori, T.; Shieh, F.K.; Wu, K.C.W.; Ariga, K.; Yamauchi, Y. Templated Synthesis for Nanoarchitected Porous Materials. *Bull. Chem. Soc. Jpn.* 88(9), 1171-1200, **2015**.
3. Fang, X.; Zhao, X.; Fang, W.; Chen, C.; Zheng, N. Self-templating synthesis of hollow mesoporous silica and their applications in catalysis and drug delivery. *Nanoscale*, 5, 2205-2218, **2013**.
4. Ogi, T.; Nandiyanto, A. B. D.; Okuyama, K. Nanostructuring strategies in functional fine-particle synthesis towards resource and energy saving applications. *Adv. Powder. Technol.* 25, 3-17, **2014**.
5. David Lou, X. W.; Archer, L. A.; Yang, Z. Hollow Micro-Nanostructures: Synthesis and Applications. *Adv. Mater.*, 20, 3987- 4019, **2008**.
6. Du, Y.; Luna, L. E.; Tan, W. S.; Rubner, M. F.; Cohen, R. E. Hollow Silica

- Nanoparticles in UV-Visible Antireflection Coatings for Poly-(methyl methacrylate) Substrates. *ACS Nano*, 4(7), 4308-4316, **2010**.
7. Wei, G.; Liu, Y.; Zhang, X.; Yu, F.; Du, X. Thermal conductivities study on silica aerogel and its composite insulation materials. *Int. J. Heat Mass Transf.*, 54(11), 2355-2366, **2011**.
 8. Gao, T.; Jelle, B. P.; Sandberg, L. I. C.; Gustavsen, A. Monodisperse Hollow Silica Nanospheres for Nano Insulation Materials: Synthesis, Characterization, and Life Cycle Assessment. *ACS Appl. Mater. Interfaces*, 3,761-767, **2013**.
 9. Fuji, M.; Shin, T.; Watanabe, H.; Takei, T. Shape-controlled hollow silica nanoparticles synthesized by an inorganic particle template method. *Adv. Powder Technol.*, 23, 562-565, **2012**.
 10. Nandiyanto, A. B. D.; Ogi, T.; Iwaki, T.; Okuyama, K. Mesopore-free silica shell with nanometer-scale thickness-controllable on cationic polystyrene core. *J. Colloid Interface Sci.*, 389, 134-146, **2013**.
 11. Zou, H.; Wu, S.; Ran, Q.; Shen, J. A Simple and Low-Cost Method for the Preparation of Monodisperse Hollow Silica Spheres. *J. Phys. Colloid Chem.*, 112, 11623-11629, **2008**.
 12. Zhang, T.; Zhang, Q.; Ge, J.; Goebel, J.; Sun, M.; Yan, Y.; Liu, Y.; Chang, C.; Guo, J.; Yin, Y. A Self-Templated Route to Hollow Silica Microspheres. *J. Phys. Colloid Chem.*, 113, 3168-3175, **2009**.
 13. Ma, Y.; Qi, L. Solution-phase synthesis of inorganic hollow structures by templating strategies. *J. Colloid Interface Sci.*, 335, 1-10, **2009**.
 14. Zhang, Q.; Wang, W.; Goebel, J.; Yin, Y. Self-templated synthesis of hollow nanostructures. *Nano Today*, 4, 494-507, **2009**.
 15. Li, G.; Liu, G.; Kang, E. T.; Neoh, K. G.; Yang, X. pH-Responsive Hollow Polymeric Microspheres and Concentric Hollow Silica Microspheres from Silica-Polymer Core-Shell Microspheres. *Langmuir*, 24(16), 9050-9055, **2008**.
 16. Nandiyanto, A. B. D.; Akane, Y.; Ogi, T.; Okuyama, K. Mesopore-Free Hollow Silica Particles with Controllable Diameter and Shell Thickness via Additive-Free Synthesis. *Langmuir*, 28, 8616-8624, **2012**.
 17. Su, Y.; Yan, R.; Dan, M.; Xu, J.; Wang, D.; Zhang, W.; Liu, S. Synthesis of

- Hierarchical Hollow Silica Microspheres Containing Surface Nanoparticles Employing the Quasi-Hard Template of Poly (4-vinylpyridine) Microspheres. *Langmuir*, 27(14), 8983-8989, **2011**.
18. Tan, M. N.; Park, Y. S. Synthesis of stable hollow silica nanospheres, *J. Ind. Eng. Chem.*, 15, 365-369, **2009**.
19. Wang, Y.; Su, X.; Ding, P.; Lu, S.; Yu, H. Shape-Controlled Synthesis of Hollow Silica Colloids. *Langmuir*, 29(37), 11575-11581, **2013**.
20. Chen, Y.; Chen, H. R.; Shi, J. L. Construction of Homogenous/Heterogeneous Hollow Mesoporous Silica Nanostructures by Silica-Etching Chemistry: Principles, Synthesis, and Applications. *Acc. Chem. Res.*, 47(1), 125-137, **2014**.
21. Wan, Y.; Yu, S. H. Polyelectrolyte Controlled Large-Scale Synthesis of Hollow Silica Spheres with Tunable Sizes and Wall Thicknesses. *J. Phys. Chem.C.*, 112(10), 3641-3647, **2008**.
22. Qiao, Z. A.; Zhang, L.; Guo, M.; Liu, Y.; Huo, Q. Synthesis of Mesoporous Silica Nanoparticles via Controlled Hydrolysis and Condensation of Silicon Alkoxide. *Chem. Mater.*, 21(16), 3823-3829, **2009**.
23. Jacob, D. S.; Gedanken, A. Effect of Reaction Parameters on the Hydrolysis of Tetramethyl Orthosilicate and Tetraethyl Orthosilicate and their Surface Morphology in an Ionic Liquid. *J. Am. Ceram. Soc.*, 91(9), 3024-3030, **2008**.
24. Néouze, M. A.; Bideau, J. L. Gaveau, P. Bellayer, S. Vioux, A. Ionogels, New Materials Arising from the Confinement of Ionic Liquids within Silica-Derived Networks. *Chem. Mater.*, 18(17), 3931-3936, **2006**.
25. Zhao, M.; Zheng, L.; Bai, X.; Li, N.; Yu, L. Fabrication of silica nanoparticles and hollow spheres using ionic liquid microemulsion droplets as templates. *Colloids Surf. Physicochem. Eng. Asp.*, 346(1), 229-236, **2009**.
26. Zerda, T. W.; Hoang, G. Effect of Solvents on the Hydrolysis Reaction of Tetramethyl Orthosilicate, *Chem. Mater.*, 2, 372-376, **1990**.
27. Bernards. T. N. M.; Van Bommel, M. J.; Boonstra, A. H. Hydrolysis-condensation processes of the tetra-alkoxysilanes TPOS, TEOS and TMOS in some alcoholic solvents. *J. Non-Cryst. Solids*, 134, 1-13, **1991**.
28. Schmidt, H. K.; Scholze, H.; Kaiser, A. Principles of hydrolysis and condensation

- reaction of alkoxysilanes. Part I: Basic investigations on hydrolysis, condensation and densification I. *J. Non-Cryst. Solids*, 63, 1-11, **1984**.
29. Liu, D.; Sasidharan, M.; Nakashima, K. Micelles of poly-(styrene-b-2-vinylpyridine-b-ethylene oxide) with blended polystyrene core and their application to the synthesis of hollow silica nanospheres. *J. Colloid Interface Sci.*, 358(2), 354-359, **2011**.
30. Ugelstad, J.; Mfutakamba, H. R.; Mork, P. C.; Ellingsen, T.; Berge, A.; Schmid, R.; Holm, L.; Jorgedal, A.; Hansen, F.K.; Nustad, K. Preparation and application of monodisperse polymer particle *Polym. Sci. J.*, 72, 225-240, **1985**.
31. Nandiyanto, A. B. D.; Ogi, T.; Okuyama, K. Control of the Shell Structural Properties and Cavity Diameter of Hollow Magnesium Fluoride Particles. *ACS Appl. Mater. Interfaces*, 6(6), 4418-4427, **2014**.
32. Li, L.; Zhai, T.; Zeng, H.; Fang, X.; Bando, Y.; Golberg, D. Polystyrene sphere-assisted one-dimensional nanostructure arrays: synthesis and applications. *J. Mater Chem.*, 21(1), 40-56, **2011**.
33. Nandiyanto, A. B. D.; Suhendi, A.; Ogi, T.; Umemoto, R.; Okuyama, K. Size and charge controllable polystyrene spheres for templates in the preparation of porous silica particles with tunable internal hole configurations. *Chem. Eng. J.*, 256, 421-430, **2014**.
34. Nandiyanto, A. B. D.; Suhendi, A.; Ogi, T.; Iwaki, T.; Okuyama, K. Synthesis of additive-free cationic polystyrene particles with controllable size for hollow template applications. *Colloids Surf. A.*, 396, 96-105, **2012**.
35. Hess, S. C.; Kohll, A. X.; Raso, R. A.; Schumacher, C. M.; Grass, R. N.; Stark, W. J. Template-Particle Stabilized Bicontinuous Emulsion Yielding Controlled Assembly of Hierarchical High-Flux Filtration Membranes. *ACS Appl. Mater. Interfaces*, 7, 611-617, **2015**.
36. Luyben, W. L.; Hoboken, N. J. Distillation design and control using Aspen simulation. Wiley: *Inter-Sci*. 2nd Edition, 510, **2006**.
37. Gmehling, J.; Onken, U. Vapor-Liquid Equilibrium Data Collection. *Dechema-Chemistry Data Series*. Frankfurt, Germany, 1-60, **1977**.

38. Beganskiene, A.; Sirutkattis, V.; Kurtinattiene, M.; Juskenas, R.; Kareiva, FTIR, TEM and NMR investigations of Stöber silica nanoparticles. *J. Mater. Sci.*, 10, 287-290, **2004**.
39. El Rassy, H.; Pierre, A. C. NMR and IR spectroscopy of silica aerogels with different hydrophobic characteristics. *J. Non-Cryst. Solids*, 351,1603-1610, **2005**.
40. Chuprov, L. A.; Sennikov, P. G.; Tokhadze, K. G.; Ignatov, S. K.; Schrems, O. HighResolution Fourier-Transform IR Spectroscopic Determination of Impurities in Silicon Tetrafluoride and Silane Prepared from it. *J. Inorg. Mater.*, 42, 924-931, **2006**.
41. Assink, R. A.; Bruce, D. K. Sol-gel kinetics I. Functional group kinetics. *J. Non-Cryst. Solids*, 99, 359-370, **1988**.
42. Zerda, T.W.; Hoang, G. Effect of Solvents on the Hydrolysis Reaction of Tetramethyl Orthosilicate. *Chem. Mater.*, 2, 372-376, **1990**.
43. Woodhead, M.; Paabo, M.; Robinson, R. A.; Bates, R. G. Dissociation of Ammonium Ion in Methanol-Water Solvents. *J. Phys. Chem.*, 70, 247-251, **1966**.

Chapter 3

Tunable Synthesis of Mesoporous Silica Particle with a Unique Radially Oriented Pore Structures from Tetramethyl Orthosilicate via Oil-Water Emulsion Process

3.1 Introduction

The synthesis of mesoporous silica (MPS) particles using oil/water (O/W) emulsion systems has attracted much attention [1-5]. MPS is widely used in applications such as catalysis, drug delivery, adsorption, separation, and biological and medical areas, because of its specific and attractive properties such as a well-ordered and open pore structure, high specific surface area, tunable morphology, low density, good biocompatibility, low toxicity, high mechanical stability, easy selective functionalization of the pore or particle surfaces, and high accessibility to guest materials [6-10].

The general formation mechanism of mesoporous particles in mixtures of water, oil, surfactants, and cosurfactants, and its phase behavior in emulsion systems have been studied for several decades.[11-13] Many researchers have investigated how mesophase structures are formed from mixtures containing a sufficient amount of surfactant and balancing amounts of water and oil.[14-16] Winsor et al. have classified the phase behaviors of emulsion systems, which depend on the water–oil–surfactant ratios, into four types, i.e., Type I [water in oil (W/O)], Type II (O/W), Type III [bicontinuous (W/emulsion/W or O/emulsion/O)] and Type IV (single phase with high surfactant concentration).[17] The emulsion type and its phase behavior significantly affect the hierarchical structures of particles formed in the reaction mixture.

In our previous study, tunable MPS particles (diameters ~20 to 80 nm and pore sizes ~4 to 15 nm) were successfully synthesized via an emulsion process. [18] These MPS

particles were successfully formed through dynamic self-assembly of silica particles generated by hydrolysis of tetraethyl orthosilicate (TEOS) and polystyrene particle generated by polymerization of styrene. Zhang et al. and Liu et al. synthesized similar MPS particles with particle diameters around 40 nm and pore sizes of 5 to 10 nm via a modified O/W emulsion process. [19, 20]. In 2016, Gustafsson et al. [21] successfully prepared MPS particles with diameter as small as 40 nm and pore size around 9 nm using a synthesis protocol adapted from our previous method. [18]

The morphologies of MPS particles synthesized from TEOS significantly affect their physical and chemical properties. [22, 23] MPS particles with radially oriented pore structures have unique properties. Increases in the center radial structure and pore size enable molecules or even nanoparticles to move easily into or out of the pores and promote loading and mass transport. These factors enhance the catalytic performance and broaden the range of biomedical applications. [24-26]

Although many reports of the preparation of MPS particles have been published, most of these have focused on the use of TEOS rather than other tetraalkoxysilanes, particularly tetramethyl orthosilicate (TMOS), as silica source. It is because of difficult to control the fast hydrolysis of TMOS, which often results in free silica particles and inner pore structures. [27-29] However, in the large-scale production of silica, especially in terms of recycling alcohol as byproduct, the fast reaction of TMOS enables the use of smaller-scale equipment (i.e., recycled streams) than is used with TEOS. [30] It also requires the minimum energy, which can reduce the silica production costs. Therefore, the use of TMOS as a silica source for preparing MPS particles should be considered. In most previous studies, the characteristic behavior of the emulsion phase, which can provide valuable insights into changes in the particle morphology, was not thoroughly analyzed. Further study is needed to achieve a better understanding of emulsion types and establish the most appropriate conditions for MPS particle formation.

The purpose of present study was to synthesize spherical MPS particles from TMOS via a modified O/W emulsion process. The process involved one-step controlled polymerization of styrene and hydrolysis of TMOS, followed by the addition of hexadecyltrimethylammonium bromide (CTAB) as a cationic surfactant and *n*-octane as the hydrophobic component. The structural properties of the particles were controlled by

selecting emulsions with appropriate water-CTAB-oil ratios. Unlike the MPS particles were generally obtained from TMOS, which have small inner pores, the synthesized MPS particles had a unique radially oriented structure, high surface area, and large pores. To the best of our knowledge, there have been no reports of similar studies. Based on the hierarchical structure of the synthesized MPS particles, a plausible mechanism for particle formation in terms of the phase behavior and type of emulsion system is proposed.

3.2 Experimental

3.2.1 Raw materials

Tetramethyl-Orthosilicate (TMOS, 98%, Aldrich, USA) and ammonium hydroxide (NH₄OH, 28%, Kanto-Chemical, Japan) were used as the silica source and basic catalyst, respectively. Styrene (99%, Kanto-Chemical, Japan) and *n*-octane (99%, Aldrich, USA) were used as the oil component. Ultrapure water and Ethanol (EtOH, 98%, Kanto-Chemical, Japan) were used as a mixed solvent. Hexadecyltrimethylammonium bromide (CTAB, 99%, Aldrich, USA) and potassium persulfate (KPS, 99%, Aldrich, USA) were used as a cationic surfactant and anionic initiator, respectively.

3.2.2 Synthesis of mesoporous silica particles

The reaction system was performed by adding styrene at various concentrations (0-44.6 mg mL⁻¹) to EtOH-water mixture solvent and stirred at 700 rpm in a three-necked flask, and heating to 70°C under N₂. When the reaction temperature was attained, a KPS aqueous solution (0.0084 mg mL⁻¹) was added. The emulsion system was controlled and stabilized by adding a cationic surfactant (CTAB) and *n*-octane simultaneously. This mixture was reacted for 3 h. TMOS and NH₄OH were then slowly added to the reaction mixture with the temperature controlled at 40°C. After mixing for 2 h, the solution was then cooled, decanted, and kept for overnight. The particles were collected by centrifugation at 10000 rpm for 10 min and washed three times with EtOH and water. The collected particles were calcined at 550°C for 5 h under air to give MPS. This experimental procedure was used to prepare MPS-(b-i) particles. MPS-a particles were synthesized without adding styrene and KPS, the other parameters were similar to those for the other samples.

3.2.3 Characterization

The morphologies and structures of the MPS particles were investigated using scanning electron microscopy (SEM; Hitachi S-5000 operated at 20 kV) and transmission electron microscopy (TEM; JEM-3000F, JEOL, operated at 300 kV). The crystallinities of the MPS particles were examined using X-ray diffraction (XRD; Bruker D2 Phaser diffractometer equipped with a Cu K α radiation source and a Linx-Eye detector). The diffraction patterns were recorded in the range $10^\circ < (2\theta) < 80^\circ$. The functional groups in, and chemical compositions of, the prepared samples were identified using Fourier-transform infrared (FT-IR) spectroscopy in the range 1000–4000 cm^{-1} (Shimadzu, IFR-Affinity-1S, JIS C6802, operated at 150 V, Japan). The specific surface areas and pore-size distributions of the prepared particles were calculated using the Brunauer-Emmet-Teller (BET) and Barrett-Joyner-Halenda (BJH) methods, respectively (BELSORP 28SA, Bel Japan; N₂ adsorption isotherms were recorded at 77.15 K). Prior to characterization, the powdered MPS samples were dried for 4 h at 200°C in N₂.

3.3 Results and discussions

3.3.1 Effect of water-CTAB-oil weight ratios on the morphology of mesoporous silica

An emulsion system is thermodynamically unstable in its fundamental equilibrium state. Even in the presence of CTAB, the oil droplets are bounded by surfaces with high interfacial energies, and eventually break down and separate into a multiphase layer [31, 32]. Control of the water, CTAB, and oil mixing ratios can therefore be used to promote phase separation in an emulsion system. This phase separation represents the equilibrium properties (i.e., hydrophilicity and hydrophobicity) of each component in the reaction system. The types and characteristic phase behaviors of emulsion systems for the synthesis of MPS particles are shown in **Table 3.1**.

Table 3.1. Types and characteristic phase behaviors of emulsions system of the synthesized MPS particles

sample	initial styrene conc. [mg ml ⁻¹] ^a	water: CTAB: oil weight ratio ^b	n-octane: water weight ratio	oil: TMOS weight ratio	phase behavior ^c	emulsion type ^d
MPS-a	0	7.0 : 1.0 : 0.0	0.77	0.35	Two separated layer	Type II
MPS-b	12.3	7.0 : 1.0 : 2.5	0.77	0.52	Two separated layer	Type II
MPS-c	19.6	7.0 : 1.0 : 6.0	0.84	0.52	Two separated layer	Type II
MPS-d	27.7	7.0 : 1.0 : 7.5	0.84	0.52	Two separated layer	Type II
MPS-e	36.6	6.0 : 1.0 : 10.5	0.91	0.77	Three separated layer	Type III
MPS-f	36.6	5.5 : 1.0 : 10.5	0.91	0.77	Three separated layer	Type III
MPS-g	36.6	4.0 : 1.0 : 10.5	0.91	0.77	Three separated layer	Type III
MPS-h	43.3	4.0 : 1.0 : 13.0	0.95	1.31	Bulk gel	Type I
MPS-i	44.6	4.0 : 1.0 : 14.0	0.95	1.31	Bulk gel	Type I

^aThe initial concentration of styrene is expressed in mg per total volume of solution of 110 to 120 ml.

^bThe oil weight ratio involved the total concentration of styrene and n-octane in reaction system.

^dType I, II, and III based on the WINSOR emulsion system. The concentration of KPS was kept at 0.0084 to 0.01 g ml⁻¹. The initial weight ratio of TMOS/NH₄OH was controlled at 0.24 for MPS-a to MPS-g; and at 0.55 for MPS-h and MPS-i particles.

The results show that when *n*-octane was gradually added into the reaction system, the equilibrium state of the mixture solution changed from a one-phase to a multiphase system. A Type II emulsion was formed when the system contained an excessive amount of water, (i.e., greater than that needed to dissolve CTAB). In this system, the weight ratios of water and CTAB were fixed and the amount of styrene in the emulsion was varied. The MPS particles which were formed in Type II emulsion systems are denoted by MPS-a, MPS-b, MPS-c, and MPS-d. In Type III emulsion system, the three-phase layer consisted of both excessive oil and water separate from the bicontinuous emulsion, in which oil at the top layer, bicontinuous emulsion (composed of mostly CTAB and about equal amount of water and oil) in the middle layer, and water at the bottom layer. In this system, the composition ratio in emulsion layer was unchanged even when the relative concentration of the total components changed, which resulted in a unique radially oriented mesoporous structured of the materials. The MPS particles which were formed in Type III emulsion systems are denoted by MPS-e, MPS-f, and MPS-g.

Meanwhile, in a Type I emulsion, oil separates from the O/W emulsion layer because of excess styrene. This system was formed when the weight ratio of styrene to CTAB was fixed and the amount of water in the emulsion was varied. MPS-h and MPS-i particles were formed in this emulsion phase. In this emulsion system, most of the silica particles were dispersed within the droplet interfaces because of the excessive amount of styrene. The emulsion system was observed in a bulk gel formation. The surface morphologies of the MPS particles were examined using SEM, the results are shown in **Figure 3.1**.

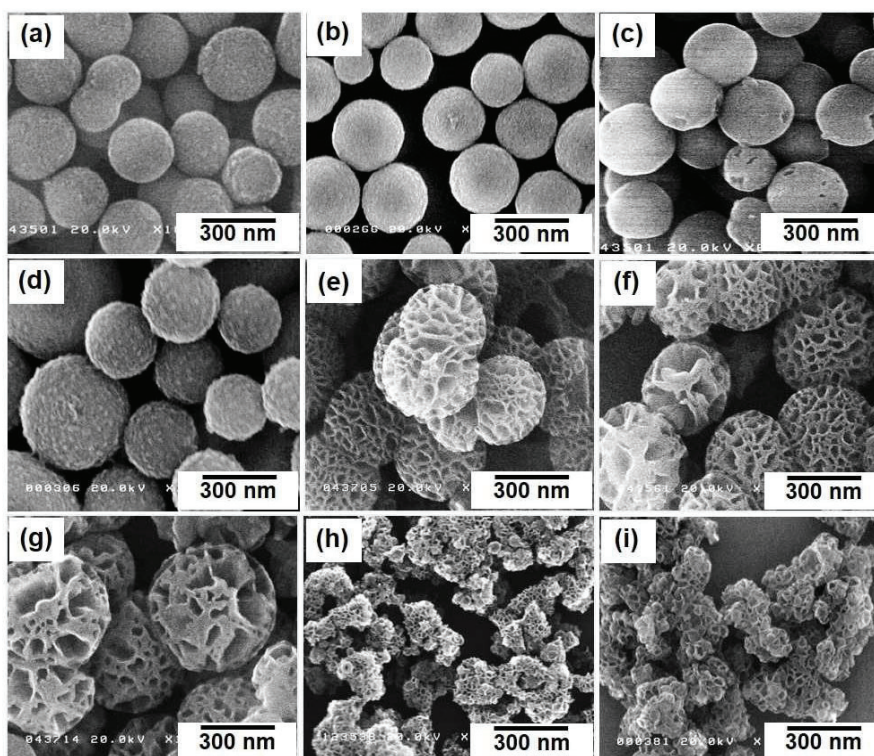


Figure 3.1 SEM images of MPS particles prepared using various water-CTAB-oil weight ratios: (a) MPS-a, 7.0:1.0:0.0; (b) MPS-b, 7.0:1.0:2.5; (c) MPS-c, 7.0:1.0:6.0; (d) MPS-d, 7.0:1.0:7.5; (e) MPS-e, 6.0:1.0:10.5; (f) MPS-f, 5.5:1.0:10.5; (g) MPS-g, 4.0:1.0:10.5; (h) MPS-h, 4.0:1.0:13.0; and (i) MPS-i, 4.0:1.0:14.0. Other synthesis conditions are summarized in **Table 3.1**.

Submicron spherical particles were obtained in all cases, except the MPS-h and MPS-i particles (**Figure 3.1 (h) and (i)**). The surfaces of the MPS particles prepared without addition of styrene and KPS were slightly rough, as shown in Figure 1a. In contrast, when styrene and KPS were added to the reaction system, MPS particles with various morphologies were formed (**Figure 3.1 (b-g)**). When a small amount of styrene

(12.3 mg mL⁻¹) was added, large pore structures on the particle surface cannot be observed (**Figure 3.1 (b)**). The surface morphology of the MPS particles gradually changed with increasing amount of styrene from 19.6 to 36.6 mg mL⁻¹, as shown in **Figure 3.1 (c-g)**. The addition of excess styrene (i.e., 43.3 and 44.6 mg mL⁻¹) created aggregated and ruptured particles, as shown in **Figure 3.1 (h)** and **(i)**. These results indicate that styrene plays an important role in formation of the MPS particle structure. The equilibrium phases of the mixed solution with different styrene concentrations prepared after cooling overnight and before centrifugation was shown in **Figure 3.2**.

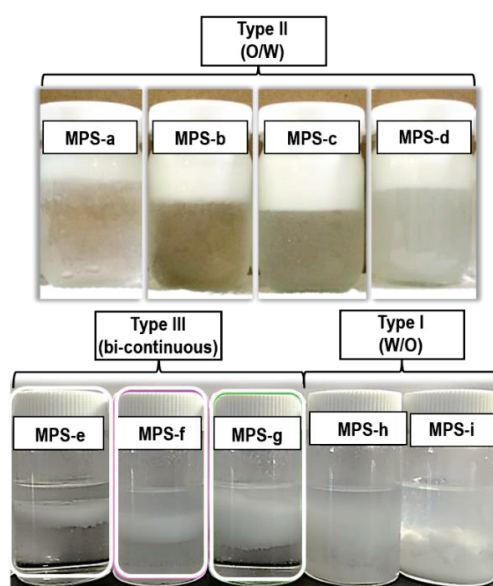


Figure 3.2 Photograph of MPS samples freshly prepared after cooling overnight and before centrifugation. The mixed precursor was left without mixing for 1 d prior to observing the presence of a transparent and translucent mixed solution (change of solution phase).

When the initial styrene concentration was increased from 0 (without styrene addition) to 27.7 mg mL⁻¹, two distinct phases were observed. The upper layer of solution containing aqueous solution and n-octane could be observed when the was further increased to 36.6 mg mL⁻¹, thereby confirming that the mixed system was in the Winsor III system region. The middle layer of this system should ideally comprise a bicontinuous structure. From these results, it was confirmed that the bicontinuous emulsion phase of the Winsor III system is essential to the formation of radially oriented pore structure of MPS particle. However, MPS particle synthesized from the bicontinuous phase of the

separated upper layer were aggregated with those from the emulsion system obtained by the fast mechanical stirring of the two separated layers. When this emulsion sample were added to pure water or n-octane, they diluted quickly in n-octane but stayed in a separated phase in water, thereby confirming that this macroemulsion system is water in-oil (W/O) type emulsion within which the bicontinuous emulsion. TEM was used to examine the inner structures of the particles, the results are shown in **Figure 3.3**.

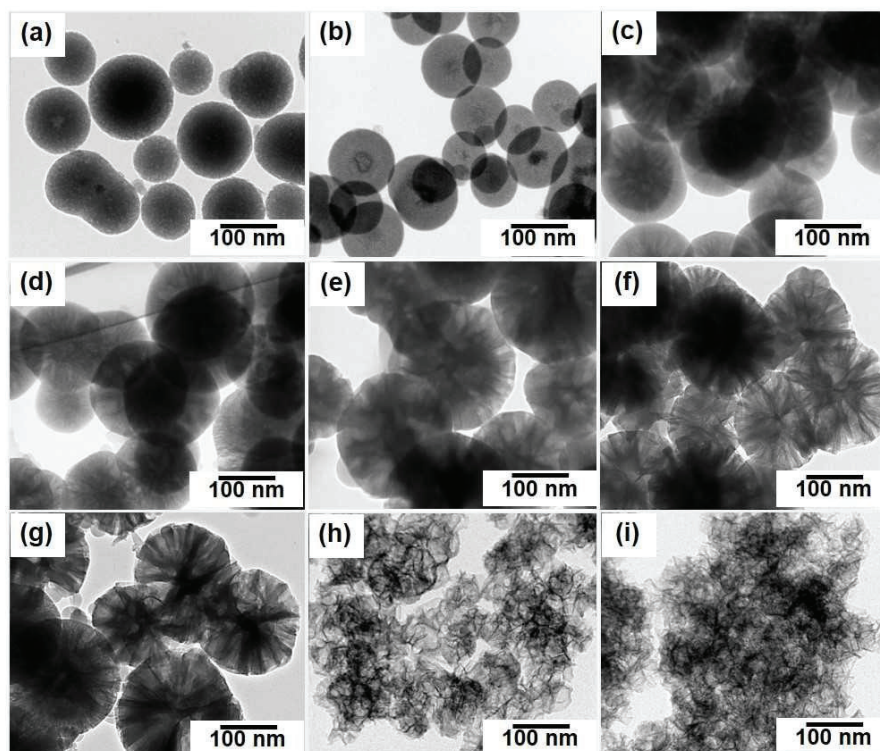


Figure 3.3 TEM images of MPS particles prepared using various water/CTAB/oil weight ratios: (a) MPS-a, 7.0:1.0:0.0; (b) MPS-b, 7.0:1.0:2.5; (c) MPS-c, 7.0:1.0:6.0; (d) MPS-d, 7.0:1.0:7.5; (e) MPS-e, 6.0:1.0:10.5; (f) MPS-f, 5.5:1.0:10.5; (g) MPS-g, 4.0:1.0:10.5; (h) MPS-h, 4.0:1.0:13.0; and (i) MPS-i, 4.0:1.0:14.0.

Based on TEM results, the MPS particle morphologies can be classified into four types, namely: (i) spherical with inner pores (**Figure 3.3 (a)** and **(b)**); (ii) radial with small inner pores (**Figure 3.3 (c)** and **(d)**); (iii) radial with large outer pores (**Figure 3.3 (e-g)**); and (iv) aggregated and ruptured particles (**Figure 3.3 (h)** and **(i)**). The TEM images show that the particles obtained without styrene and KPS addition had small pores uniformly distributed inside the particles (**Figure 3.3 (a)**). The addition of 12.3 mg mL^{-1} styrene did not significantly affect the pore structure of the MPS-b particles (**Figure 3.3 (b)**). The

morphology and pore structure of particle gradually changed with increasing styrene addition from 19.6 to 36.6 mg mL⁻¹. The TEM results are in good agreement with the SEM results.

3.3.2 Proposed formation mechanism of hierarchical mesoporous silica particle

The proposed effect of the initial concentration of styrene on hierarchical MPS particle formation is shown in **Figure 3.4**.

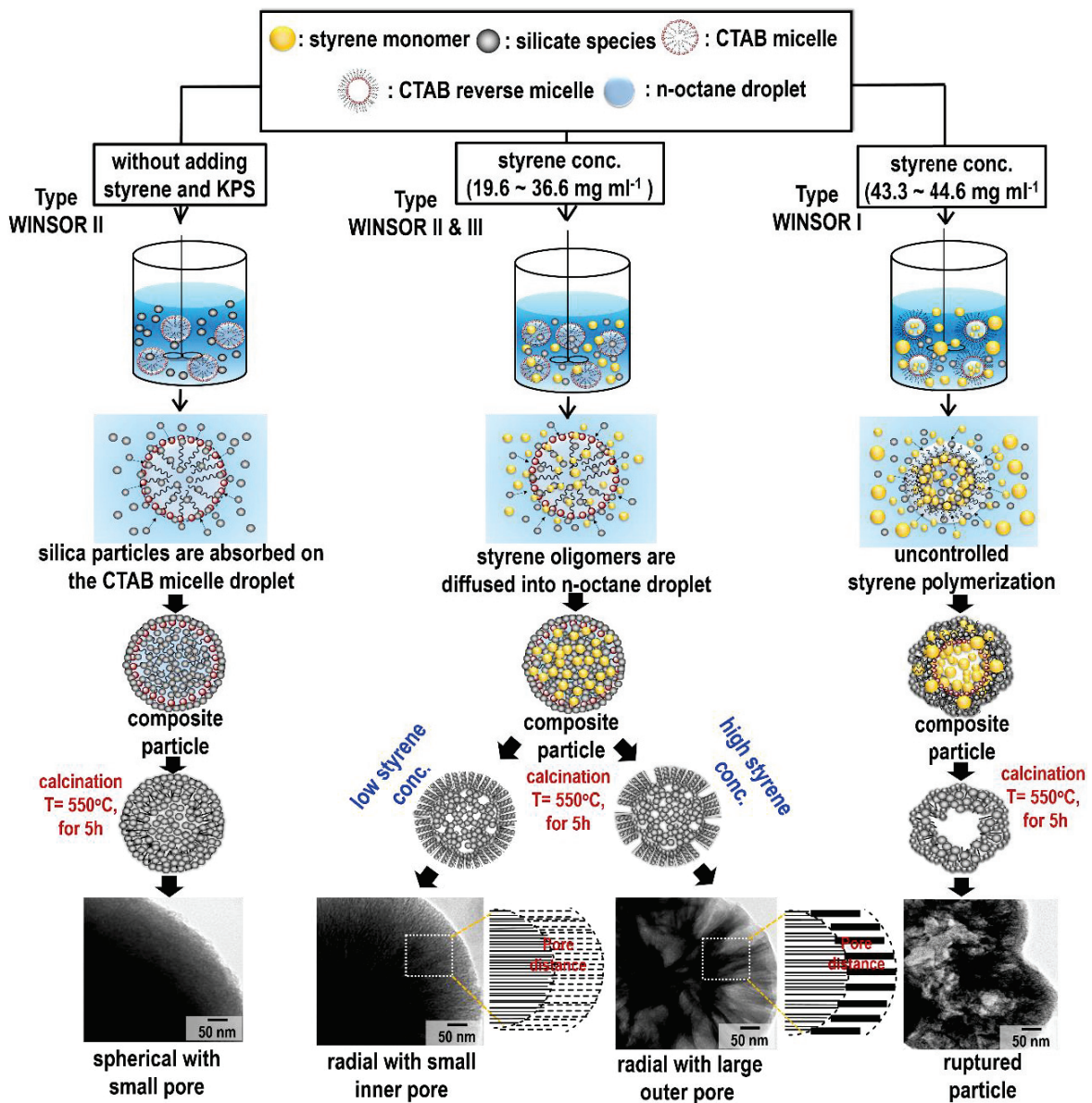


Figure 3.4 A plausible formation mechanism of mesoporous silica through dynamic polystyrene template particle via O/W emulsion process.

The arrangement of mesoporous particle structures in an emulsion system is a complex process involving bulk solution formation, viscosity and mobility of particle, colloidal stability, electrostatic forces, diffusion and transport of the aggregated particles to form droplets during the emulsion process. [33-35] The shear force from stirring induces the particle aggregation, and finally structured arrangements of MPS particles are obtained. Overall process of the formation mechanism of MPS particle is as follows: (i) Growth of silica oligomers and addition of *n*-octane in emulsion system result in a thermodynamically unstable mixture (i.e. silica/CTAB/oil/solvent), (ii) Transition of emulsion phase is formed, which spontaneously giving the formation of droplets in a multiphase system (i.e. oil-rich phase, water-rich phase and bicontinuous emulsion), (iii) The droplets are colloidally stabilized by electrostatic or steric stabilization, and adsorption of silica oligomers into CTAB micelle may also played a key role here, (iv) Polymerization of styrene via free-radical initiator (KPS) and hydrolysis of TMOS which simultaneously occurred within the droplets, give rise to the formation of mesostructured particles.

In the case of the MPS-a particles, when styrene and KPS are excluded from the reaction system, the phase of emulsion was identified as Type II system, which contains an excessive amount of water (greater than that needed to dissolve CTAB). This excess water may cause the reaction of TMOS rapidly proceed, even after adding ethanol (EtOH) as co-solvent. As a result, some fractions of TMOS molecules may be remained in the bulk emulsion system as partially hydrolyzed, and some fractions are remained in the oil droplets as hydrolyzed molecules. In this state, the reaction rate of TMOS can be assumed faster than the formation rate of CTAB micelle. Based on the MPS particle formation mechanism proposed by Du et al. [36], MPS-a particle is probably formed through the electrostatic interactions between negatively charged silica and the cationic surfactant at the oil droplet interfaces. After hydrolysis reaction was proceed, the silica clusters are absorbed into the CTAB micelle surfaces. This reduces inter-micellar repulsion and enables the formation of CTAB-silica clusters, which grow to form MPS-a particle.

In the case of MPS-(b-g) particle synthesis, in which styrene, KPS, *n*-octane, and CTAB are mixed, the shear rate is higher, and emulsion droplets are formed. In this system, MPS particle formation can be attributed to dynamic self-assembly in a two-stage

process. The first stage is KPS-initiated styrene polymerization to form styrene oligomers in the EtOH–water mixed solvent system. The second stage involves continuous growth of silicate species through hydrolysis and condensation of TMOS. Under continuous stirring, the styrene oligomers and silica particles both move into the *n*-octane droplets because they are hydrophobic. Simultaneously, dynamic self-assembly of CTAB micelles and silica particles at the O/W interface can induce the formation of CTAB–silica nanoclusters. The silica composite particles then randomly move into the aqueous phase, reach the O/W interface, and interact with the CTAB micelles, resulting in further assembly and growth. During this complex process, the dynamic self-assembly of styrene, silica, and CTAB micelles inside *n*-octane droplets can induce the formation of MPS particles.

Lee et al. suggested that when TEOS is used to prepare MPS particles using an emulsion process, the mechanism behind of particle formation involves a transition from an O/W or W/O system to a bicontinuous system.[37] They also reported that the MPS particle morphology could be precisely controlled by regulating the phase behaviors of a Winsor III system, which can be achieved by adjusting the water–surfactant–oil mixing ratios.[38] In principle, the same mechanism should be involved when TMOS is used, and a similar phase transition was observed in this study. However, here, the diameters of the MPS particles synthesized from TMOS were larger (i.e. ~400 nm) than those of the MPS particles synthesized from TEOS (i.e. 40-50 nm). [18-21] The MPS particle in the present case are larger than those previously reported for the following reasons: (i) In the present case, the hydrolysis of TMOS was performed using relatively high amount of NH₄OH (4.26 g) with the initial weight ratio of H₂O/TMOS/NH₄OH at 70/1/4. This high NH₄OH amount may cause the increasing number of silanol (Si-OH) groups at the surface of silica network and favors the aggregation of the particles into bigger ones. [39,40] Compared with the previous studies, [18, 20, 21] the hydrolysis of TEOS was performed using L-lysine as catalyst, which resulting in small silica particle. Nevertheless, these results should be considered with the other caution, namely, (ii) The different ratio of *n*-octane/water in the reaction process, which may cause the phase transition of emulsion system was changed, due to the different solubility of surfactant (CTAB) in the reaction system. The presence of *n*-octane as a hydrophobic agent, which acts for: (1) Stabilizes

the emulsion system, (2) Swelling agent and homogenizing the hydrophobic molecules (i.e., styrene and silica), and (3) Controls droplet formation and sphere growth at the O/W interface by incorporating styrene molecules. [18] This is consistent with the results of this study. When the *n*-octane/water ratio was increased from 0.77 to 0.91, and the oil/TMOS ratio was increased from 0.35 to 0.77, large MPS particles of average size around 400 nm were produced. However, when an *n*-octane/water ratio of 0.95 and oil/TMOS ratio of 1.3 were used, spherical MPS particles were not observed. These values were the limits of the ratios of *n*-octane/water and oil/TMOS in the reaction system and were not appropriate for controlling droplet formation and stabilizing the emulsion system. Spherical MPS particles therefore could not be obtained, the ruptured particles were formed.

MPS particles with radially oriented structures and large pores were observed in Type III emulsions. The samples obtained in this system correspond to MPS-e, MPS-f, and MPS-g particles. In this system, a three-phase layer is formed, in which the middle layer is a bicontinuous emulsion. The initial concentration of *n*-octane significantly affects the interface between the continuous and dispersed phases. The dispersed phase corresponds to the formation of silica clusters through hydrolysis and condensation of TMOS. The continuous phase corresponds to the surfactant and oil system. The free organic solvent (*n*-octane) and the other components (i.e., water, silica, styrene, and CTAB) are assumed to be in equilibrium. The addition of EtOH as a cosolvent may have helped to stabilize the emulsion stability by reducing the interfacial tension and increasing the solubility of oil in water. [41] In this region, the silica nucleation rate during hydrolysis is stable. However, the attractive forces and the ionic interactions between the silicate species and CTAB micelles may increase. Consequently, more clusters collide with each other in the middle layer of the emulsion, resulting in formation of a Type III emulsion. The emulsion system for the MPS-a, MPS-b, MPS-c, and MPS-d particles was Type II. The BET results show that the average pore size of the MPS particles gradually increased from 1.2 (i.e., MPS-b particles) to 20 nm (i.e., MPS-g particles) with increasing initial amount of styrene from 12.3 to 36.6 mg mL⁻¹. On addition of excess styrene, (i.e., 43.3 and 44.6 mg mL⁻¹), the phase behavior of the emulsion system gradually changed to Type I (oil-rich phase), reverse CTAB micelle formation occurred, and a group of these

micelles arranged themselves with their hydrophobic tails pointing together to avoid interactions with water. The formation of silicate species in the continuous-phase system also decreased because of the oil-rich area. This caused spontaneous rupture of the emulsion droplets, and resulted in aggregated particles (i.e., MPS-h and MPS-i).

3.3.3 Effect of initial styrene concentrations on the surface and pore properties of mesoporous silica particle

The N₂ adsorption-desorption isotherms and pore-size distribution plots of the MPS-c and MPS-f particles are shown in **Figure 3.5**.

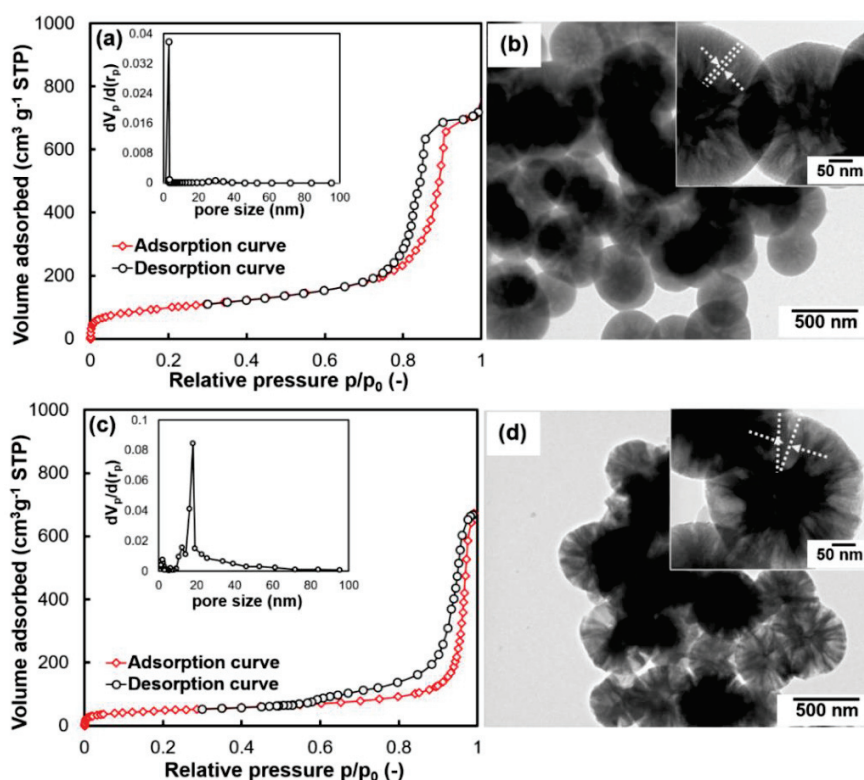


Figure 3.5 (a) N₂ adsorption-desorption isotherms and pore-size distribution plots for MPS-c particles; (b) low- and high-magnification TEM images of MPS-c particles; (c) N₂ adsorption-desorption isotherms and pore-size distribution plots of MPS-f particles; and (d) low- and high-magnification TEM images of MPS-f particles.

The N₂ adsorption-desorption isotherms of the MPS-c particles are Type IV according to the IUPAC classification and have an H₄ hysteresis loop, which clearly shows two-step capillary condensation, at relative pressures (p/p_0) of 0.3-0.6 and 0.7-1.0, indicating the presence of mesopores. The pore size and distribution (inset Figure 4a)

were confirmed using the BJH method. There is a sharp peak centered at 3.2 nm in the pore-size distribution curve. These results basically agree with the TEM results, as shown in **Figure 3.5 (b)**. A high-magnification TEM image (inset in **Figure 3.5 (b)**) confirmed that small pores were distributed uniformly inside the particles. The smaller mesopores are thought to be generated from the interparticle void spaces, and calcination may cause a slight shrinkage of the pore structure. The isotherms of the MPS-f particles also show Type IV structure and H₄ hysteresis loop, as shown in **Figure 3.5 (c)**. The MPS-f particles had pores of size 17.2 nm, calculated using the BJH method. The BET results show that the specific surface area of the MPS-f particles was higher than that of the MPS-c particles (**Table 3.2**).

Table 3.2 Surface areas and pore properties of the synthesized MPS particles

sample	initial styrene conc. [mg ml ⁻¹]	water: CTAB: oil weight ratio	n-octane: water weight ratio	surface area S _{BET} [m ² g ⁻¹] ^a	pore size [nm] ^b	pore volume [cm ³ g ⁻¹] ^c
MPS-a	0.0	7.0 : 1.0 : 0.0	0.77	109	0.8	0.77
MPS-c	19.6	7.0 : 1.0 : 6.0	0.84	560	3.2	1.18
MPS-f	36.6	5.5 : 1.0 : 10.5	0.91	891	17.2	2.44
MPS-g	36.6	4.0 : 1.0 : 10.5	0.91	814	21.7	2.55

^a specific surface area based BET method, ^{b, c} the pore size and pore volume were obtained by using BJH analysis.

The increases in the surface area and pore size can be attributed to pore expansion caused by rapid diffusion of styrene. Other factors, e.g., strong electrostatic interactions between silica species from TMOS and CTAB, could also induce fast assembly growth of the CTAB–silica clusters after calcination, leading to the formation of MPS-f particles with large pores. This was confirmed by a high-magnification TEM image (inset in Figure 4d), which shows large pores radially distributed inside the particles. This is consistent with the previous reports. [42] It is concluded that styrene plays an important role in pore expansion in the MPS particles.

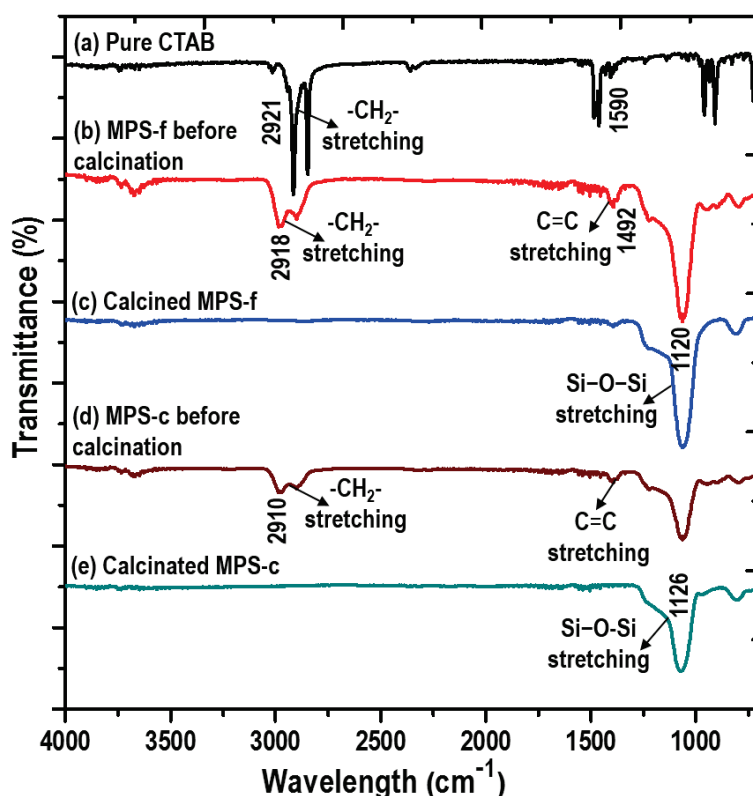


Figure 3.6 FT-IR spectra of (a) pure CTAB; (b, c) MPS-f particles before and after calcination; and (d, e) MPS-c particles before and after calcination.

FT-IR spectroscopy was used to confirm that CTAB was completely removed by calcination. Figure 5 shows that the spectrum of dried CTAB powder has two intense peaks, at 2921 and 2839 cm^{-1} , which are assigned to the asymmetric stretching vibrations of $-\text{CH}_2-$ in methylene chains. [18, 43] These peaks were also observed in the spectra of the MPS-c and MPS-f particles before calcination, indicating that CTAB cannot be easily removed by washing. In the cases of calcined MPS-c and MPS-f particles, the characteristic peaks of silica were clearly observed at 1096 , 970 , and 804 cm^{-1} , corresponding to Si-OH bending, Si-OH symmetrical stretching, and Si-O-Si bending, respectively. The characteristic peaks of CTAB, in the region $2800\text{-}2900\text{ cm}^{-1}$ disappeared, indicating complete removal of CTAB and the presence of only pure intact MPS after calcination at 550°C for 5 h. Calcination also led to an increase in the diffraction peak intensities because of the increased contrast with the intensity of the diffraction peaks of the channel pore structure even after reheated [44].

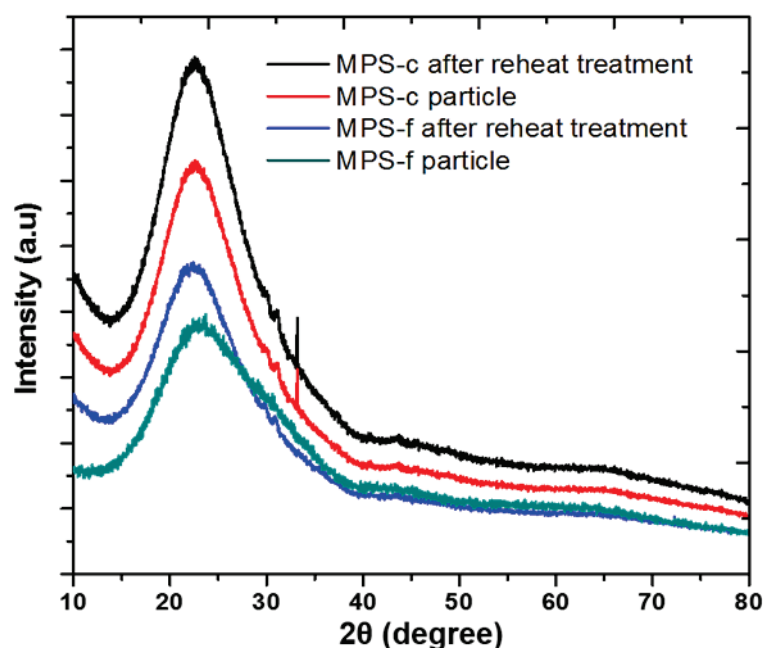


Figure 3.7 XRD patterns of the calcined mesoporous silica particle and after reheat treatment

Figure 3.7 shows that the XRD patterns of the calcined and reheated MPS-c and MPS-f particles showed a strong diffraction peak centered at an angle of $2\theta = 26^\circ$ (range 20° - 30°) corresponding to typical silica particle. The X-ray pattern confirms that the powders are silica with few other impurities detected. The peak with a wide 2θ range also indicates that the produced MPS particles is amorphous and that no crystalline structure appeared.

3.4 Conclusions

Spherical submicron MPS particles with radially oriented structures, high specific surface areas (up to $800 \text{ m}^2 \text{ g}^{-1}$), and large pores (20 nm) were successfully synthesized from TMOS via an O/W emulsion process. The morphologies of the MPS particles were tuned from spherical with inner pores to inner-radial with small pores, outer-radial with large pores, and finally aggregated and ruptured particles, by controlling the water–CTAB–oil weight ratios. Styrene played an important role as a pore-forming agent. The pore size of the MPS particles gradually increased from 1.2 to 20 nm with increasing initial styrene concentration from 12.3 to 36.6 mg mL^{-1} . From the results, it is suggested that the formation of various morphology of MPS particle were obtained depend on the balance between the rate of styrene polymerization, reaction of TMOS and the rate of CTAB micelle formation. If the polymerization of styrene and hydrolysis of TMOS are

slow, relative to the rate of CTAB micelle formation, there is a time for a highly ordered mesostructures particle to develop. However, if the both reactions (i.e, styrene and silica) are relatively fast, the viscosity will increase and the mobility of particle will be restricted before the mesostructures particle can be completely formed. Further, it is confirmed that the emulsion system at a specific condition could form the Winsor-III system and MPS particles with radially oriented structure were produced in the bicontinuous emulsion phase. For further research, this material is expected to be useful for various potential applications, e.g., in drug delivery, adsorption, filtration, and catalyst supports.

3.5 References

1. Zhao, Z.; Wang, X.; Jiao, Y.; Miao, B.; Guo, X.; Wang, G. Facile, low-cost, and scalable fabrication of particle size and pore structure tunable monodisperse mesoporous silica nanospheres as supports for advanced solid acid catalysts. *RSC. Adv.*, 6(11), 9072-9081, **2016**.
2. Ogi, T.; Nandiyanto, A. B. D.; Okuyama, K. Nanostructuring strategies in functional fine-particle synthesis towards resource and energy saving applications. *Adv. Powder. Technol.* 25, 3-17, **2014**.
3. Nandiyanto, A. B. D.; Iskandar, F.; Okuyama, K. Nanosized polymer particle-facilitated preparation of mesoporous silica particles using a spray method. *Chem. Lett.* 37(10), 1040-1041, **2008**.
4. Balgis, R.; Ogi, T.; Wang, W. N.; Anilkumar, G. M.; Sago, S.; Okuyama, K. Aerosol synthesis of self-organized nanostructured hollow and porous carbon particles using a dual polymer system. *Langmuir.* 30(38), 11257-11262, **2014**.
5. Iskandar, F.; Mikrajuddin, A.; Okuyama, K. In Situ Production of Spherical Silica Particles Containing Self-Organized Mesopores. *Nano Lett.*, 1(5), 231-234, **2001**.
6. Beltrán-Osuna, A. A.; Perilla, J. E. Colloidal and spherical mesoporous silica particles: synthesis and new technologies for delivery applications. *J. Sol-Gel Sci. Technol.* 77(2) 480-496, **2016**.
7. Pang, J.; Li, X.; Zhou, G.; Sun, B.; Wei, Y. Fabrication of mesoporous silica nanospheres with radially oriented mesochannels by microemulsion templating for adsorption and controlled release of aspirin. *RSC. Adv.*, 5(9), 6599-6606, **2015**.

8. Yamamoto, E.; Kitahara, M.; Tsumura, T.; Kuroda K. Preparation of Size-Controlled Monodisperse Colloidal Mesoporous Silica Nanoparticles and Fabrication of Colloidal Crystals. *Chem. Mater.*, 26(9), 2927-2933, **2014**.
9. Yamada, H.; Urata, C.; Higashitamori, S.; Aoyama, Y.; Yamauchi, Y.; Kuroda, K. Critical Roles of Cationic Surfactants in the Preparation of Colloidal Mesostructured Silica Nanoparticles: Control of Mesostructure, Particle Size, and Dispersion. *ACS Appl. Mater. Interfaces*. 6(5), 3491-3500, **2014**.
10. Yamada, H.; Ujiie, H.; Urata, C.; Yamamoto, E.; Yamauchi, Y.; Kuroda, K. A multifunctional role of trialkylbenzenes for the preparation of aqueous colloidal mesostructured-mesoporous silica nanoparticles with controlled pore size, particle diameter, and morphology. *Nanoscale.*, 7(46), 19557-19567, **2015**.
11. Binks, B. P. Relationship between microemulsion phase behavior and macroemulsion type in systems containing nonionic surfactant. *Langmuir*. 9, 25-28, **1993**.
12. Hazlett, R. D.; Schechter, R. S. Stability of Macroemulsions. *Colloids Surf.*, 29, 53-69, **1988**.
13. Kahlweit, M.; Strey, R.; Busse, G. Microemulsions: A Qualitative Thermodynamic Approach. *J. Phys. Chem.* 94, 3881-3894, **1990**.
14. Ikari, K.; Suzuki, K.; Imai, H. Structural control of mesoporous silica nanoparticles in a binary surfactant system. *Langmuir*, 22(2), 802-806, **2006**.
15. Blas, H.; Save, M.; Pasetto, P.; Boissière, C.; Sanchez, C.; Charleux, B. Elaboration of Monodisperse Spherical Hollow Particles with Ordered Mesoporous Silica Shells via Dual Latex-Surfactant Templating: Radial Orientation of Mesopore Channels. *Langmuir*, 24(22), 13132-13137, **2008**.
16. Li, W.; Yue, Q.; Deng, Y.; Zhao, D. Ordered Mesoporous Materials Based on Interfacial Assembly and Engineering. *Adv. Mater.*, 25(37), 5129-5152, **2013**.
17. Winsor, P. A. Hydrotropy, solubilisation and related emulsification processes. *Trans. Faraday Soc.* 44, 376-398, **1948**.
18. Nandiyanto, A. B. D.; Kim, S. G.; Iskandar, F.; Okuyama, K. Synthesis of spherical mesoporous silica nanoparticles with nanometer-size controllable pores and outer diameters. *Microporous Mesoporous Mater.* 120(3), 447-453, **2009**.

19. Zhang, M. j.; Wang, W.; Yang, X. L.; Ma, B.; Liu, Y. M.; Xie, R.; Ju, X. J.; Liu, Z.; Chu, L. Y. Uniform Microparticles with Controllable Highly Interconnect Hierarchical Porous Structures. *ACS Appl. Mater. Interfaces.* 7(25), 13758-13767, **2015**.
20. Liu, Q.; DeShong, P.; Zachariah, M. R. One-step synthesis of dye-incorporated porous silica particles. *J. Nanoparticle Res.*, 14(7), 923, **2012**.
21. Gustafsson, H.; Isaksson, S.; Altskar, A. Holmberg, K. Mesoporous silica nanoparticles with controllable morphology prepared from oil-in-water emulsions. *J. Colloid Interface Sci.* 467(4), 253-260, **2016**.
22. Lv, X.; Zhang, L.; Xing, F.; Lin, H. Controlled synthesis of monodispersed mesoporous silica nanoparticles: Particle size tuning and formation mechanism investigation. *Microporous Mesoporous Mater.*, 225, 238-244, **2016**.
23. Du, X.; Qiao, S. Z. Dendritic Silica Particles with Center-Radial Pore Channels: Promising Platforms for Catalysis and Biomedical Applications. *Small.*, 11(4), 392-413, **2015**.
24. Febriyanti, E.; Suendo, V.; Mukti, R. R.; Prasetyo, A.; Arifin, A. F.; Akbar, M. A.; Triwahyono, S.; Marsih, I. N.; Ismunandar. Further Insight into the Definite Morphology and Formation Mechanism of Mesoporous Silica KCC-1. *Langmuir.*, 32(23), 5802-5811, **2016**.
25. Chen, J. He. Fine control over the morphology and structure of mesoporous silica nanomaterials by a dual-templating approach. *Chem. Commun.*, 37, 4422, **2008**.
26. Hyde, E. D. E. R.; Seyfaee, A.; Neville, F.; Moreno-Atanasio, R. Colloidal Silica Particle Synthesis and Future Industrial Manufacturing Pathways: A Review, *Ind. Eng. Chem. Res.*, 55(33), 8891-8913, **2016**.
27. Zhang, K.; Xu, L. L.; Jiang, J. G.; Calin, N.; Lam, K. F.; Zhang, S. J.; Wu, H. H.; Wu, G. D.; Albela, B.; Bonneviot, L.; Wu, P. Facile Large-Scale Synthesis of Monodisperse Mesoporous Silica Nanospheres with Tunable Pore Structure. *J. Am. Chem. Soc.*, 135(7), 2427-2430, **2013**.
28. Schmidt, H. K.; Scholze, H.; Kaiser, A. Principles of hydrolysis and condensation reaction of alkoxysilanes. Part I: Basic investigations on hydrolysis, condensation and densification I. *J. Non-Cryst. Solids.*, 63, 1-11, **1984**.

29. Urata, C.; Aoyama, Y.; Tonegawa, A.; Yamauchi, Y.; Kuroda, K. Dialysis process for the removal of surfactants to form colloidal mesoporous silica nanoparticles. *Chem. Commun.*, 34, 5094, **2009**.
30. Ernawati, L.; Ogi, T.; Balgis, R.; Okuyama, K.; Stucki, M.; Hess, S. C.; Stark, W. J. Hollow Silica as an Optically Transparent and Thermally Insulating Polymer Additive. *Langmuir*. **2016**, 32(1), 338-345.
31. Cai, Q.; Geng, Y.; Zhao, X.; Cui, K.; Sun, Q.; Chen, X.; Feng, Q.; Li, H.; Vrieling, E. G. Morphological classification of mesoporous silicas synthesized in a binary water-ether solvent system. *Microporous Mesoporous Mater.*, 108 (1-3), 123-135, **2008**.
32. Syed, H. K.; Peh, K. K. Identification of phases of various oil, surfactant/co-surfactants and water system by ternary phase diagram. *Acta Pol. Pharm. Drug Res.*, 71(2), 301-309, **2014**.
33. Nallamilli, T.; Binks, B. P.; Mani, E.; Basavaraj, M. G. Stabilization of Pickering Emulsions with Oppositely Charged Latex Particles: Influence of Various Parameters and Particle Arrangement around Droplets. *Langmuir*, 31(41), 11200-11208, **2015**.
34. Chan, H. B. S.; Budd, P. M.; Naylor, T. deV. Control of mesostructured silica particle morphology. *J. Mater. Chem.*, 11(3), 951-957, **2001**.
35. Grosso, D.; Cagnol, F.; de, G. J.; Soler-Illia, A. A.; Crepaldi, E. L., Amenitsch, H.; Brunet-Bruneau, A.; Bourgeois, A.; Sanchez, C. Fundamentals of Mesostructuring Through Evaporation-Induced Self-Assembly. *Adv. Funct. Mater.*, 14(4), 309-322, **2004**.
36. Du, X.; Li, X.; Huang, H.; He, J.; Zhang, X. Dendrimer-like hybrid particles with tunable hierarchical pores. *Nanoscale.*, 7(14), 6173-6184, **2015**.
37. Lee, J. K.; Moon, D. S. Tunable Synthesis of Hierarchical Mesoporous Silica Nanoparticles with Radial Wrinkle Structure. *Langmuir*, 28(33) 12341-12347, **2012**.
38. Lee, J. K.; Moon, D. S. Formation of Wrinkled Silica Mesostructures Based on the Phase Behavior of Pseudoternary Systems. *Langmuir*, 30(51), 15574-15580, **2014**.
39. Mackenzie J. D.; Ulrich, D. R. Ultrastructure processing of advanced ceramics. Wiley, New York, **1988**.

40. Zhao, H.; Xin, Y.; Wang, H.; Zhang, Z.; Liu, S. A Comparison of the Formation of SiO₂ Particles Under the Catalysis of Dodecylamine and Ammonia Solutions. *J. Inorg. Organomet. Polym. Mater.*, 21(4), 925-928, **2011**.
41. Mathew, D. S.; Juang, R. S. Role of alcohols in the formation of inverse microemulsions and Back extraction of proteins/enzymes in a reverse micellar system. *Sep. Purif. Technol.*, 199-215(53), **2007**.
42. Polshettiwar, V.; Cha, D.; Zhang, X.; Basset J. M. High-Surface-Area Silica Nanospheres (KCC-1) with a Fibrous Morphology. *Angew. Chem. Int. Ed.*, 49(50), 9652-965, **2010**.
43. Naik, S. P.; Elangovan, S. P.; Okubo, T.; Sokolov, I. Morphology Control of Mesoporous Silica Particles. *J. Phys. Chem. C.*, 111(30), 11168-11173, **2007**.
44. Drmosh, Q.A.; Gondal, M.A.; Yamani, Z.H.; Saleh, T.A. Spectroscopic characterization approach to study surfactants effect on ZnO₂ nanoparticles synthesis by laser ablation process. *Appl. Surf. Sci.*, 256, 4661-4666, **2010**.

Chapter 4

Role of Acetone in the Formation of Highly Dispersed Cationic Polystyrene Nanoparticle as a Template for Preparing Hollow Silica Nanospheres

4.1 Introduction

Polystyrene (PS) nanoparticles, both anionic and cationic, have attracted much interest owing to their excellent properties such as low density, high hydrophobicity, large specific surface area, good mechanical and chemical stability [1-4]. They have many potential applications as templates, calibration standards, film coatings, ink toners, or polymer fillers, or in chromatographic separation and drug delivery [5-8]. The size and distribution of PS particle are considered to be the most important parameters that succeeded in these applications [9, 10]. Hence, how to synthesize and control highly dispersed PS particles with the size around 50 nm or less becomes a critical issue.

Numerous polymerisation methods, including dispersion, suspension, miniemulsion, microemulsion, and living radical polymerisation, have been used for preparing PS nanoparticles [11-13]. Among these methods, the emulsion method is widely used because of its rapid polymerisation rate, high conversion, and environmental friendly and readily scalable characteristics [14-16]. An emulsion system, to control the stability and to reduce the size of PS particle, high amount of surfactant (up to 20 wt%) and/or emulsifier are often required [17, 18]. It is because of the adsorbed surfactant molecules at the oil-water (O/W) interface which can effectively reduce the O/W interfacial tension, further against the droplet coalescence and increase the emulsion stability. However, the use of high level amount of surfactant is often not acceptable, as it leaves uncommon residues in products and contaminants in the reaction medium which have to be removed. Moreover, particle coagulation also readily occurs during the

emulsion process and becomes the major drawback of this method.

The addition of co-solvents such as alcohols, acetone and some organic solvents into emulsion system also played an important role in controlling formation and size of PS particle [19]. For instance, the synthesis of anionic PS nanoparticles using potassium persulfate as the initiator and acetone/water as the mixture solvent medium was reported for the first time by Okubo and co-workers [20]. Acetone was used to increase the solubility of styrene in the aqueous-phase system. This approach could effectively prevent particle coagulation and generate small PS particles. Subsequent research has enabled the successful preparation of smaller anionic PS particles (50 nm) via a microwave-assisted emulsion polymerisation process [21]. Additionally, a detailed study of the nucleation and growth mechanism of anionic PS particles has been reported [22]. Besides anionic PS nanoparticles, cationic PS particles are as important, particularly as a template material in the design of nanostructures. However, to our knowledge, the synthesis of cationic PS particles with controllable size of less than 50 nm is rarely reported.

The present study reports an improved synthesis route for the preparation of highly dispersed cationic PS nanoparticles as small as 31 nm in diameter by the combined use of acetone/water as the mixture solvent medium and 2,2'-azobis[2-(2-imidazolin-2-yl) propane] dihydrochloride as the cationic initiator. Acetone was selected as a co-solvent because of its rapid diffusion characteristic and ability to promote the formation of small droplets in an emulsion system. 2,2'-Azobis[2-(2-imidazolin-2-yl) propane] dihydrochloride was used to control both the surface charge and size of the particles. Additionally, as prepared PS particle was used as template for preparing hollow silica particle. The present research is expected to be useful for the improvement of particle technology, especially concerned to the fields of chemical and material engineering.

4.2 Experimental

4.2.1 Raw materials

Monomer styrene (99%, Kanto Chemical Co., Inc., Japan) was purified using sodium hydroxide (NaOH) prior to use. Cationic initiator 2,2'-azobis[2-(2-imidazolin-2-yl) propane] dihydrochloride (VA-044; 99%) was obtained from Wako Pure Chemical

Industries, Ltd. (Japan). Acetone (99%, Kanto Chemical Co., Inc.) and ultra-pure water were used as a mixture solvent medium without further purification.

4.2.2 Preparation of cationic PS nanoparticle

The reaction set-up consisted of a 300-mL three-neck round-bottom flask equipped with a stirrer (the rotation speed was adjusted to 700 rpm), a reflux condenser, a heating jacket to control the temperature, a temperature controller, and a nitrogen (N₂) gas source. The polymerisation process was performed as follows. Ultra-pure water and acetone at known compositions were introduced into the reactor vessel and heated at 60°C under N₂ atmosphere for 30 min. After the reaction temperature and oxygen-free conditions were attained, styrene and VA-044 were added simultaneously. The acetone-to-water mass ratio and VA-044 concentration were varied from 0 to 2.33 and 0.0048 to 0.0193 mol L⁻¹, respectively. The reaction time was varied from 2 to 14 h. Other parameters i.e., styrene concentration and reaction temperature were maintained at 9.24 mol L⁻¹ and 60°C, respectively. The polymerisation conditions are given in Table 1. After polymerisation, acetone was removed by heating at 60°C for 3 h. The samples were then dried in a vacuum oven at 60 °C overnight prior to calculating total solid content (TSC).

4.2.3 Characterizations

The morphology of prepared particles was observed by scanning electron microscopy (SEM; Hitachi S-5000, Japan; operating at 20 kV) and transmission electron microscopy (TEM; JEM-3000F, JEOL, Japan; operating at 300 kV). To obtain the average diameter and size distribution of the particles, more than 200 particles ($\Sigma n_i = 200$) were statistically examined. The hydrodynamic diameter (D_h) distribution of PS particles was determined using dynamic light scattering (DLS). For the measurement, colloidal PS particle suspensions were diluted with deionised water and sonicated for 1 h at room temperature. The zeta potential (ζ) of the particles was measured on a Zetasizer (Malvern Instruments, Nano ZS, UK). The surface tension of PS particles in colloidal solution was measured using a surface tensiometer (KF14001139, Japan; operating at 100 V). Hence, for the measurement of surface tension, the use of VA-044 initiator was negligible.

4.3 Results and discussions

4.3.1 Influence of acetone/water mass ratio on PS particle sizes

The effect of the acetone-to-water mass ratio on the surface charge of the PS nanoparticles was examined by measuring the zeta potential of the PS samples. PS particles with zeta potentials of approximately +43 to +47 mV, were obtained for the PS samples prepared with varying acetone-to-water mass ratios as given in **Table 4.1**.

Table 4.1 Polymerization conditions employed for synthesis of cationic polystyrene particles

Sample	C_{VA-044}^a (mol L ⁻¹)	Acetone/ water mass ratio	VA-044/ styrene mass ratio	Reaction time (h)	R_h (DLS) (nm)	D_p (SEM) (nm)	Zeta potential (ζ) (mV)	TS C ^b wt. %
CPS1	0.0064	0	0.055	8	330	272	+43	7.4
CPS2	0.0064	0.28	0.055	8	192	163	+45	6.4
CPS3	0.0064	0.67	0.055	8	101	88	+46	4.1
CPS4	0.0064	1.04	0.055	8	47	35	+47	3.6
CPS5	0.0064	1.50	0.055	8	44	31	+48	2.4
CPS6	0.0064	1.86	0.055	8	-	coagulated	+46	-
CPS7	0.0064	2.33	0.055	8	-	coagulated	+47	-
CPS8	0.0064	> 2.33	0.055	8	-	no particle	+47	-
CPS9	0.0064	1.04	0.055	2	41	32	+45	0.6
CPS10	0.0064	1.04	0.055	4	43	33	+46	1.5
CPS11	0.0064	1.04	0.055	6	44	34	+48	3.2
CPS12	0.0064	1.04	0.055	10	46	42	+47	3.7
CPS13	0.0064	1.04	0.055	12	48	45	+48	3.8
CPS14	0.0064	1.04	0.055	14	55	48	+49	3.9
CPS15	0.0048	1.50	0.041	8	coagulated	coagulated	+41	-
CPS16	0.0091	1.50	0.077	8	46	33	+46	2.2
CPS17	0.0128	1.50	0.112	8	47	35	+48	2.3
CPS18	0.0193	1.50	0.167	8	48	37	+49	2.4

The concentration of styrene was kept constant at 9.24 mol L⁻¹. ^a Initial concentration of VA-044 initiator in mixture solution system. ^b TSC was determined using a gravimetric method and calculated as follows

$$W_1$$

where W_1 and W_2 are the weights of the dried and wet PS samples, respectively.

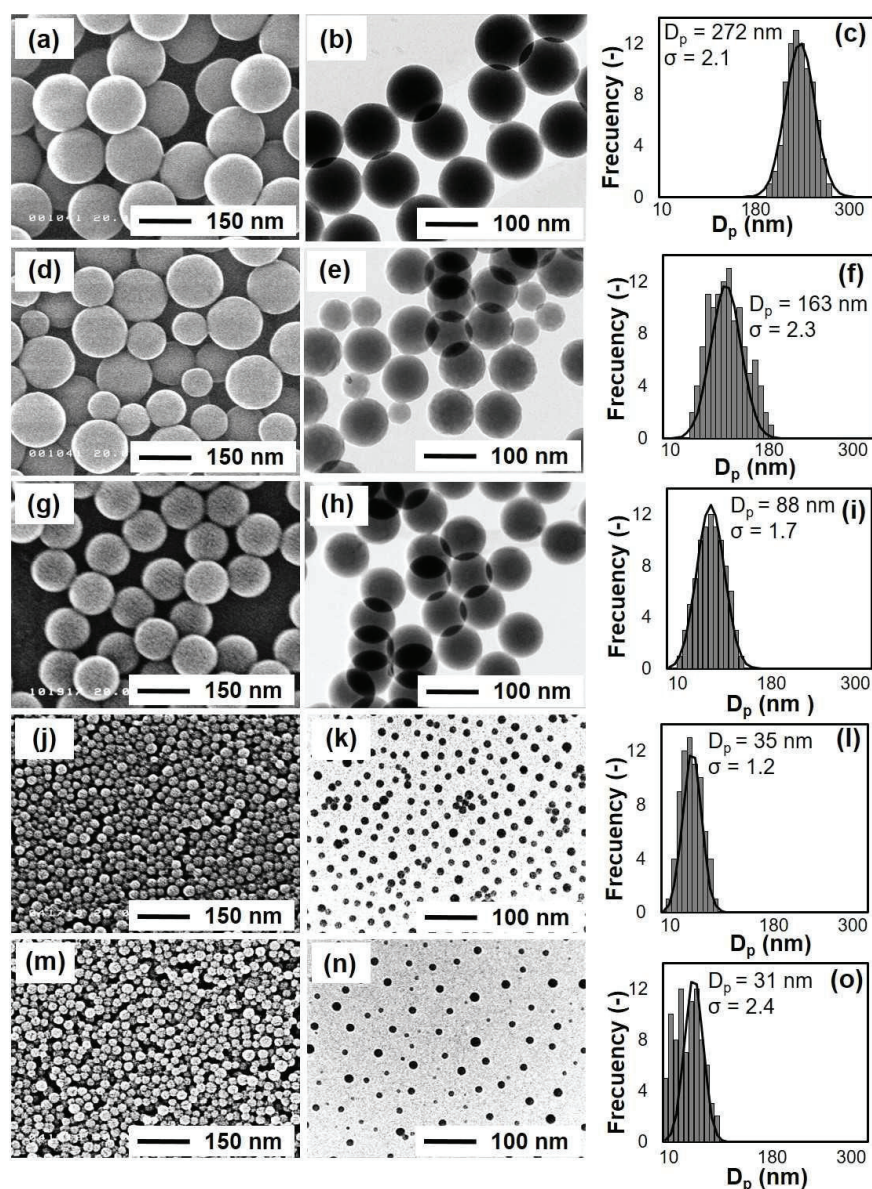


Figure 4.1 SEM and TEM images, and size distribution profiles of the PS particles prepared at different acetone/water mass ratios of (a, b, c) 0, (d, e, f) 0.28, (g, h, i) 0.67, (j, k, l) 1.04, and (m, n, o) 1.50. Other parameters were kept constant: VA-044 initiator-to-styrene mass ratio, 0.055; reaction temperature, 60°C.

As shown in **Figure 4.1**, large cationic PS particle of ~272 nm was obtained in the absence of acetone. The particle size could be significantly reduced to 31 nm when the acetone-to-water mass ratio was increased to 1.50. It is well known that high-polarity solvents, such as acetone, can form small droplets owing to rapid diffusion of the solvent. The emulsion droplets formed upon addition of the styrene monomer to the acetone/water

mixture solvent medium. Acetone quickly diffused and spread into the styrene monomer, subsequently leading to rupture of styrene into small droplets. Assume that one PS particle is formed in each emulsion droplet, the particles shrink after evaporation of acetone, resulting in the formation of PS nanoparticles. Thus, a good correlation between the initial droplet size and final size of the PS particles can be expected.

4.3.2 Plausible formation mechanism of PS particle influenced by acetone addition

The role of acetone on the formation of cationic PS nanoparticles is illustrated in **Figure 4.2**.

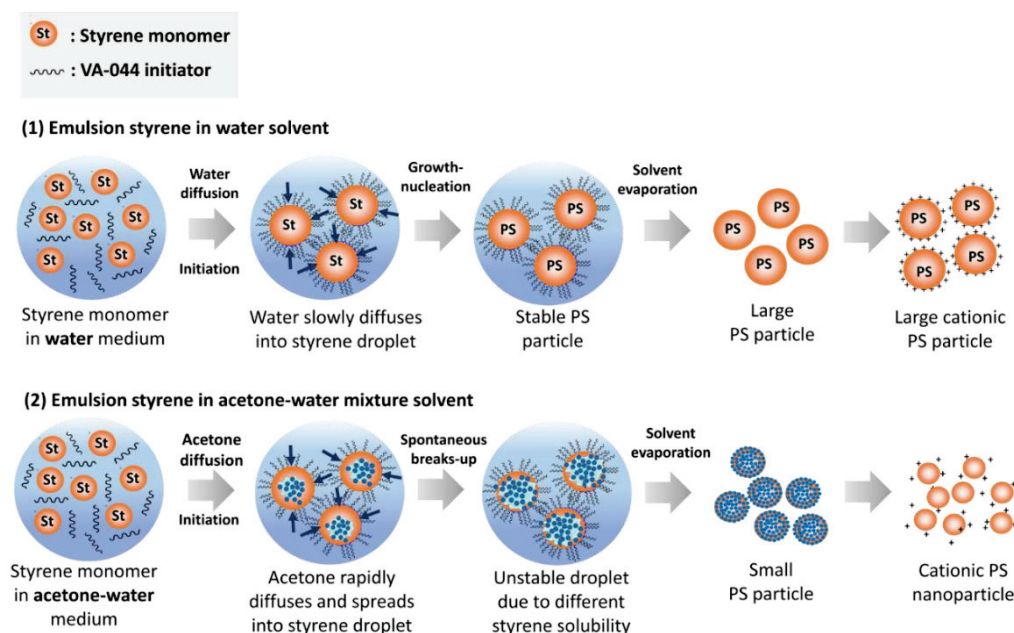


Figure 4.2 Schematic formation of the cationic PS nanoparticles influenced by differences in the diffusion rate of acetone in the emulsion system.

The solvent diffusion phenomenon, which causes spontaneous rupture of droplets, depends on the mass ratio of acetone to water. In the presence of water medium only, droplet rupture is slower owing to the slower diffusion rate of water (when compared with that of acetone), thereby resulting in the formation of large droplets. In contrast, when acetone is added to the emulsion system, emulsion droplets can readily break into small droplets owing to rapid diffusion of acetone. Based on the proposed mechanism in **Figure 4.2**, rapid diffusion of acetone, which promotes the formation of cationic PS nanoparticles with diameter of 31 nm, was successfully attained when the mass ratio of acetone to water

was 1.50 (**Figure 4.1 (m, n)**). In contrast, when the mass ratio of acetone to water was greater than 1.50, particle coagulation occurred (**Figure 4.3 (a, b)**).

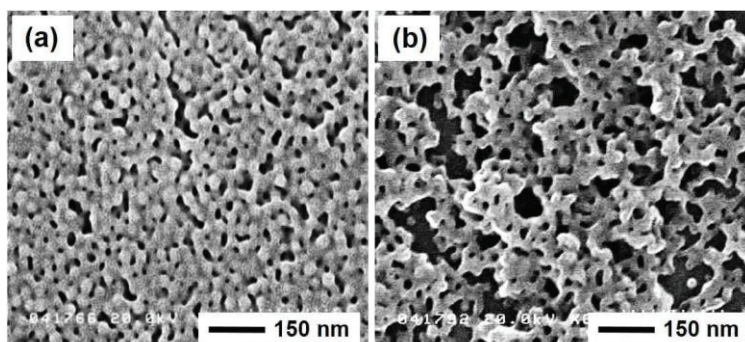


Figure 4.3 SEM images of the PS particles prepared at different acetone/water mass ratios of (a) 1.86, and (b) 2.33. Other parameters were kept constant: styrene and VA-044 initiator concentrations, 9.24 and 0.15 mol L⁻¹, respectively; reaction temperature, 60 °C, and reaction time, 8h.

The coagulated PS particles was observed at acetone-to-water mass ratios of 1.86 and 2.33, occurred because the equilibrium solubility of styrene was surpassed. Furthermore, the increase in the diffusion of acetone, while the amount of styrene monomer was constant, likely led to increased particle collision events and gelling effects. Further increases in the acetone-to-water mass ratios to above 2.33 did not generate any PS nanoparticles. Styrene monomers tend to dissolve in acetone rather than in aqueous phase, thereby accelerating the diffusion process. Consequently, the formation of particle nuclei becomes difficult because of the imbalance in the hydrophobic and hydrophilic properties of the different solvents involved in the system. As noted, the droplet size was mainly influenced by the acetone/water composition, diffusion and shrinkage processes. The size of PS particles could be adjusted by controlling the mass ratio of the acetone/water mixture solvent. With increasing acetone contents, the diffusion of acetone becomes rapid and the extent of shrinkage of the particle becomes greater owing to the evaporation of more acetone molecules. Both processes synergistically reduce the diameter of PS particles.

In the present system, the rapid diffusion of acetone has important roles in instigating spontaneous droplet break-up and preventing particle re-coalescence, thereby generating PS nanoparticles. However, the balanced mass ratio between acetone and water should be properly maintained; excessive amounts of acetone will result in increased

supersaturation of styrene, thus impeding the subsequent growth and nucleation of emulsion droplets, consequently impeding the formation of PS nanoparticles. Moreover, as previously reported [31-33], the effect of interfacial phenomena during diffusion contributes to the formation of nanoparticles. In this work, a similar trend was observed as represented by the effect of increasing acetone-to-water mass ratios on the solubility of styrene and the reduction of surface tension.

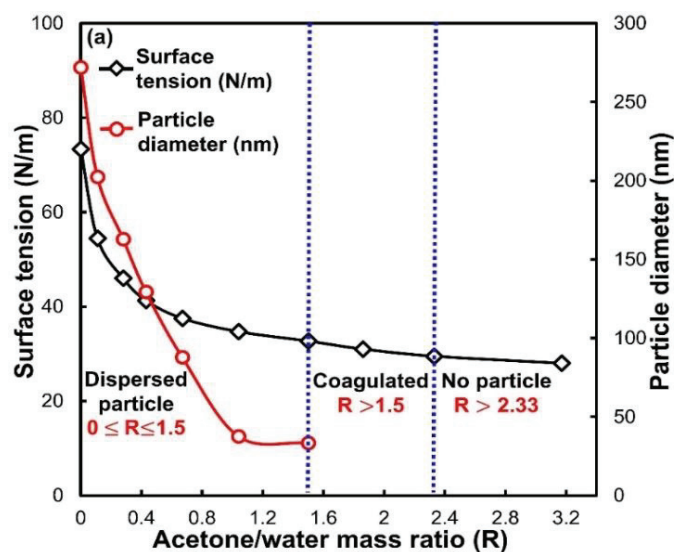


Figure 4.4 Influence of the acetone/water composition on the average diameter of the PS particles and surface tension of the emulsion system.

Figure 4.4 shows that a high acetone content reduced the surface tension of the emulsion system, consequently inducing a reduction in the particle size. (The surface tension of acetone is lower than that of water). Specifically, when the acetone-to-water mass ratio was 1.50, a low interfacial tension of 32.73 N m^{-1} was attained. As the interfacial tension of the aqueous phase was decreased further by increasing the content of acetone, the affinity and/or electrostatic force between the initiator and the PS particle surface was not as high as the affinity among the initiator molecules. Consequently, the initiator molecules were loosely packed on the PS particle surface, and the degree of particle dispersion became high owing to the enhanced solubility of styrene, thereby promoting the formation of PS nanoparticles. The correlation between acetone/water compositions and solubility of styrene was evaluated by Hansen solubility parameters, (see **Table 4.2**).

Table 4.2 Hansen solubility parameter values of acetone, water and styrene

Solvent	δ_d (Mpa) ^{1/2}	δ_p (Mpa) ^{1/2}	δ_h (Mpa) ^{1/2}	δ (Mpa) ^{1/2}
Acetone	15.5	10.4	7.0	19.9
Water	15.5	16.0	42.3	47.8
Styrene	9.1	0.5	2.0	9.3

A. Lafaurie, et al., *Adv. Powder Technol.*, 192, 92-98, 2009

In this case, changing acetone/water mass ratio affect to the surface tension and solubility of styrene, which was evaluated by using the model established by Beerbower

$$\text{et. al : } \Sigma \delta^2 = \delta_d^2 + 0.632\delta_p^2 + 0.632\delta_h^2 = 13.9 \left(\frac{1}{V_m} \right)^{1/3} \gamma_L \quad (\text{for non-alcohols}) \quad (1)$$

The experimental data were then linearly fitted using the model established by Koenhen

$$\text{and Smolders: } \Sigma \delta^2 = \delta_d^2 + \delta_p^2 = 13.5 \left(\frac{1}{V_m} \right)^{1/3} \gamma_L \quad (\text{for all substances}) \quad (2)$$

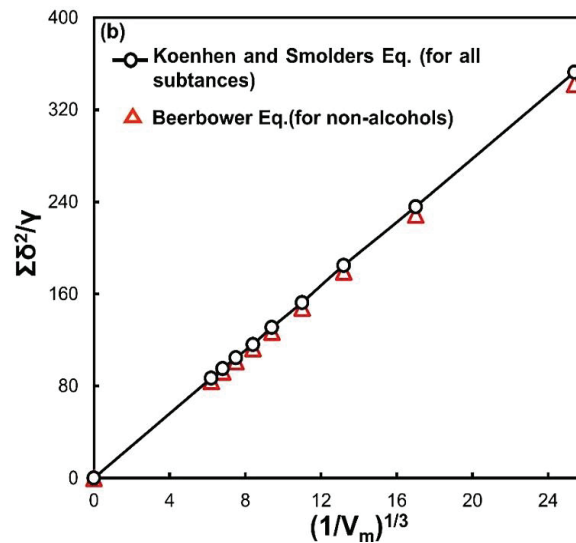


Figure 4.5 Correlation between the acetone/water composition to the surface tension and the solubility parameter of styrene in the mixture solvent system calculated using Beerbower model (1971) and fitted using Koenhen-Smolders equation model (1975).

The solubility parameter values represent the relative solvency behaviour of a specific solvents. The solvents with similar solubility parameters will be able to interact with each other, resulting in solvation, miscibility or swelling. It can be explained that acetone dissolves styrene, then one might expect the styrene to be soluble in neighboring solvents with increasing acetone concentration, like acetone and water, since these

solvents have similar internal energies. As deduced from these calculations, increasing the acetone-to-water mass ratio increased the solubility of styrene and reduced the interfacial tension of the solution system simultaneously. Furthermore, it enabled the formation of a homogenous mixture emulsion system and an increased number of particle nuclei, while preventing aggregation and coagulation among the particles, consequently leading to the formation of small PS particles.

4.3.3 Influence of VA-044 initiator concentration on PS particle sizes

The effect of VA-044 concentration on the average size and zeta potential of the prepared PS particles was evaluated. The results are given in **Figure 4.6**.

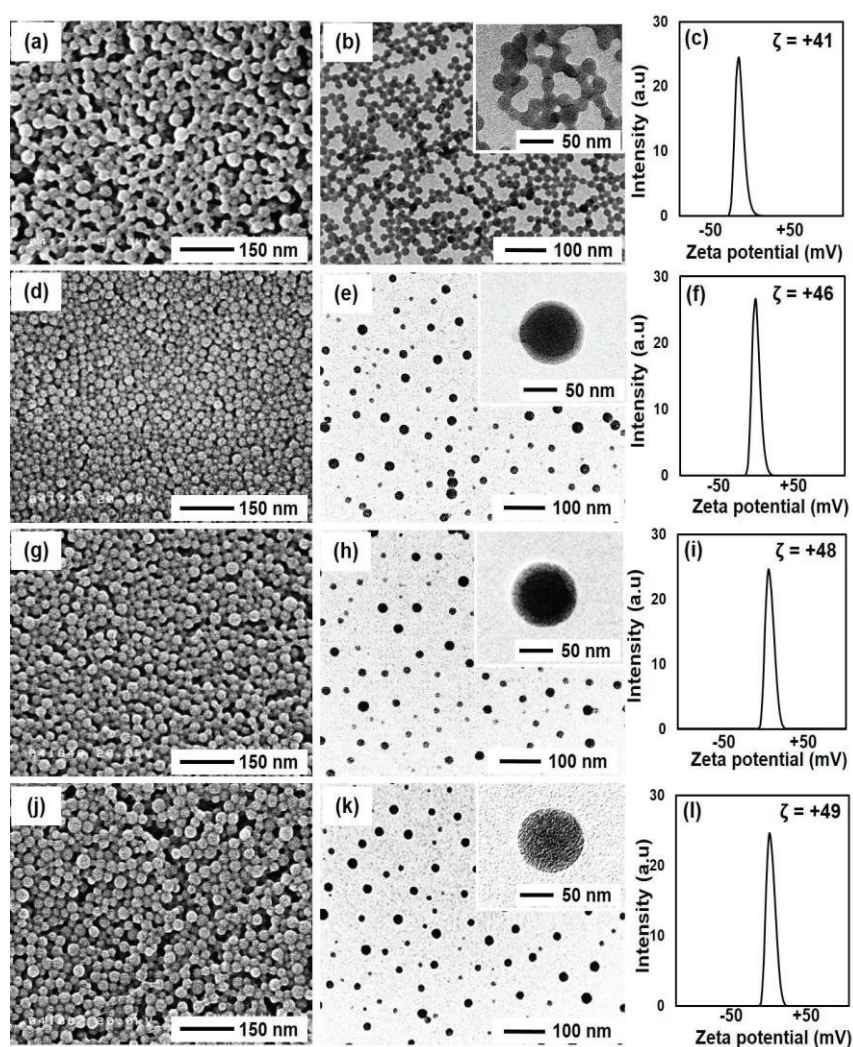


Figure 4.6 SEM and TEM images, and zeta potential distribution (ζ) of the PS particles prepared at various VA-044 concentrations of (a, b, c) 0.0048, (d, e, f) 0.0091, (g, h, i)

0.0129, and (j, k, l) 0.0193 mol L⁻¹. Other parameters were kept constant: acetone/water mass ratio, 1.50; styrene, 9.24 mol L⁻¹; reaction temperature, 60°C.

As observed in **Figure 4.6**, the VA-044 concentration had a slight effect on the particle size. The size of PS particles increased slightly from 33 to 37 nm with increasing VA-044 concentrations from 0.0091 to 0.0193 mol L⁻¹. As reported, the formation of considerably larger PS particles is expected by increasing the VA-044 concentration. However, the trend obtained herein differed from that previously reported using excessively high VA-044 concentrations and did not have a significant effect on the size of the particles; only a small difference in the particle size was observed. This result indicated that when a high VA-044 concentration was used, both the consumption and initiation rates of the styrene monomers increased simultaneously. As the amount of styrene monomers was constant, the number of styrene units that could be attacked by the initiator was limited by the solubility of the monomer itself. This promoted the uncontrolled formation of free-radical initiators, thereby generating particle nuclei. In contrast, using excessively low VA-044 concentrations cause the formation of necked PS particles as shown in **Figure 4.6 (a)**. This is due to the low initiation and consumption rates of the styrene monomers in the emulsion system. Likewise, the zeta potential of PS particles increased slightly from +41 to +50 mV with increasing VA-044 concentrations. This result implied that the presence of VA-044 initiator stabilised the emulsion system by a combined electrostatic and attractive force mechanism. To investigate the effect of increasing VA-044 concentrations on the stability of PS particles, D_h of PS particles in aqueous medium was evaluated as shown in **Figure 4.7**.

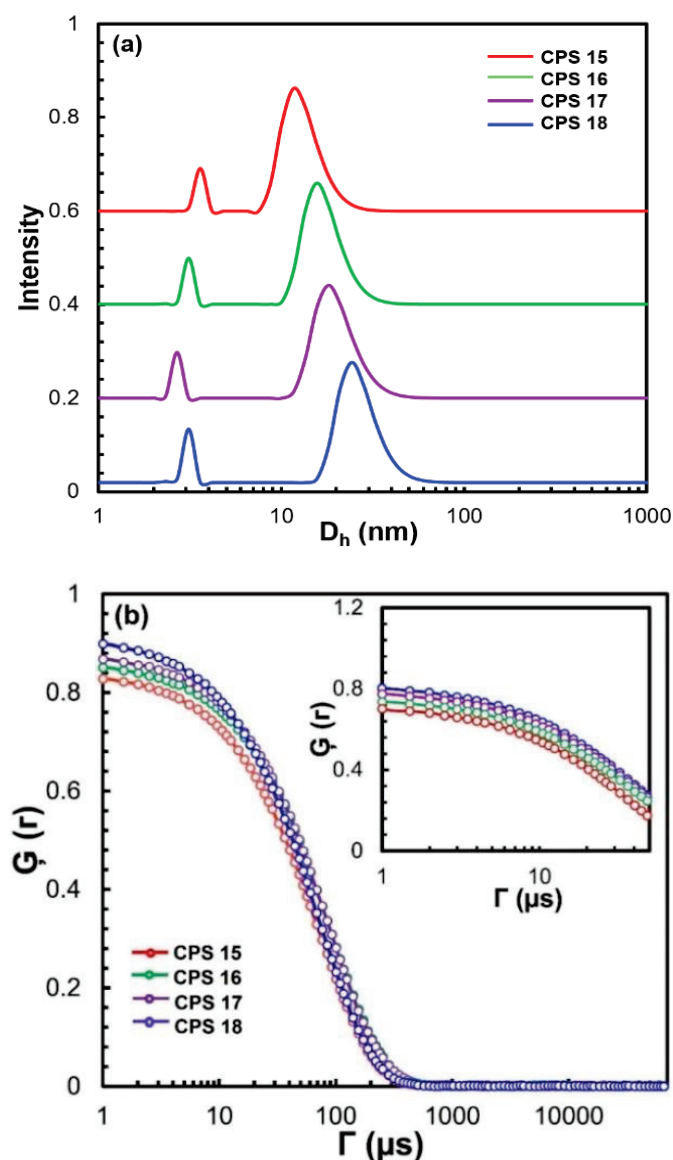


Figure 4.7 (a) Hydrodynamic diameter (D_h) distributions of the colloidal PS particles measured by DLS. (b) Force at distance, of the colloidal PS particles as a function of lag time, (r). The inset shows an enlarged view at the shorter lag-time intervals.

Figure 4.7 (a) shows that the D_h of cationic PS nanoparticles, as measured by DLS, was ~ 50 nm. The diameter of the particles, as measured by SEM, was 30 nm. The smaller size determined by SEM was related to the shrinkage of the particles upon drying for the measurement. The principle of DLS for D_h particle measurement depends on the measuring of fluctuation intensity caused by interference of laser light that is scattered by diffusing particles. The evolution time of these fluctuations depends on the particle movement caused by Brownian motion, as well as the size of particle. Hence, it is possible

to observe the correlation between the force at distance, $G(r)$, of colloidal PS particles and lag time, (r) . Force at distance is also referred to as the first-order autocorrelation function $G(r)$. This parameter describes temporal aggregated formation and/or coagulation of particles in a particular orientation within scattering light. At short time, the system is nearly stationary and the value of the correlation function is approximately equal to unity (1). Due to the random nature (i.e., Brownian motion effect), at longer time, the force appeared in the system, meaning that the system with the initial state approaches zero. On the other hand, lag time (r) describes the required time to reach a steady-state of particle size distribution (PSD) which is determined as a function of the relative rates of coagulation. Herein, the intensity of $G(r)$ represents the degree of interaction between interfacial PS particles in the colloidal system that is controlled by regulating the VA-044 concentration. As observed in Fig. 6(b), at short lag times ($<50 \mu\text{s}$), the $G(r)$ intensity changed slightly with increasing VA-044 concentrations from 0.0048 to 0.0193 molL^{-1} (inset of **Figure 4.7 (b)**). This result revealed that by using VA-044 initiator, the nucleation and growth rates of particles could be greatly suppressed, thereby affording control over the formation of smaller PS particles without any coagulation. This result agreed with the results of previous reports. The authors reported high electron density and strong hydration capabilities of VA-044 initiator that resulted in weak adsorption between particle interfaces. Thus, VA-044 initiator has potential in preventing the formation of large particles through coagulation.

4.3.4 Influence of reaction time on the yield and PS particle size

The effect of reaction time on the size of PS particles was evaluated, and the results are shown in **Figure 4.8**.

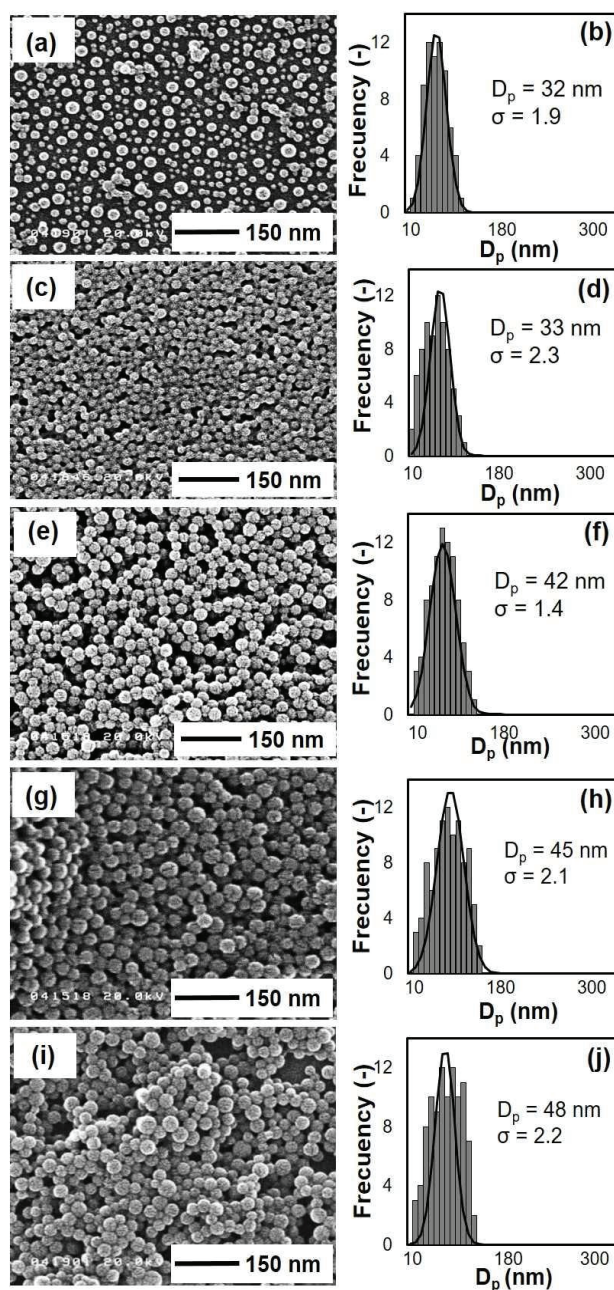


Figure 4.8 SEM images and associated size distribution profiles of the PS particles prepared under different reaction times of (a, b) 2, (c, d) 4, (e, f) 10, (g, h) 12, and (i, j) 14 h. Other reaction parameters were kept in constant: acetone/water and VA-044 initiator-to-styrene mass ratio, 1.04 and 0.055, respectively, reaction temperature, 60°C.

Figure 4.8 shows that the size of PS particles increased slightly from 32 to 48 nm when the reaction time increased from 2 to 14 h. The PS particles grew continuously during the early stages of the reaction (2-8 h), after which the growth rate became steady. These results revealed that as the reaction time increased, the monomer concentration in the emulsion system decreased continually as it was converted into an oligomer and a polymer. The growth of PS particles decreased slowly, and then stopped. Using a short reaction time of 2 h produced small PS particles of ~32 nm in size. PS nanoparticles with controllable sizes less than 50 nm were also obtained when the reaction time was increased from 8 to 14 h (Table 1). This result shows that the reaction time is important for controlling the size of PS particles. Based on the DLS results, the size of PS particles could be controlled to less than 60 nm even under prolonged polymerisation ($t=4$ h).

4.3.5 Synthesis of hollow silica using different sizes of PS particle

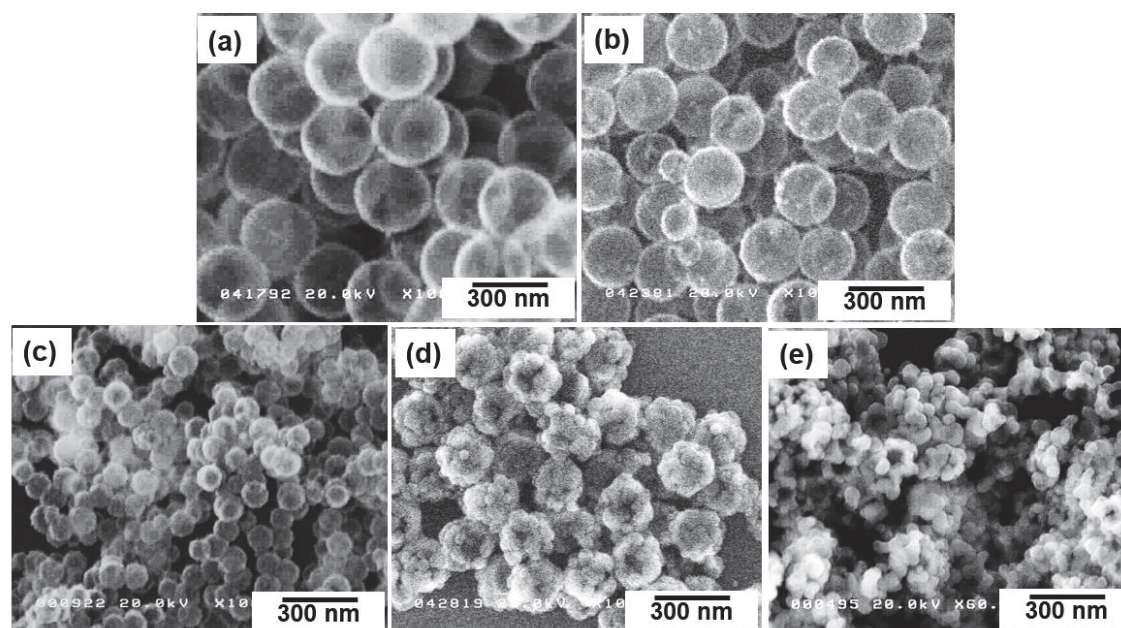


Figure 4.9 SEM images of hollow silica particles prepared with different PS diameter of: (a) 272, (b) 163, (c) 88, (d) 35, and (e) 31 nm. The molar ratio of $\text{NH}_4\text{OH}/\text{MeOH}$ and TMOS concentration were kept at 0.055 and 0.015 molL^{-1} , respectively. Detail synthesis condition was summarized in **Table 4.3**.

Table 4.3 Synthesis condition of hollow silica particle prepared under different PS particle sizes

PS size [nm]	PS conc. [mg mL ⁻¹]	TMOS conc. [mol L ⁻¹]	MeOH conc. [mg mL ⁻¹]	Hollow size [nm]
272	0.97	0.04	0.78	195
163	0.84	0.04	0.76	144
88	0.75	0.04	0.76	71
35	0.47	0.04	0.81	aggregated
31	0.47	0.04	0.81	aggregated

Total amount of precursor solution is 79 mL, NH₄OH concentration 0.05 mg mL⁻¹. Reaction temperature at 40°C, reaction time 285 min.

PS particles with different sizes from 272, 163, 88, 35 and 31 nm, were employed as a template to prepare hollow silica particle. In all cases, the concentration of the PS templates in the reactant solutions was fixed at 1.2 wt %. Hollow silica spheres with smooth surface were successfully formed, when cationic PS particle with the sizes of 272, 163 and 88 nm were used, as shown in **Figure 4.9 (a-c)**. On the contrary, hollow silica particle could not be obtained when PS particle with diameter smaller than 80 nm was used as template. It can be explained that the deposition of silica on the PS surface occurs competitively with homogenous nucleation of PS nanoparticle during the reaction. However, the silica shells tend to collapse, due to insufficient template size can be deposited by the silica. As the results, irregular and aggregated silica particles were obtained, after PS removal. It is confirmed that the prepared PS nanoparticle is not effective as template for preparing smaller hollow silica.

4.4 Conclusions

Highly dispersed cationic PS nanoparticles were successfully synthesised via a modified emulsion polymerisation method. Specifically, the combined use of VA-044 initiator and acetone/water mixture solvent enabled the preparation of cationic PS nanoparticles with enhanced stability and controllable sizes of ~31 nm. Moreover, highly dispersed cationic PS nanoparticles could be obtained using high styrene concentrations without any added surfactant. The optimum polymerisation condition was achieved by using VA-044 initiator concentration of 0.0064 mol L⁻¹, acetone-to-water mass ratio of 1.50, reaction time of 8 h, styrene concentration of 9.24 mol L⁻¹, and reaction temperature

of 60°C. The addition of acetone increased the solubility of styrene and reduced the surface tension between the PS particle surface and aqueous phase. Additionally, rapid diffusion of acetone contributed to the formation of small droplets in the emulsion system, further enabling the formation of PS nanoparticles. The VA-044 initiator could effectively control the stability of both the surface charge and size of PS particles. This study provides important insights and a new methodology for further research and application, especially for preparing polymer nanoparticles via a convenient, low-temperature, and chemical handling process.

4.5 References

1. Abadi A.R.S., Darabi A., Jessop P.G. Cunningham M.F. Preparation of redispersible polymer latex using cationic stabilizers based on 2-dimethylaminoethyl methacrylate hydrochloride 2,2'-azobis [2-(2-imidazolin-2 yl)-propane] dihydrochloride. *J. Polym.*, 60(1), 18, **2015**.
2. Balgis R., Anilkumar G.M., Sago S., Ogi T., Okuyama K., Nanostructured design of electrocatalyst support materials for high-performance PEM fuel cell application. *J. Power Sources*, 203, 26-33, **2012**.
3. Balgis R., Ogi T., Wang W. N., Anilkumar G. M., Sago S., Okuyama K. Aerosol synthesis of self-organized nanostructured hollow and porous carbon particles using a dual polymer system. *Langmuir*, 30(38), 11257-11262, **2014**.
4. Beerbower A. Surface free energy: A new relationship to bulk energies. *J. Colloid Interface Sci.* 35 (1), 126-132, **1971**.
5. Camli S.T., Buyukserin F., Balci O., Budak G.G. Size controlled synthesis of sub-100 nm poly(methylmethacrylate) nanoparticles using surfactant-free emulsion polymerization. *J. Colloid Interface Sci.*, 344(2), 528-532, **2010**.
6. Chou C., Chiu W.Y. Novel Synthesis of Multi-Scaled, surfactant-free monodisperse latexes via alcoholic dispersion polymerization in a mixed ionic-nonionic initiation system. *Macromolecules*, 46(9), 3561-3569, **2013**.
7. Chou I. C., Chen S. I., Chiu W. Y. Surfactant-free dispersion polymerization as an efficient synthesis route to a successful encapsulation of nanoparticles. *RSC Adv.*, 4(88), 47436-47447, **2014**.

- 8 Ernawati, L., Ogi T., Balgis R., Okuyama K., Stucki M., Hess S. C., Stark W.J. Hollow silica as an optically transparent and thermally insulating polymer additive. *Langmuir*, 32(1), 338-345, **2016**.
- 9 Ganachaud F., Katz J.L. Nanoparticles and nanocapsules created using the ouzo effect: spontaneous emulsification as an alternative to ultrasonic and high-shear devices. *Chem. PhysChem*, 6 (2), 209-216, **2005**.
- 10 Gradon L., Janeczko S., Abdullah M., Iskandar F., Okuyama K. Self-organization kinetics of mesoporous nanostructured particle. *AIChE J.*, 50(10), 2583-2593, **2004**.
- 11 Hansen C.M. The universality of the solubility parameter. *Ind. Eng. Chem. Prod. Res. Dev.*, 8(1), 2-11, **1969**.
- 12 Hirschle P., Prei T., Auras F., Pick A., Völkner J., Valdepérez D., Witte G., Parak W. J., Rädler J. O., Wuttke S. Exploration of MOF nanoparticle sizes using various physical characterization methods is what you measure what you get. *Cryst. Eng. Comm.*, 18(23), 4359-4368, **2016**.
- 13 Horn D., Rieger J. Organic nanoparticles in the aqueous phase-theory, experiment, and use. *Angew. Chem. Int. Ed.*, 40(23), 4330-4361, **2001**.
- 14 Ishii H., Ishii M., Nagao D., Konno M. Advanced synthesis for monodisperse polymer nanoparticles in aqueous media with sub-millimolar surfactants. *Polymer*, 55(12), 2772-2779, **2014**.
- 15 Ito F., Ma G., Nagai M., Omi S. Study of particle growth by seeded emulsion polymerization accompanied by electrostatic coagulation. *Colloids Surf. Physicochem. Eng. Asp.* 201(1), 131-142, **2002**.
- 16 Kim, G., Lim, S., Lee, B.H., Shim, S.E., Choe, S. Effect of homogeneity of methanol/water/monomer mixture on the mode of polymerization of MMA: Soap-free emulsion polymerization versus dispersion polymerization. *Polymer*, 51, 1197-1205, **2010**.
- 17 Lee S.Y., Gradon L., Janeczko S., Iskandar F., Okuyama K. Formation of highly ordered nanostructures by drying micrometer colloidal droplets. *ACS Nano*, 4(8), 4717-4724, **2010**.

- 18 Legrand P., Lesieur S., Bochet A., Gref R., Raatjes W., Barratt G. Influence of polymer behaviour in organic solution on the production of polylactide nanoparticles by nanoprecipitation. *Int. J. Pharm.*, 344, 33-43, **2007**.
- 19 Li Zh., Cheng Z., Han H.C. C. Mechanism of narrowly dispersed latex formation in a surfactant-free emulsion polymerization of styrene in acetone-water mixture, *Macromolecules*, 45(7), 3231-3239, **2012**.
- 20 Okubo M., Yamada A., Shibao S., Nakamae K., Matsumoto T. Studies on suspension and emulsion. XLVI. Emulsifier-free emulsion polymerization of styrene in acetone-water, *J. Appl. Polym. Sci.*, 26(5), 1675-1679, **1981**.
- 21 Li L., Zhai T., Zeng H., Fang X., Bando Y., Golberg D. Polystyrene sphere-assisted one-dimensional nanostructure arrays: synthesis and applications. *J Mater. Chem.*, 21(1), 40-56, **2011**.
- 22 Liu B., Zhang M., Cheng H., Fu Z., Zhou T., Chi H., Zhang H. Large-scale and narrow dispersed latex formation in batch emulsion polymerization of styrene in methanol-water solution. *Colloid Polym. Sci.*, 292(2), 519-525, **2014**.
- 23 Liu B., Sun S., Zhang M., Ren L., Zhang H. Facile synthesis of large scale and narrow particle size distribution polymer particles via control particle coagulation during one-step emulsion polymerization. *Colloids Surf. Physicochem. Eng. Asp.*, 484(2), 81-88, **2015**.
- 24 Liu Q., Li Y., Duan Y., Zhou H. Research progress on the preparation and application of monodisperse cationic polymer latex particles. *Polym. Int.*, 61(11), 1593-1602, **2012**.
- 25 Liu Q., Tang Z., Zhou Z., Zhou H., Liao B., Shen S., Chen L. A novel route to prepare cationic polystyrene latex particles with monodispersity, *J. Macromol. Sci.* 51(4), 271-278, **2014**.
- 26 Maiti A., Mc Grother S. Bead-bead interaction parameters in dissipative particle dynamics: Relation to bead-size, solubility parameter, and surface tension. *J. Chem. Phys.*, 120(3), 1594, **2004**.
- 27 Nandiyanto A.B.D., Iskandar F., Okuyama. K. Nanosized polymer particle-facilitated preparation of mesoporous silica particles using a spray method. *Chem. Lett.*, 37(10), 1040-1041, **2008**.

- 28 Nandiyanto A.B.D., Suhendi A., Ogi T., Iwaki T., Okuyama K. Synthesis of additive-free cationic polystyrene particles with controllable size for hollow template applications. *Colloids Surf. Physicochem. Eng. Asp.*, 396, (96-105), **2012**.
- 29 Nandiyanto A.B.D., Suhendi A., Ogi T., Umemoto R., Okuyama K. Size and charge controllable polystyrene spheres for templates in the preparation of porous silica particle with tunable internal hole configurations. *Chem. Eng. J.*, 256, 421-430, **2014**.
- 30 Natu A.M., Wiggins M., Van De Mark M.R. Synthesis and characterization of cationic colloidal unimolecular polymer (CUP) particles. *Colloid Polym. Sci.*, 293(4), 1191-1204, **2015**.
- 31 Ngai T., Wu C. Double roles of stabilization and destabilization of initiator potassium persulfate in surfactant-free emulsion polymerization of styrene under microwave irradiation, *Langmuir*, 21(18), **2005**.
- 32 Ogi T., Nandiyanto, A. B. D., Okuyama, K. Nanostructuring strategies in functional fine-particle synthesis towards resource and energy saving applications. *Adv. Powder. Technol.* 25, 3-17, **2014**.
- 33 Koenhen D. M., Smolders C. A. Determination of solubility parameters of solvents and polymers by means of correlations with other physical quantities. *J. Appl. Polym. Sci.*, 19(4), 1163-1179, **1975**.
- 34 Rao J. P., Geckeler K. E. Preparation techniques and size-control parameters. *Prog. Polym. Sci.*, 36(7), 887-913, **2011**.
- 35 Shibuya D., Nagao H., Ishii., Konno M. Advanced soap-free emulsion polymerization for highly pure, micron-sized, monodisperse polymer particles. *Polymer*, 55(2), 535-539, **2014**.
- 36 Sood A. Particle size distribution control in emulsion polymerization. *J. Appl. Polym. Sci.*, 92(5), 2884-2902, **2004**.

Chapter 5

Summary

5.1 Summary and Conclusions

Hollow and mesoporous silica particle from tetramethyl-orthosilicate were successfully synthesized using organic polystyrene particle through wet-chemical process followed by calcination. Advanced research on the synthesis of highly dispersed cationic polystyrene nanoparticles with controllable size smaller than 50 nm via modified emulsion polymerization process was also presented. For the conclusion of this dissertation, the major results are summaries as follows:

1. The size and shell thickness of hollow silica particles were controlled by changing the size of PS particle and the concentration of TMOS. A high concentration of MeOH (75 to 90 wt%) was required to produce hollow silica particles. The measured shell-thickness of hollow silica particles as function of the TMOS concentrations was in a good agreement with theoretical calculation. Hollow silica particle with the shell-thickness of 6.2 nm displayed a high light transmittance intensity of 97.1%, in the wavelength at 680 nm. The thermal conductivity of the PES/hollow silica composite film (silica composition, 2.5 wt%, film thickness, $35 \pm 5 \mu\text{m}$) shows a low value ($0.03 \pm 0.005 \text{ W m-K}^{-1}$) if compared to the pure PES film. These results indicate that the prepared hollow silica particle has a high potential to be used for flexible optical devices, thermal insulator, yet visible-transparent composite film applications. For future work, more detail study the effect of MeOH concentration in the degree hydrolysis and condensation of TMOS and the theoretical result for thermal conductivity of composite film are suggested.
2. Spherical submicron MPS particles with radially oriented structures, high specific surface areas (up to $800 \text{ m}^2 \text{ g}^{-1}$), and large pores (20 nm) were successfully synthesized from TMOS via an O/W emulsion process. Styrene played an important role as a pore-forming agent. The pore size of the MPS particles gradually increased from 1.2 to 20 nm with increasing initial styrene concentration from 12.3 to 36.6 mg mL^{-1} . From the results, it is suggested that the formation of various morphology of

MPS particle were obtained depend on the balance between the rate of styrene polymerization, reaction of TMOS and the rate of CTAB micelle formation. Further, it is confirmed that the emulsion system at a specific condition could form the Winsor-III system and MPS particles with radially oriented structure were produced in the bicontinuous emulsion phase. For further research, this material is expected to be useful for various potential applications, such as for adsorption, filtration, and catalyst supports.

3. Research finding on the synthesis of highly dispersed polystyrene (PS) nanoparticle with diameter as smaller than 50 nm was presented in this current research. Specifically, the combined use of VA-044 initiator and acetone/water mixture solvent enabled the preparation of cationic PS nanoparticles with enhanced stability and controllable sizes of ~ 31 nm. Moreover, highly dispersed cationic PS nanoparticles could be obtained using high styrene concentrations without any added surfactant. The optimum polymerisation condition was achieved by using VA-044 initiator concentration of 0.15 mol L^{-1} , acetone-to-water mass ratio of 1.50, reaction time of 8 h, styrene concentration of 9.24 mol L^{-1} , and reaction temperature of $60 \text{ }^\circ\text{C}$. The addition of acetone increased the solubility of styrene and reduced the surface tension between the PS particle surface and aqueous phase. Additionally, rapid diffusion of acetone contributed to the formation of small droplets in the emulsion system, further enabling the formation of PS nanoparticles. The VA-044 initiator could effectively control the stability of both the surface charge and size of the PS particles. It is still difficult to produce small hollow silica particle using prepared PS particle. For future work, this PS particle can be considered as template nanoparticle for design and nanostructured particle. Furthermore, it is suggested that increase of the product yield is necessary in order can be applied for industrial application.
4. The present research is expected to be useful for the improvement of particle technology, especially concerned to the fields of chemical and material engineering.

List of Publications

1. L. Ernawati, T. Ogi, R. Balgis, K. Okuyama, M. Stucki, S. C. Hess, W. J. Stark, Hollow silica as an optically and thermally insulating polymer additive., *Langmuir*. 32(1), 338-345, **2016**.
2. L. Ernawati, R. Balgis, T. Ogi, K. Okuyama, Tunable synthesis of mesoporous silica particles with unique radially oriented pore structures from tetramethyl orthosilicate via oil-water emulsion process., *Langmuir*, 33(3), 783-790, **2017**.
3. L. Ernawati, R. Balgis, T. Ogi, K. Okuyama, T. Takada, Role of acetone in the formation of highly dispersed cationic polystyrene nanoparticles., *Chem. Process Eng. J.*, 38(1), **2017**.
4. R. Balgis, L. Ernawati, T. Ogi, K. Okuyama, L. Gradon, Controlled Surface Topography of Nanostructured Particles Prepared by Spray Drying Process., *AIChE J.*, 63(5), 1503-1511, **2017**.

Acknowledgment

The author wishes to acknowledge the contributions of the following people towards the successful completion of this dissertation. I am indebted to many great individuals for their support in bringing this project to completion. First, I deeply appreciate and admire my supervisor, Assoc. Prof. Takashi Ogi, for his patience and professional advices throughout the completion of this dissertation. I am also thankful for his invaluable guidance, kind and moral supports concerning all my complications apart from the studies during stay in Japan.

I also would like to thank Prof. Kikuo Okyama, and Prof. Akihiro Yabuki for their patience, wisdom and support as referee members. Special thanks to Ministry of Education, Culture, Sports, Science and Technology of Japan (MEXT) Scholarship Foundation for the financial support during my study at Hiroshima University. My deep appreciation is extended to Prof. Wendelin J. Stark (ETH university) who gave a good, comments, suggestions and many advise with great compliments towards my research. I am thankful for his input, ideas, discussions, valuable insights and constructive comments on my earlier version work of hollow silica to make it more scientifically relevant. A special tribute and thanks to his laboratory members: Mario Stucki, and Samuel C. Hess, for their nice research collaboration, good cooperation, and help for measuring thermal conductivity.

This dissertation could not have been accomplished if it had not been contributed by people surrounding this project. Therefore, I would like to thank those. First, I wish to express my deepest gratitude to Dr. Toru Iwaki and Asst. Prof. Dr. Ratna Balgis, who constant help and generous support with invaluable advice during the progress of my doctoral studies. I also wish to convey my sincere thanks to Dr. Makoto-Maeda of the Natural Science Center for Basic Research and Development (N-BARD) of Hiroshima University for his help with TEM analysis and his invaluable help for observing my prepared particles. I also would like to express my sincere thanks to all my laboratory member for all the good moments and for creating a funny and warm working atmosphere. Many thanks to all of friends in Hiroshima University for their supporting including for the daily life and food sharing. Those memorable moments are

what made it as my second home. A special thank goes to all my friends for their everlasting supports/prayers.

Finally, I am deeply indebted and grateful to my parents, my lovely brother and his wife, for their unconditional love and moral support, and for being the greatest family on earth. The love and encouragements kept me going during challenging times in Japan. They give my life purpose and meaning. They provide the day-to-day support that I need to be the best I can be. They also exposed me to environments so colorful and unique that what I experienced made a permanent impression on me.

LUSI ERNAWATI

Higashi Hiroshima, September 2017